STRUCTURAL GEOLOGY OF THE BIG BEND ANTICLINE, BROOKS RANGE FOOTHILLS, ALASKA

By

Cheryl M. Sanders

RECOMMENDED:

Dr. Catherine Hanks

Dr. Anupma Prakash

Dr. Wesley Wallace
Advisory Committee Chair

Dr. Paul McCarthy, Chair
Department of Geosciences

APPROVED:

Dr. Paul Layer
Dean, College of Natural Science and Mathematics

Dr. John Eichelberger
Dean of the Graduate School

12/7/14
Date

STRUCTURAL GEOLOGY OF THE BIG BEND ANTICLINE, BROOKS RANGE FOOTHILLS, ALASKA

A

THESIS

Presented to the Faculty

of the University of Alaska Fairbanks

in Partial Fulfillment of the Requirements

for the Degree of

MASTER OF SCIENCE

By

Cheryl M. Sanders, B.S., B.A. Elementary Education, B.A. Secondary Education

Fairbanks, Alaska

December 2014

Abstract

Big Bend anticline is near the northern edge of the Brooks Range foothills of northern Alaska. The structure of the foothills is a low-taper triangle zone or passive-roof duplex within Brooks Range foreland basin deposits. The dominant structures are detachment folds locally cut by thrust faults and Big Bend anticline is one of these. This research combines detailed surface mapping (1:25,000) with interpretation of aerial photos and satellite imagery of the Big Bend anticline and seismic reflection data from the Umiat anticline to reconstruct its surface and subsurface geometry.

The research area surrounds the Big Bend of the Chandler River and covers approximately 10 km^2. The mechanical stratigraphy of the area consists of the competent Nanushuk sandstones between two incompetent units-the overlying Seabee and underlying Torok shales. The structure of the area consists of an east-trending anticline with a hinge that branches westward into two open, broad anticlines and an intervening syncline. A forethrust near the southern hinge and a backthrust near the northern hinge have broken through the anticline west of the branch point.

Subsurface data of Umiat anticline combined with surface projected cross sections from the study area provide an analog of the subsurface structure in the Big Bend area. These cross sections show gentle anticlines separated by flat bottomed synclines in competent Nanushuk Formation sandstone. The anticlines overly Torok Formation thickened by north vergent folds and thrust faults above a detachment zone. Collectively, these structures form a low-taper triangle zone. Cross section restoration suggests more shortening in the Torok duplex than in the overlying folds and breakthrough faults. Results of this research provide an analog for other anticlines in the region that are currently the focus of oil and gas exploration.

For my father for all the inspiration he gave.

Table of Contents

Page

Page

Page

Page

List of Figures

Page

Page

Page

Page

List of Tables

Page

List of Supplemental Files

M.1 Preferred geologic interpretation of the Big Bend anticline

M.2 Alternate geologic interpretation of the Big Bend anticline

M.3 Domain map of the study area

List of Appendices

Page

Acknowledgements

I would like to acknowledge the following organizations and individuals for their support of this research.

Support for this research was provided by the University of Alaska Fairbanks Geophysical Institute, the Bureau of Land Management, the Department of Energy contract DE-FC26-08NT0005641, Renaissance Alaska LLC and Linc Energy. Funding was provided by an EDMAP grant from the United States Geologic Survey to assist with the costs of field research including equipment, food, an assistant and transportation. Support from the Alaska Division of Geological and Geophysical Surveys was instrumental in providing the helicopter access into and around the study area.

Wes Wallace provided the encouragement and guidance to help me complete the field research, process and analyze the data and create the maps and models for this research.

Anupma Prakash provided the inspiration to look beyond the field and dive into the world of remote sensing.

The content and organization of this thesis is the result of support and assistance from my committee members, Wes Wallace, Anupma Prakash and Cathy Hanks. Their guidance provided clarity, motivation, and suggestions for improvement.

Bill Witte, Chris Wyatt and Santosh Panda gave hours of valuable technical support and patience.

Joel Brann was the most wonderful, gun toting, GPS tracking, musically inclined field assistant.

My fellow students, Raelene Wentz, Jeremy Davis and Grant Shimer provided their friendship, encouragement and insight.

Thanks to my family for everything.

Chapter 1 Introduction

1.1. Importance of Brooks Range foothills

The Brooks Range foothills, in northern Alaska, form the southern part of the North Slope of Alaska and are dominated over a vast area by folds formed in foreland basin deposits (Figure 1.1). These folds are conspicuous in regional maps and satellite imagery. They have been a target throughout the history of North Slope oil and gas exploration and promise to be of significant interest in the future. Some anticlines in the region are known to be structural traps for hydrocarbons such as the Umiat and Gubik anticlines. Exploration for oil and gas in the Umiat region north of the study area is proving promising as drilling and production technology advance and the price of oil increases. The source and extent of these petroleum resources are not fully understood due to the limited information available because of the remoteness and inaccessibility of the region. Few detailed maps or studies of these structures have been published.

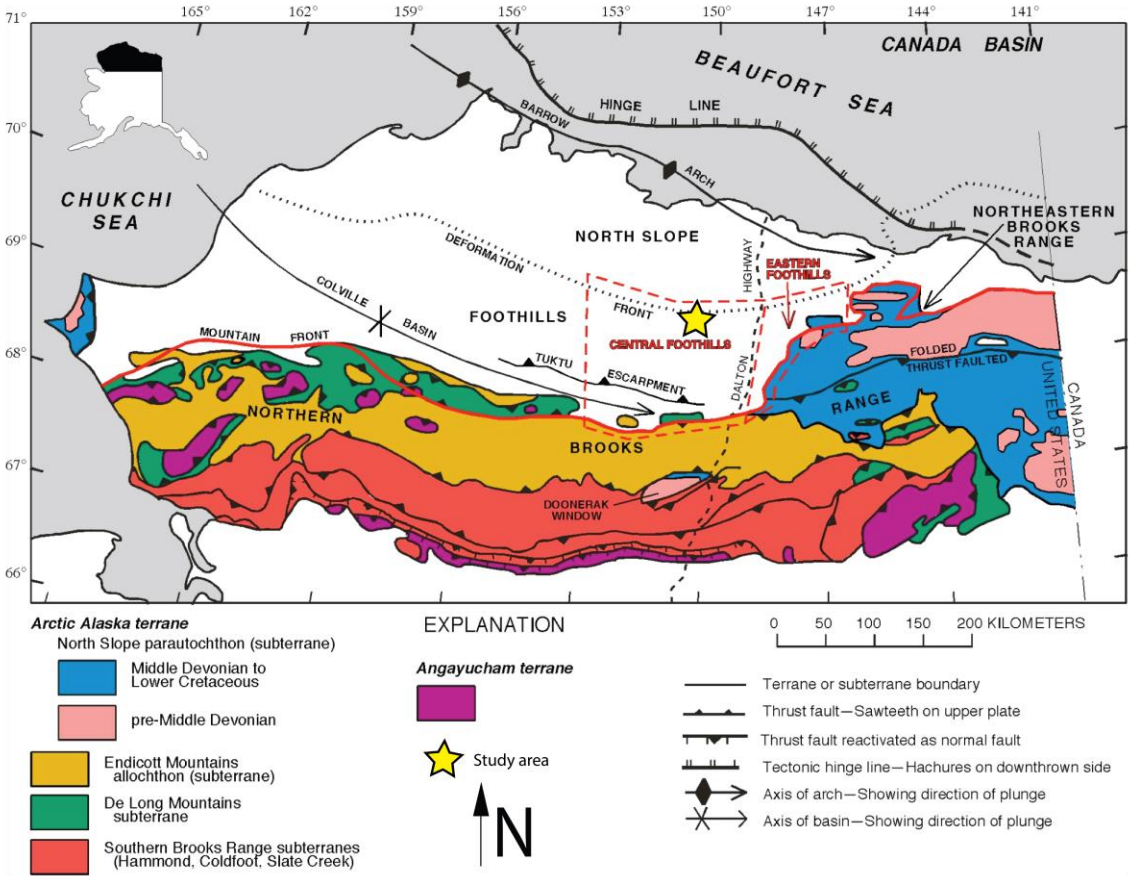

Figure 1.1 Generalized tectonic map of northern Alaska. The central foothills are located between the Brooks Range to the south and the deformation front to the north. Modified from Moore et al., 1994.

Inaccessibility is the main factor contributing to the lack of detailed documentation about the study area. More is known about traps closer to the road system. The nearest road, the Dalton Highway, is approximately 100 km to the east and the nearest airstrip, Umiat airstrip, is 30 km north of the study area. The level of detail of the available geologic mapping defines many of the structurally important features with only limited certainty (Figure 1.2). Interpretations of the surface and subsurface structural geometry are limited or largely outdated and interpretations of the kinematic evolution of the area are generalized and simplistic. A deeper understanding of the geology and kinematic evolution of the region will be beneficial as the feasibility to produce from the central part of the northern Brooks Range foothills increases with rising demand and prices for petroleum.

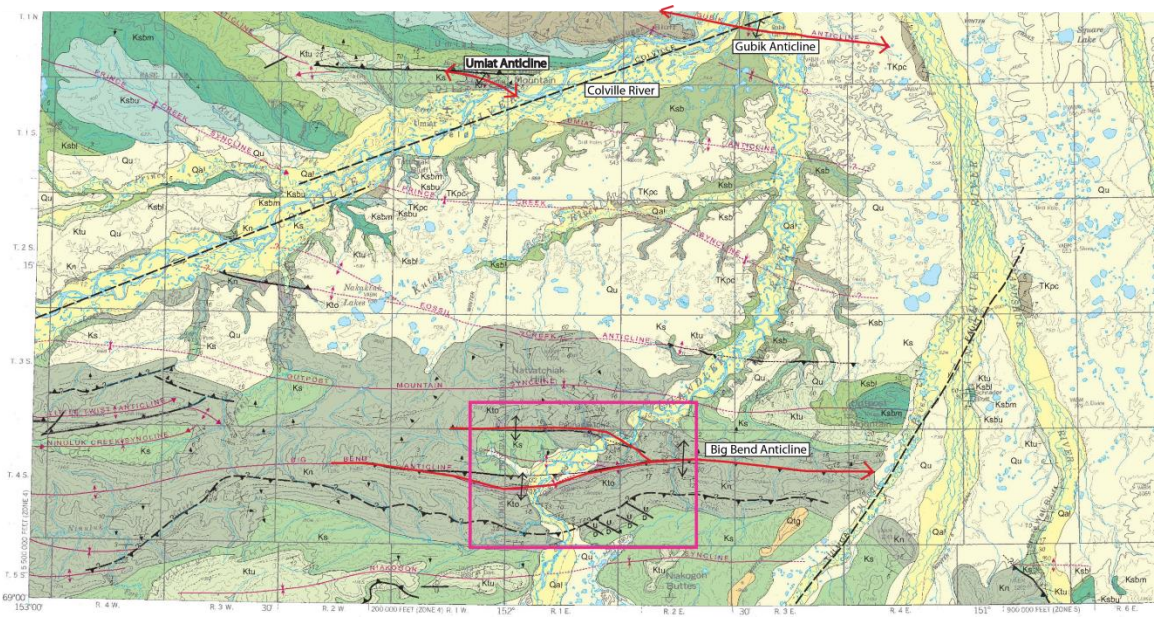

Figure 1.2 Published 1:250,000-scale geologic map of the region. Notice that many of the major geologic structures are mapped with a very low level of certainty. Study area is outlined with a pink box. Umiat and Gubik anticlines are known hydrocarbon traps that are labeled. Modified from Mull et al., 2004

Understanding the sequence of deformation is critically important to recognizing how the fold-and-thrust belt works as a whole. This Master's thesis research is a study of Big Bend anticline, an example of a central foothills anticline near the deformation front. The research combines detailed surface mapping, seismic interpretation, and aerial platform and satellite data analysis to create a map (1:25,000) of the Big Bend anticline in order to reconstruct the surface and subsurface geometry of a representative example of the structure of the foothills and to interpret its kinematic evolution.

1.2. Objectives of study

The main objectives of this research were to document the three-dimensional geometry of an anticline that displays characteristics and complexities representative of foothills anticlines and to determine the reason for the opposing thrust faults that cut the anticline; to assess the applicability of the idealized triangle zone model by Jones (1982) to the folds in the study area.

Other objectives included determining the kinematic evolution as an analog for other foothills folds and relating the findings to the Umiat anticline, which hosts a known oil field.

I am using the Big Bend anticline as an analog for other northern Brooks Range foothills folds because relatively good outcrops along the Chandler River define an anticline that changes geometry along strike and displays thrust faults cutting both limbs.

1.3. Introduction to study area

The foothills of the Brooks Range are prominent features extending across the Colville basin from the northern mountain front (Figure 1.1). The main structural features in the northern foothills are broad anticline-syncline pairs in folded foreland basin deposits. Most structures parallel the deformation front and trend east-west.

The study area is in the northern Brooks Range foothills, approximately 40 km south of the deformation front (Figure 1.1). The Chandler River bisects the study area as it flows north towards its union with the Colville River and on toward the Arctic Ocean. "Big Bend" is a named large bend in the river in the study area, so I have used this name for the geologic structures in the area. The area contains one well-documented east-west trending gentle anticline, the southern Big Bend anticline (Figure 1.3). Another anticline branches to the north from the main southern Big Bend anticline just east of the Chandler River. The Seabee syncline separates these two anticlines west of the branch point. Two major east-west striking thrust faults are present in the study area. A south-dipping forethrust cuts through the north limb of southern Big Bend anticline near its hinge and west of the branch point, but its location and displacement are uncertain because of poor exposures. A north-dipping backthrust cuts through the northern anticline, near its hinge and north of the Seabee syncline.

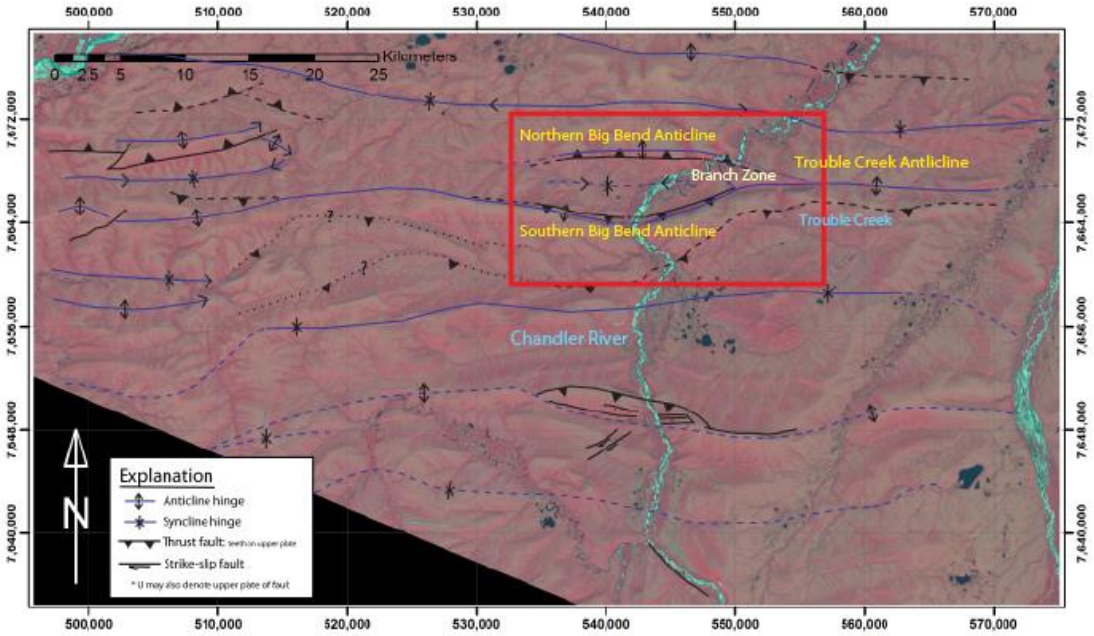

Figure 1.3 General structural names and locations within the study area. To clarify the identity of structures throughout this paper, the southern Big Bend anticline is the southern anticline west of the branch zone and the Trouble Creek anticline is the single anticline east of the branch zone. The entire northern branch of the anticline west of the branch zone is the northern Big Bend anticline.

1.4. Problem Definition

Current, published information about the Big Bend area leaves some questions unanswered. The purpose of this research is to answer these questions and gain a deeper understanding of the structure and kinematic evolution of the northern foothills of the Brooks Range. Some of the questions I had at the beginning of this research include:

- What is the structural relation between the northern and southern Big Bend anticlines to the west and to the single anticline to the east at Trouble Creek? Is this consistent with other folds in the area?
- Why are the thrust faults located where they are? Do they extend farther east or west? How are the thrust faults related to the underlying structures? Is the amount of

shortening different between the eastern and western portions of the study area and why?

- What is the nature of the normal faults and the ambiguous thrust fault in the southeastern corner of the Mull et al. (2004) map? What is the role of extensional structures in an area dominated by contractional structures? Are extensional structures present anywhere else in the study area or the region?
- What is the subsurface structure? What is the vertical extent of deformation and how have the different units of the mechanical stratigraphy responded to deformation? What structural patterns occur in the subsurface that could be helpful in understanding other areas of the Brooks Range foothills fold-and-thrust belt? How do the subsurface structures help to explain the exposed pattern of stratigraphy and structure or vice versa?
- How did deformation progress? What is the total amount of shortening within the study area? How did each mechanical stratigraphic unit respond to contraction?

In order to provide some context for the basic scientific questions being addressed by this study Chapter 3 (Previous Work) summarizes the basic concepts related to mechanical stratigraphy (section 3.2), detachment folds (section 3.3), forethrust and backthrust faults (section 3.4), branching anticlines (section 3.5) and passive roof duplexes (section 3.6) and how each of them applies to the study area.

1.5. Structure of the thesis

The thesis is designed to present the reader with relevant background on the region, the methods and analyses that were used to address the questions identified, and the results and interpretations. The field and satellite data and methods were quite different and so are presented in two separate chapters. Seismic reflection data from the Umiat anticline, a nearby structurally analogous anticline, are used to identify and define the sub-surface structure to provide further clarification for interpretation. An appendix is included to help fully document detailed information that is not included in the text. The topics of each chapter are outlined below.

Chapter 1-General introduction of the thesis and study area including the Problem Definition.

Chapter 2-Regional geologic setting to provide context including geologic location, tectonic history, stratigraphic setting and structural setting.

Chapter 3-Previous work on topics relating to this research to include mechanical stratigraphy, detachment folds, triangle zones or passive roof duplexes, thrust faults and branching anticlines.

Chapter 4-Methods applied to field data, aerial photos, seismic data and remote sensing data.

Chapter 5-Observations and results used to create the final geologic maps and surface projected cross sections.

Chapter 6-Discussion and interpretations.

Chapter 7-Conclusions and recommendations for further study.

Chapter 2 Regional Background

2.1. Geologic context: location and relation to the Brooks Range

The study area is located 33 km southeast of Umiat airstrip and covers an area approximately 10 x 10 km^2 (Figure 2.1). This part of the foothills is 40 km south of the deformation front of the fold-and-thrust belt. The nearest road is the Dalton Highway, 125 km to the east, which provides access to Prudhoe Bay and other North Slope oil fields. The latitude and longitude coordinates for the area are N 69.015 to 69.150, W 152.120 to 151.695 (Figure 2.2). The Chandler River bisects the study area and flows northward towards the Colville River and on to the Arctic Ocean.

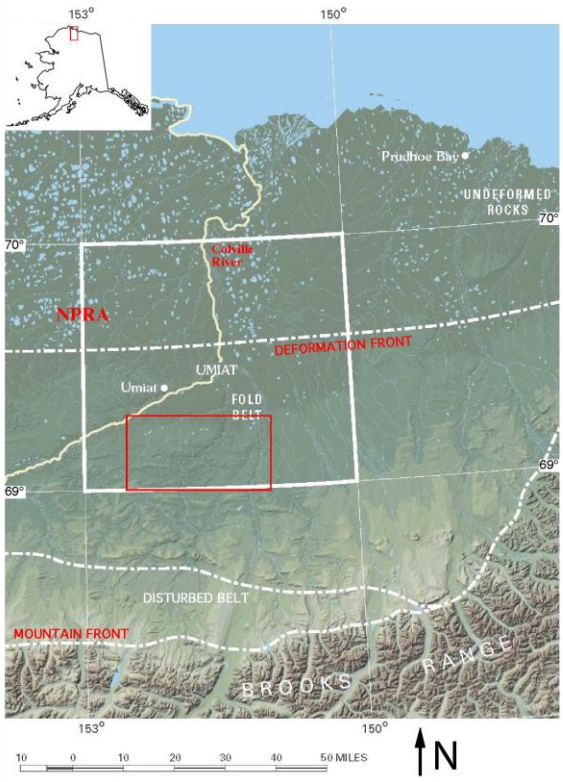

Figure 2.1 Brooks Range foothills regional map of northern Alaska. Study area is located within the red box approximately 33 km southeast of the Umiat airstrip. Study area is located near the northern edge of the foothills fold belt and thus near the deformation front. Modified from Mull et al., 2004

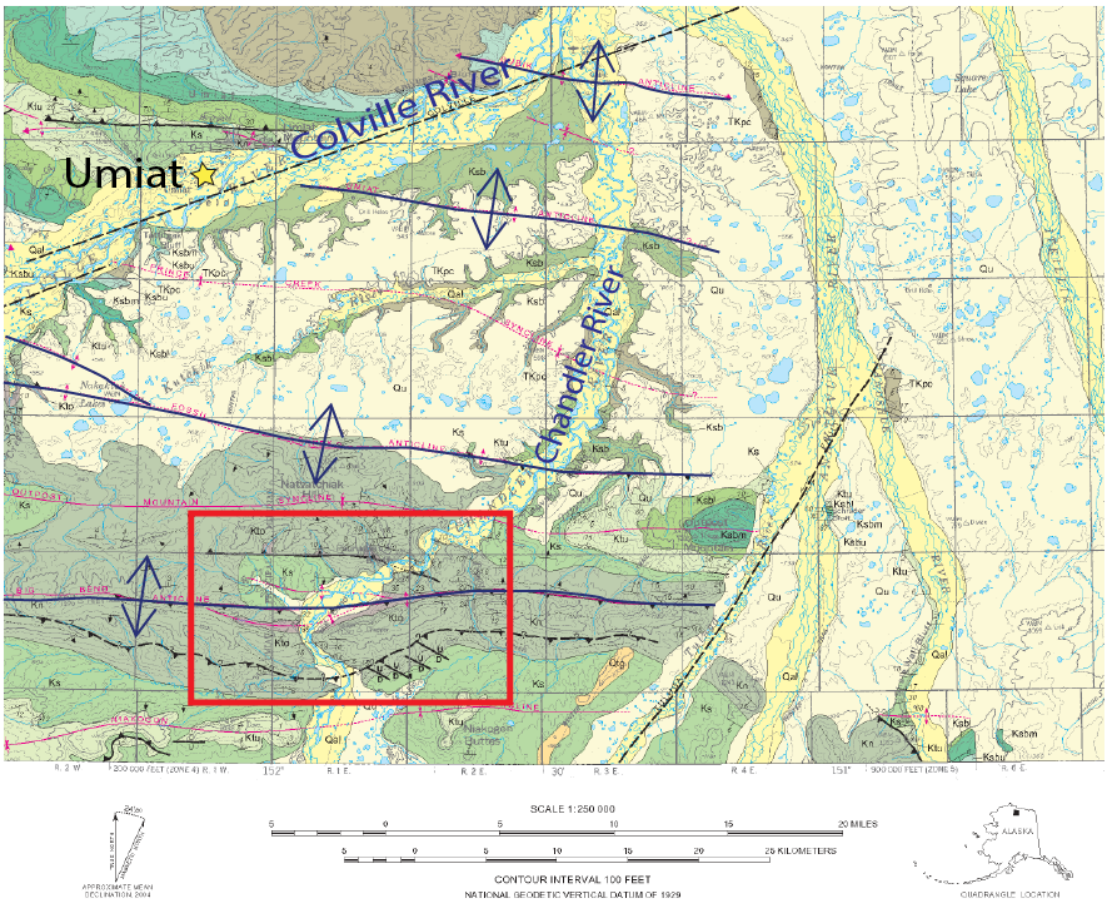

Figure 2.2 Excerpt from the published 1:250,000-scale geologic map by Mull et al., 2004. Anticline hinges have been traced with dark lines to show trends. Umiat airstrip is shown with a yellow star located in the northwest corner of the map. The red box indicates my study area.

2.2. Regional tectonic history: formation and evolution of the Brooks Range foothills

The Brooks Range is the northwestern end of the Rocky Mountain fold-and-thrust belt. Two main episodes of deformation have affected the central Brooks Range. The first occurred in Middle Jurassic to Early Cretaceous time and was responsible for the majority of the contraction (Moore et al., 1994). Mid-Cretaceous uplift and erosion in the Brooks Range and to the west caused rapid filling of the Colville foreland basin to the north by large clinoforms that prograded north and northeastward (Bird and Molenaar, 1992). Renewed contraction in Paleocene time (~60 Ma) formed the present east-trending mountain front and caused the foreland basin

deformation that formed the foothills (O'Sullivan, 1996; O'Sullivan et al., 1997; Moore et al., 2004).

2.3. Stratigraphic setting

The stratigraphy of the study area consists primarily of Brooks Range foreland basin deposits that rest on an older passive margin succession (Bird and Molenaar, 1992; Moore et al., 1994; Mull et al., 2003, 2004) (Figure 2.3). The Brooks Range foreland basin deposits thin from south to north, reflecting onlap onto a basement high to the north. Before Early Cretaceous time, the shelf and continent were to the north, and were the source of deposition for the Ellesmerian sequence. The Ellsmerian sequence is a gently south-dipping passive margin succession that is capped by the Jurassic to Lower Cretaceous Kingak and pebble shale units. These are overlain by the Brookian sequence, which consists of Aptian and younger foreland basin fill derived from the west and south. In the northern foothills, the lower part of this sequence consists of base-of-slope sandstone and shale deposits of the lower Torok Formation (also referred to by some workers as distal Fortress Mountain Formation) (Molenaar et al., 1988). These rocks grade upward into slope mudstone to shale of the upper Torok Formation, which in turn grade upward into shallow marine to fluvial sandstone and local conglomerate of the Nanushuk Formation. The Nanushuk is overlain by the Seabee Formation, which consists of shale, mudstone and fine-grained sandstone.

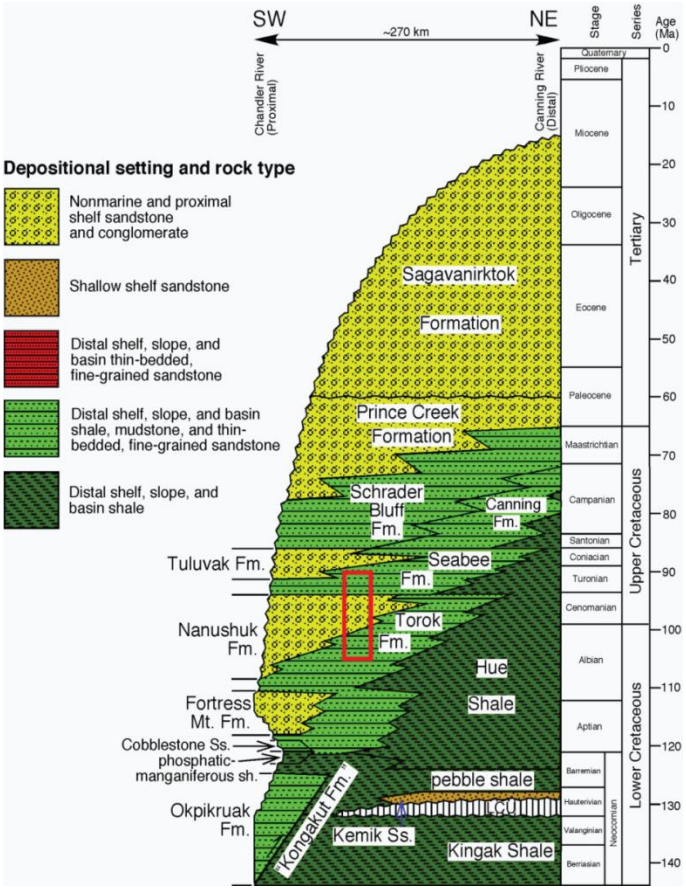

Figure 2.3 Regional Cretaceous stratigraphy of the North Slope. Red box indicates part of stratigraphy exposed in the study area. Redrafted and modified from Mull et al., 2003.

The three main stratigraphic units exposed in the study area are the Torok, Nanushuk and Seabee Formations. The information about these units most relevant for the purposes of this research is that the Nanushuk is a competent sandstone unit bounded between two very incompetent shale units (Figure 2.3). Torok Formation characteristically consists of shale and thin sandstone interbeds but is poorly exposed in the study area (Figure 2.4). All Torok Formation observed in the study area was highly weathered to a mud containing small sandstone fragments.

Figure 2.4 Torok Formation with shale and thin sandstone interbeds. Scale is 15 cm and inside yellow box. Torok Fm. is very poorly exposed in the study area, so image is from elsewhere. Photograph by W. K. Wallace.

Competent sandstone beds are characteristic of the Nanushuk Formation (Figure 2.5). The lower part of the Nanushuk Fm. consists of a thick section of intertonguing shallow marine sandstone with neritic shale and siltstone that graded seaward into mudstone of the Torok Formation (Ahlbrandt et al., 1979; Molenaar, 1985). The upper part of the Nanushuk Fm. consists dominantly of nonmarine facies of paludal shale, fluvial sandstone, and coal that grade upward from the marine facies (Bird and Molenaar, 1992). Conglomerate is present at the top of the upper Nanushuk Fm.(Ahlbrandt et al., 1979; Molenaar, 1985, 1988, Shimer et al., 2014).

Figure 2.5 Competent sandstone beds of the Nanushuk Formation. Photograph of the south limb of the southern Big Bend anticline from the Chandler River. View to the east. Geologist for scale.

All outcrop of the Seabee Formation observed in the study area consisted of bentonitic clays, with subordinate interbeds of very fine-grained sandstone with concretionary cement (Figure 2.6).

Figure 2.6 Seabee Formation as seen looking down on a typical exposure of the Seabee Formation in the study area, with characteristic bentonitic clay and concretionary cemented sandstone. Seabee Formation is only exposed within the study area in poor outcrops that are disrupted by surface processes. Pencil for scale.

2.4. Structural setting

The character of the stratigraphy has greatly influenced the structural geometry and evolution in the foothills (Moore et al., 2004; Wallace, 2009; Wallace et al., 2011). The northern foothills province is underlain by a broad axe-like wedge of Brookian strata, that tapers northward and incorporates a train of detachment folds that overlies the nearly planar, south-dipping homoclinal Ellesmerian sequence (Kirschner and Rycerski,1988). Collectively, these structures form a low-taper triangle zone (Figure 2.7) (Jones, 1982; McMechan, 1985) or passive-roof duplex (Banks and Warburton, 1986; Wallace, 1993).

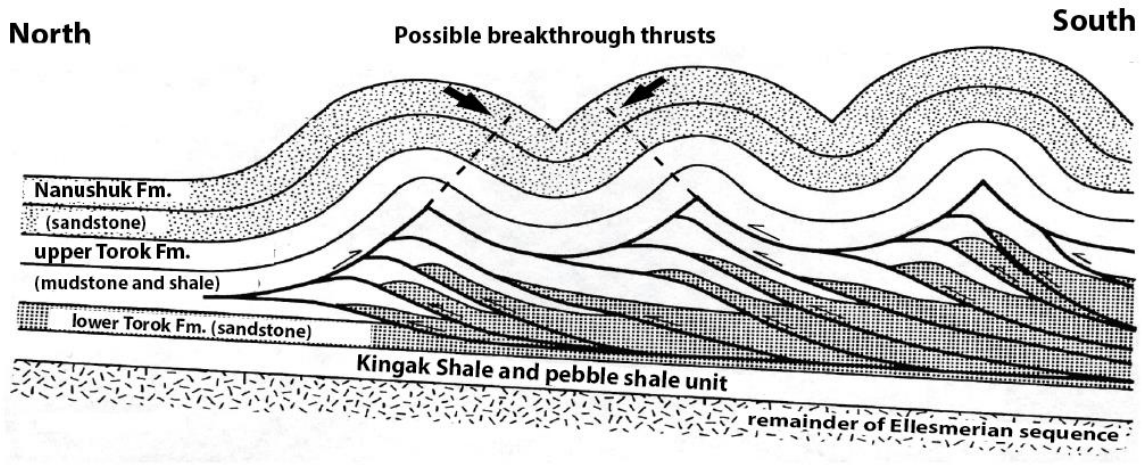

Figure 2.7 Idealized model of the folds and faults of the Brooks Range foothills fold-and-thrust belt. Gentle anticline-syncline pairs form over fault-thickened Torok above a basal detachment in the lower Torok. The entire system defines a triangle zone. Modified from Jones, 1982.

The relatively thick, structurally competent, sandstone of the Nanushuk Formation forms a folded roof above structurally incompetently deformed Torok Formation. The overlying Seabee Formation is very incompetent and allows the Nanushuk Formation. to be detached relative to overlying competent units. Cuspate anticlines in the Nanushuk Formation. are separated by flat-bottomed synclines. The anticlines are detachment folds that display local thrust breakthrough (Poblet and McClay, 1996; Wallace and Homza, 2004). Anticlines are spaced ~5-10 km apart (Wallace, 2009; Wallace et al., 2011). Detachment beneath the Nanushuk Formation. occurs in shales of the middle and upper parts of the Torok Formation. Deformed strata overlie a very gently south-dipping detachment in or below the lower Torok Formation (Wallace, 1993). Seismic reflection data along with local exposures of the upper Torok Formation. suggest that the Torok Formation. is thickened in the cores of anticlines by smaller-scale folds and thrust faults. Torok Formation in this area most likely contains several anastomosing detachment planes in the south that die out progressively northward (Kirschner and Rycerski, 1988).

Regional trends of folds and thrust faults are east-west (Figure 2.8). The gentle dip of the basal detachment and the low taper of the triangle zone are consistent with the variable vergence of the folds and thrust faults. The Nanushuk anticlines may verge either to the north or south and commonly are cut by small-displacement thrust faults that may dip either to the south or north (Wallace, 2009; Wallace et al., 2011).

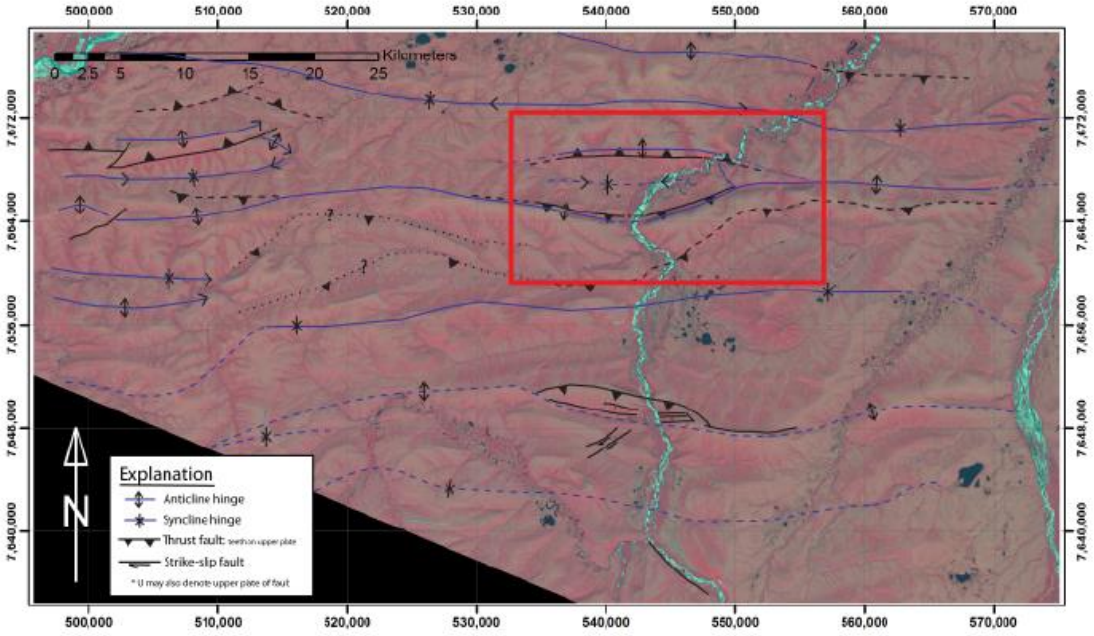

Figure 2.8 Regional map around the Big Bend anticlines to show east-west trend of the folds and thrust faults in the area. The base of this map is from the Landsat 4/5 TM image used in the remote sensing portion of this research. Structural interpretations are modified from Mull et al.,(2004), Detterman et al.,(1963), and the final map for this research.

Chapter 3 Previous Work

3.1. Focus of previous work

This chapter addresses the previous work on the various topics related to this research. Each section contains a summary of previous work and how it relates to this study. Basic concepts include mechanical stratigraphy (section 3.2), detachment folds (section 3.3), forethrust and backthrust faults (section 3.4), branching anticlines (section 3.5), and passive roof duplexes (section 3.6).

3.2. Mechanical stratigraphy

Layered sequences of rock subjected to layer-parallel shortening may either fold or fault (Erickson, 1996). The strength and thickness of each rock layer in a sequence relative to the other layers in the sequence defines the mechanical stratigraphy of that sequence and plays an important role in how the rocks within the sequence deform. The stratigraphic sequence within many fold-and-thrust belts consists of a weak decollement layer of shale or salt, a strong layer of carbonate rocks, and a cover layer of clastic rocks (Woodward and Rutherford, 1989, Goff, 1990). Slip surfaces within a sequence are also important, allowing the sequence to behave as a multilayer rather than a single layer and thereby enhancing folding over faulting (Johnson, 1980). Erickson determined that high strength contrasts, a weak decollement layer, a thin cover layer and free-slip contacts between layers favor folding over faulting. Understanding the role of mechanical stratigraphy in the study area will help to further understanding of how the layers deformed geometrically and in relation to each other. The mechanical stratigraphy in the Big Bend area includes a lower shale that acts as a weak decollement (Torok Formation), a strong middle sandstone interval (Nanushuk Formation), and a weak cover interval of shale and clay (Seabee Formation) (Figure 3.1).

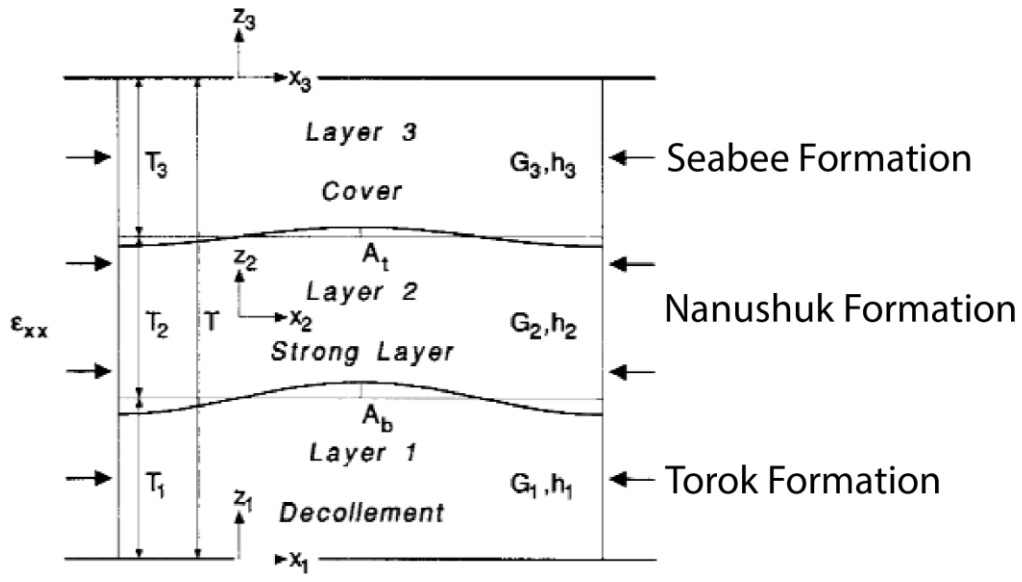

Figure 3.1 Schematic of mechanical stratigraphic layers. Geometry of the models used by Erickson (1996) showing thicknesses and material properties of the decollement (layer 1), the strong layer (layer 2) and the cover (layer 3). This is analogous to the stratigraphy of the study area with Torok as the decollement, strong Nanushuk sandstone and Seabee cover.

3.3. Detachment folds: geometry and characteristics

A detachment fold forms when a layer of rock deforms above a bedding-parallel thrust fault (also referred to as a detachment surface or decollement) (Jamison, 1987). Detachment folds form in stratigraphic packages with high competency contrasts between units in which the upper competent unit exhibits parallel fold geometries and the lower weak unit displays structural thickness variation commonly by disharmonic folding (Homza and Wallace, 1995, 1997; Poblet and McClay, 1996; Mitra, 2003). The flow of weak material into the cores of anticlines may be necessary for the development of detachment folds (Wiltschko and Chapple, 1977). Three common models of the geometry and kinematics of detachment folds differ in how thickness and bed length change in the competent and incompetent units (Figure 3.2).

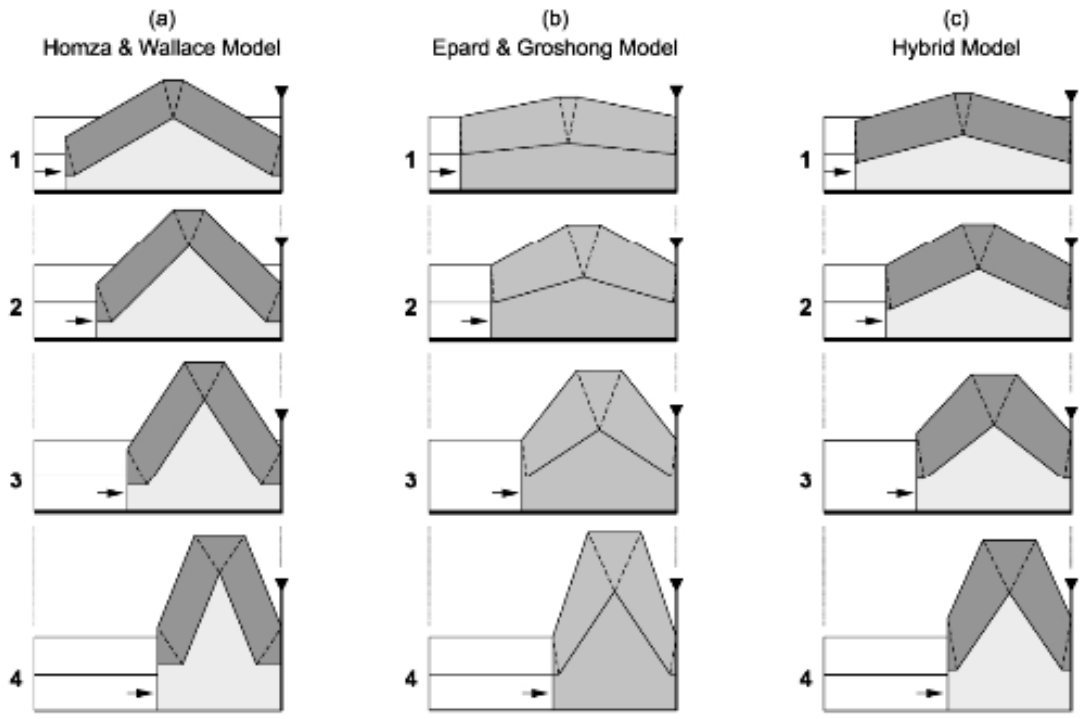

Figure 3.2 Comparison of three models describing the geometry and kinematics of detachment folds. Dark grey units are competent and the underlying light grey units are incompetent. Epard and Groshong make no distinction in competency. (a) Homza and Wallace (1995) model. (b) Epard and Groshong (1995) model. (c) Hybrid model (Atkinson and Wallace, 2003) that combines the two others. Figure modified from Atkinson and Wallace (2003).

The Homza and Wallace (1995) model shows constant thickness in the competent layer and a variable depth to detachment. The Epard and Groshong (1995) model shows no contrast in competency, variable thickness and constant depth to detachment. The hybrid model of Atkinson and Wallace (2003) shows variable thickness and a variable depth to detachment. In the study area, the competent layer is Nanushuk Formation and the underlying incompetent layer is Torok Formation.

3.4. Triangle zone or passive roof duplex

The Brooks Range fold-and-thrust belt is an example of a triangle zone because the leading edge of deformation is a monocline without an observed major thrust (Jones, 1982; Kirschner and Rycerski, 1988; Moore et al., 2004). The Jones (1982) triangle zone model (Figure 3.3) is

applicable to the mechanical stratigraphy, fold geometries and characteristics of the study area. The Jones (1982) model was originally created from surface, well and seismic data from the Alberta Foothills of the Canadian Rockies. A triangle zone is a duplex in a layered sequence in which thrust imbrications are bound by a lower detachment with forward displacement and an upper detachment with hindward displacement. The originally horizontal upper detachment becomes uplifted by the thrusting beneath it (Jones, 1982).

Typical fold geometry near the deformation front of fold-and-thrust belts includes gently folded anticline-syncline pairs. Fold axes trend parallel to the deformation front and normal to the shortening direction. In the study area, folds trend east-west parallel to the deformation front. Wallace (2009) suggested that the foothills folds formed within the competent Nanushuk Formation sandstone according to the model by Jones (1982) (Figure 3.3). In this model the basal decollement is in the lower Torok formation. The anticline-syncline pairs consist of Nanushuk and upper Torok Formations folded above a passive roof detachment. The Torok mudstone between the two detachments was structurally thickened by forward displacement of horses in a duplex. Periodically spaced thickening by thrust faults in the Torok Formation defines the cores of the overlying anticlines.

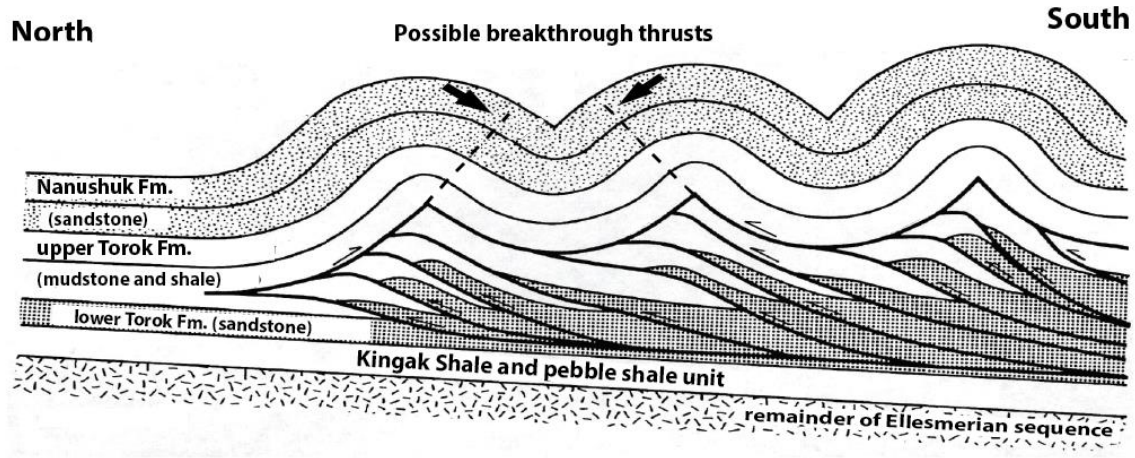

Figure 3.3 Idealized model of the folds and faults of the Brooks Range foothills fold-and-thrust belt. Gentle anticline-syncline pairs form over fault-thickened Torok Formation above a basal detachment in the lower Torok Formation. The entire system defines a triangle zone. Modified from Jones (1982).

3.5. Geometry, characteristics and origin of forethrust and backthrust faults in folds

Faulting is usually secondary to detachment folding and occurs primarily to accommodate variations in strain with structural and stratigraphic position (Mitra, 2003). Fold belts with a weak and subhorizontal detachment are usually characterized by folds and thrust faults that verge in both forward and hindward directions (Davis and Engelder, 1985). The low taper angle of such fold belts, defined as the sum of the topographic slope and the slope of the basal detachment, means that the two potential slip planes in opposite directions have approximately the same dip and so motion in either direction is equally possible (Davis and Engelder, 1985; McMechan, 1985). Consequently, thrust faults may break through either the forelimb or the backlimb of an anticline.

The study area contains at least one forethrust. This is a common structure in fold-and-thrust belts, which form by breaking through folds. Both forethrusts and backthrusts have been recognized in folds in the Brooks Range foothills fold-and-thrust belt, with several examples of each in or near the study area (Figure 1.2) (Mull et al., 2004). The Jones (1982) model shown here (Figure 3.3) has been modified to depict the possible locations and vergence of such faults in the Brooks Range fold-and-thrust belt. These thrust faults branch upward from the roof detachment and break through the limbs of the anticlines in the Torok Formation.

3.6. Geometry, characteristics and origin of branching anticlines

A branching anticline may form either when a single anticline splits or two adjacent anticlines merge together at some point during their evolution. Understanding the geometry and evolution of a branching anticline is of significant interest for oil and gas exploration and for understanding fold-and-thrust belts. Will a hydrocarbon trap beneath a branching anticline differ in its characteristics from one in a single doubly plunging anticline? What stratigraphic or structural characteristics may cause separate and parallel folds to form in one location and branching anticlines to form in another? These questions about branching anticlines are rarely addressed in published papers and when they are, the discussion about their structure and evolution is very limited. However, branching anticlines are evident in existing maps and thus may be much more common than is generally recognized. The study area includes a branching

anticline based on the map pattern of stratigraphic units and bedding dips shown on the published geologic map by Mull et al. (2004) (Figure 2.2). The location and direction of dip of the two previously mapped thrust faults in the study area also suggest a change in structure along strike.

Chapter 4 Methods

4.1. Methods and work flow

Four types of data were used for this research: field data, high resolution aerial photos, seismic data from Umiat anticline and satellite data including optical, synthetic aperture radar (SAR) and Advanced Spaceborne Thermal Emission and Reflection Radiometer digital elevation model (ASTER DEM) data (Figure 4.1). Field observations and remote sensing analysis were combined to create an updated geologic map of the study area. This map was used with the Umiat seismic data and ASTER DEM data to produce the surface projected cross sections and cross section restoration.

Figure 4.1 Workflow of methods used in this research. Data used includes field observations, seismic, and remote sensing images such as aerial photos and satellite data.

.

4.2. Fieldwork

The Alaska Division of Geological and Geophysical Surveys (DGGS) provided helicopter transportation. Their schedule allowed twelve days for field mapping of the area. My advisor, Dr. Wesley K. Wallace, was able to assist during the first six days in the field. The EDMAP grant also afforded me a field assistant for the full field time to assist with data collection and predator protection.

The short time available for field work required that the methods for collection of data and observations be as efficient and thorough as possible, while covering the most area. All helicopter reconnaissance was planned very carefully to maximize data collection. Four different camps were utilized, three along the Chandler River and one along Trouble Creek. Camp locations, as well as GPS station locations show coverage of the area (Figure 4.2). Rubble zones are common along the hillsides but generally lack outcrops with measurable bedding. Foot travel was restricted by large waterways and swamps in the low-lying areas. The higher elevations are drier but covered with tussocks. Tussocks make footing very unstable and make foot travel slow and arduous. We mainly stayed close to the river and creeks because the best available outcrops were created by river erosion. However, more outcrops were present than we had first estimated and we were able to gain a considerable amount of information during our short time in the field.

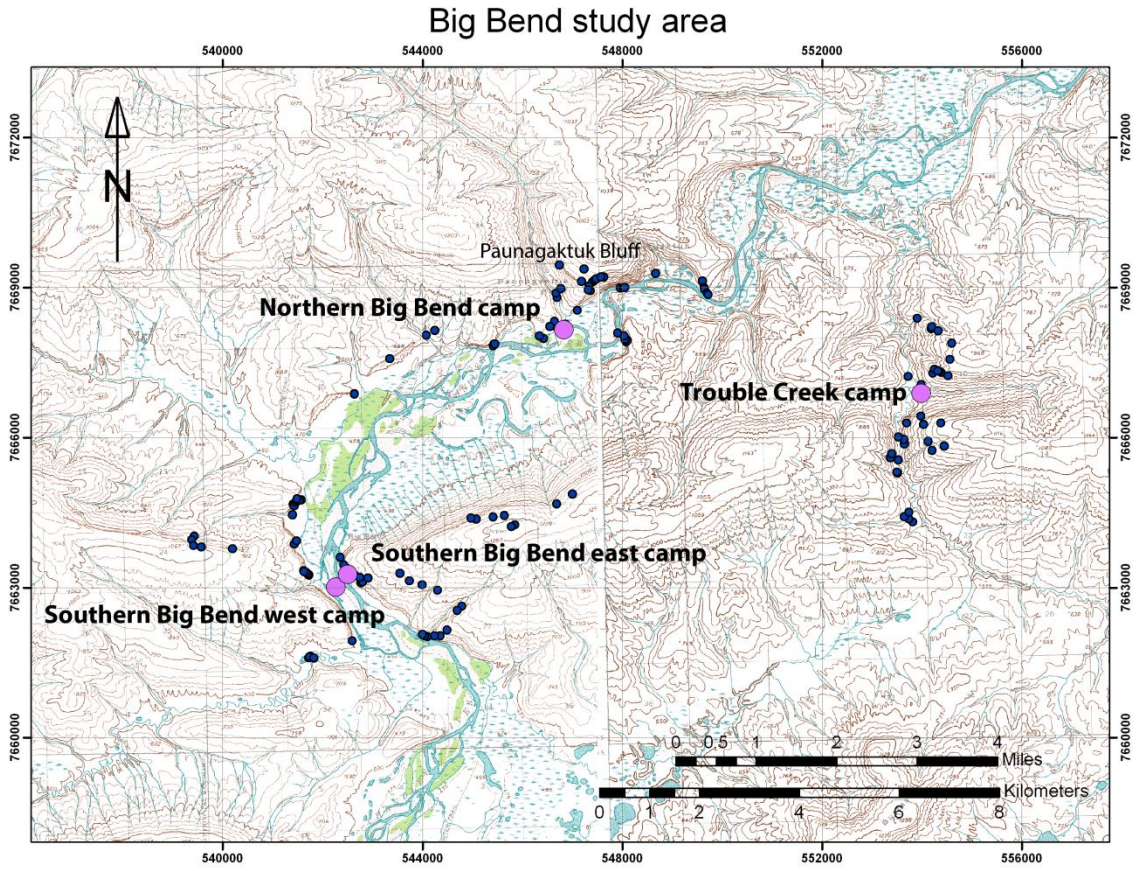

Figure 4.2 Topographic map of the study area with GPS points as small blue dots and camp sites as larger purple dots.

The actual field work and observations included locating outcrops, describing stratigraphy and structures present, taking attitude measurements where possible, collecting samples and mapping unit contacts. A GPS location, including elevation, was taken at each stop as well. I decided to create and use my own topographic maps because they would be more detailed and specific for my study area. All of the topographic maps used in the field were created from the Umiat Quadrangle at 1:250,000 scale, and the Umiat A-3 and Umiat A-4 quadrangles at 1:63,360 scale. Umiat A-3 and Umiat A-4 quadrangle maps were mapped by the U.S. Army Topographical Command. Umiat Quadrangle map was produced by the USGS. All three quadrangle maps were published for civil use by the USGS in Universal Transverse Mercator (UTM) projection and North American 1927 datum. Samples of my field maps are included in Appendix D.

The attitude measurements are compiled on stereoplots, using RockWare, to show trends in regional folding. Some attitude measurements were not included in the stereoplots because of their high uncertainty. A table of all attitude measurements is in Appendix G.

Samples were collected at many observation stops during the field research. Many of the samples were collected for comparison of variations within the stratigraphic succession of the study area and within the region. Interbeds containing organic material such as coal were also sampled for vitrinite reflectance analysis. Special care was taken to collect in-place samples of Nanushuk sandstone from the top and base of continuous bedding to be used for thermochonological analysis such as apatite U/Th-He and fission-track analysis. Timing and lack of funds did not allow completion of sample analyses during this research, but the samples may be used in future studies to better understand the depth of burial and time of unroofing.

4.3. Aerial Platform

For ease of explanation, I divided the study area into six domains. Domains were based on mapped bedding traces that were continuous and not cut by the river or suspected faults. I analyzed aerial photos of the area in order to identify features that were hard to map on foot such as bedding traces (Figure 4.3). I traced the visible bedding throughout the entire study area and interpreted the continuation of those beds based on vegetation patterns or topography (Figure 4.4).

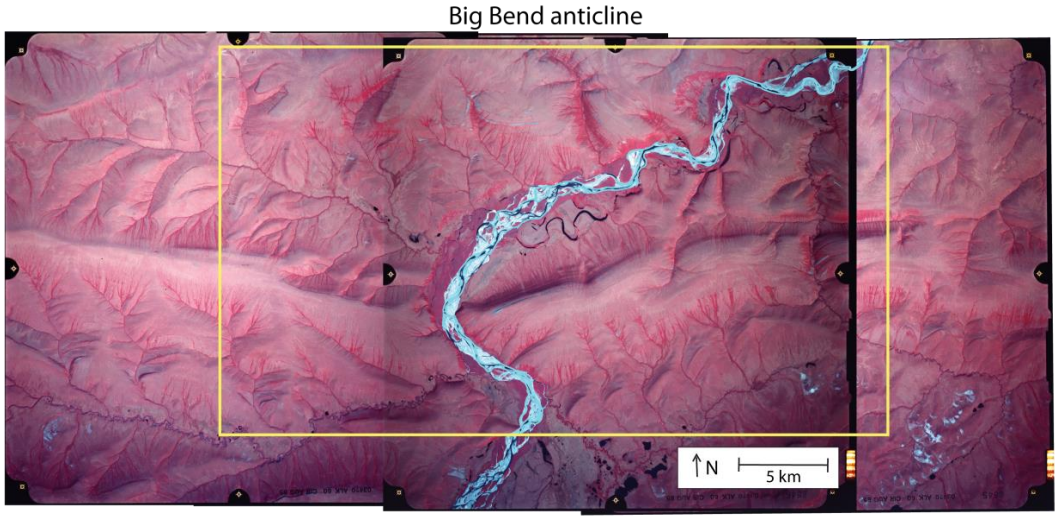

Figure 4.3 Compilation of aerial photographs used to help create geologic map. Study area outlined in yellow.

Bedding was traced on the aerial platform data and verified with the satellite data. The satellite data are discussed in more detail in Appendix A. Distinction is made on each domain map between beds that are clearly visible and those that are inferred. Visible beds were determined on air photos by color, character and shape of exposure and location and orientation relative to other beds. Inferred beds were determined by vegetation pattern, drainage pattern or rubble zones. Continuous beds in each domain are numbered with the domain letter and number increasing up section. A larger view of the domain map is included in the supplemental materials (Maps M.3).

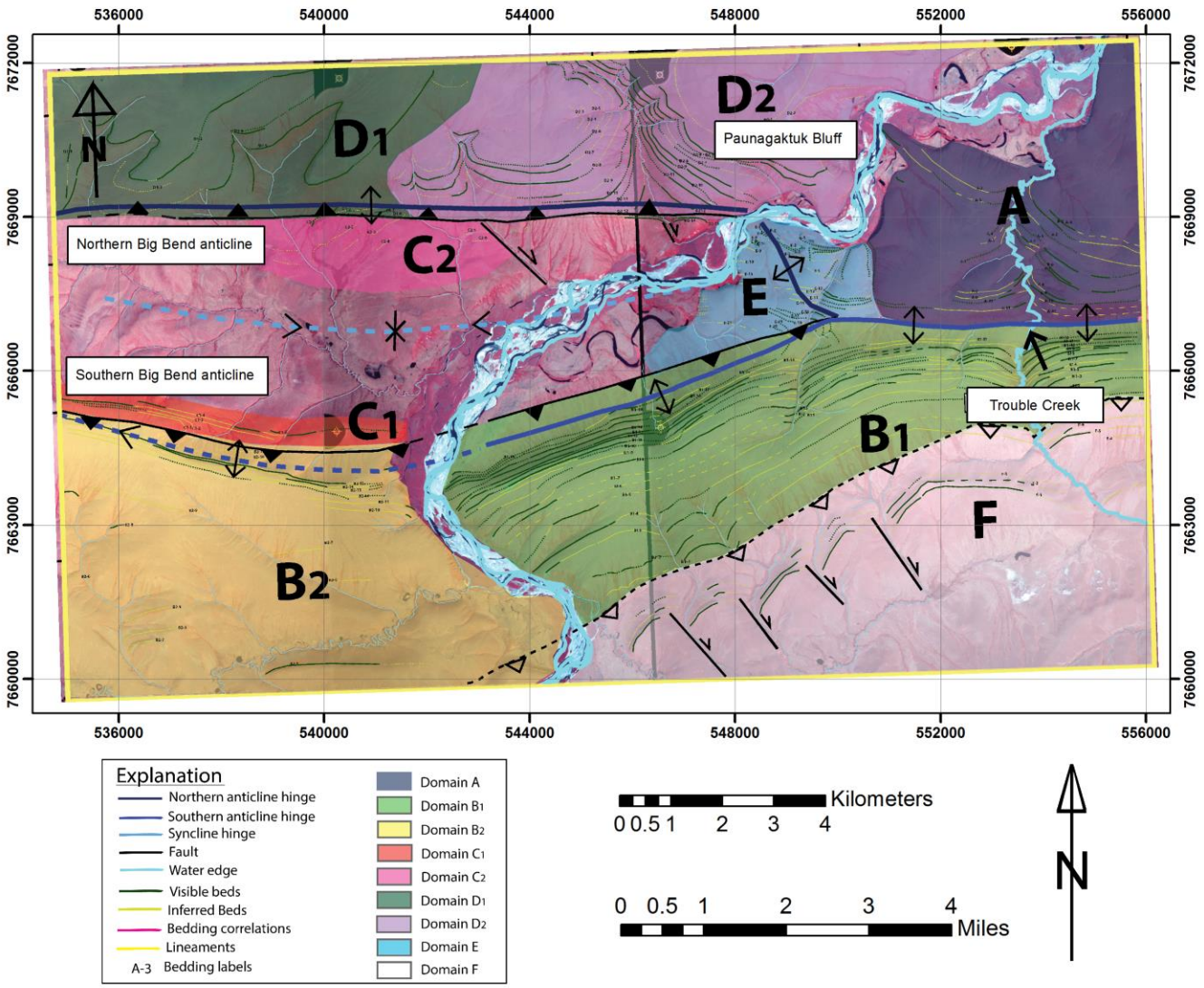

Figure 4.4 Domains used on the bedding trace map to help to identify possible correlations of beds between the southern Big Bend anticline, northern Big Bend anticline and Trouble Creek anticline.

4.4. Satellite data

The field data define the distribution of stratigraphic units and the structural geology of the study area. However, many questions remained unanswered after analysis of these data. Limited time in the field required another source of information in order to further analyze the area and more fully define its geology. Satellite data and remote sensing processing techniques allowed for additional information to be collected and analyzed. These data were then combined with analysis of field results and aerial photography to produce a final interpretation of the stratigraphic distribution and structural geology of the study area. Optical data from Landsat satellite and SAR data from ERS-1 and 2 are used to predict and confirm geologic structures and sedimentary unit boundaries. A complete description for the satellite portion of this research including all background information, methods, data, results and implications is included in Appendix A. The most relevant data will be discussed briefly in Chapter 5 Observations and Results.

4.5. Seismic reflection data

Subsurface data of the Big Bend anticline area is not publically available. However, a 3-D seismic data volume from Umiat anticline was provided by Renaissance Alaska. Umiat anticline is an analogous fold to the Bid Bend anticlines because of similarities in stratigraphy, geometry and kinematic history and is part of the same fold-and-thrust belt. Interpretations of this data were combined with surface projected cross sections of the study area in order to better understand deformation of the Torok Formation.

Chapter 5 Observations and Results

5.1. Introduction

This chapter presents the preferred geologic map of the Big Bend anticline area (Figure 5.1) in order to fully explain the observations made of the field work and remote sensing analysis used to create the geologic maps and surface projection cross sections. Content in this section is separated between Trouble Creek anticline, southern Big Bend anticline, northern Big Bend anticline and the branch zone, based on complexity and areas visited in the field (Figure 5.2). Observations were collected on a pattern of lineaments and structures associated with them. The most pertinent remote sensing data is included as this aided construction of the geologic maps. Three cross sections were created from field and remote sensing surface data using surface projection. Seismic reflection data from an analogous structure, the Umiat anticline, was used to explore the subsurface geometry of this type of fold.

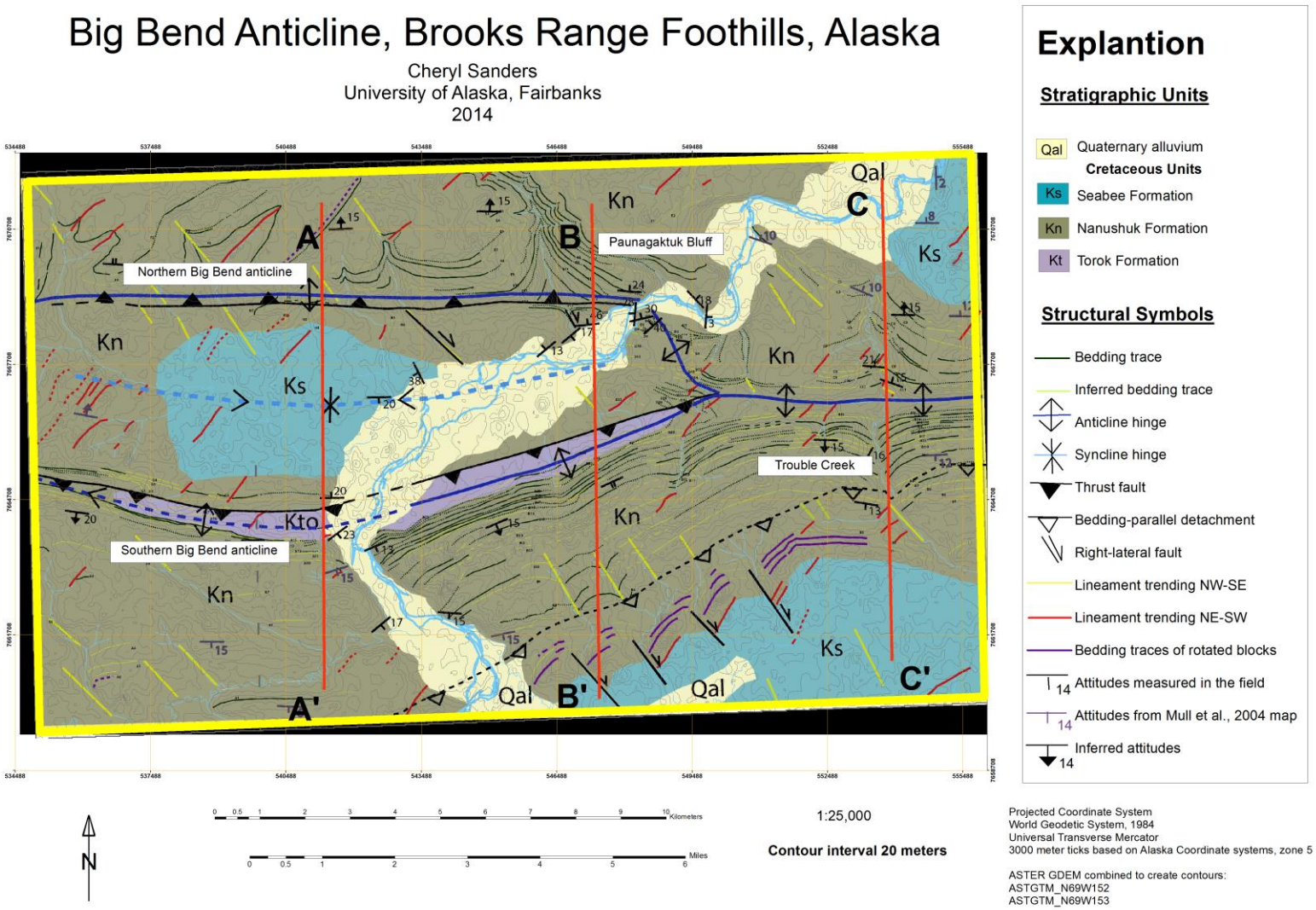

Figure 5.1 Geologic map of the study area shows the preferred interpretations of the stratigraphic contacts and structures of the Big Bend study area. All attitude measurements or interpretations that I made are represented in black. Measurements from Mull et al., (2004) are in gray.

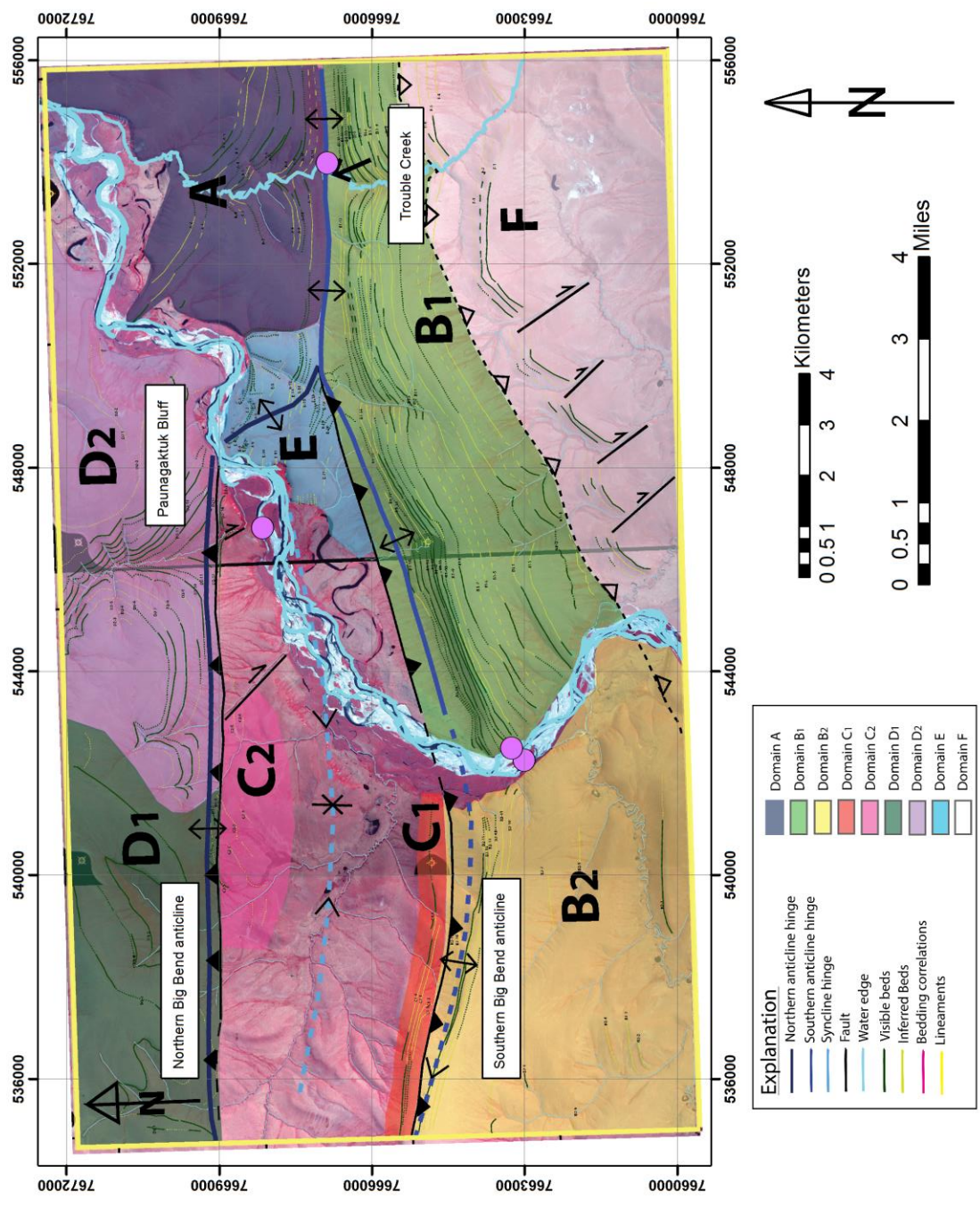

Figure 5.2 Domain map with camp locations. Domains are based on stratigraphic and structural patterns and similarities.

5.2. Trouble Creek

5.2.1. Field observations

The Trouble Creek area is included in domains A and B1. Trouble Creek crosses a single, gently folded, east-west trending anticline. The only unit observed at Trouble Creek is the Nanushuk Formation. Its stratigraphic characteristics change up section. Thin beds, 1mm to 3 cm thick, of fine to medium-grained sandstone are at the base. Cross bedding and bioturbation are abundant with some low swales and rip-up clasts present. The beds contain many fractures, but I recorded no other observations about the fractures in this area. Sandstone rubble is gravel to boulder sized. Up section toward the top of the hill, to the north and east of the Trouble Creek camp (Figure 5.2), bed thickness increases as does the resistance to erosion of the layers. Boulders the size of small cars that consist of coarse-grained sandstone are scattered throughout the hillside and along the ridge to the north. This same pattern of rock characteristics was observed all along Trouble Creek.

5.2.2. Attitude measurements

North of the campsite all the beds dip to the north at approximately 15°. South of the campsite the beds dip to the south at about 15°. I took attitude measurements at outcrops along Trouble Creek from the southern-most helicopter drop off 3.5 km south of Trouble Creek camp to at least 1 km north of the camp. I plotted these measurements on equal area stereographic projections in order to document the general pattern in the trend and plunge of the fold (Figure 5.3). The fold axis trends 98.3° and plunges 0.5° E, which is consistent with the east-west trend of anticlines in the region. The stereoplot also indicates a very low plunge to the east consistent with the field observations.

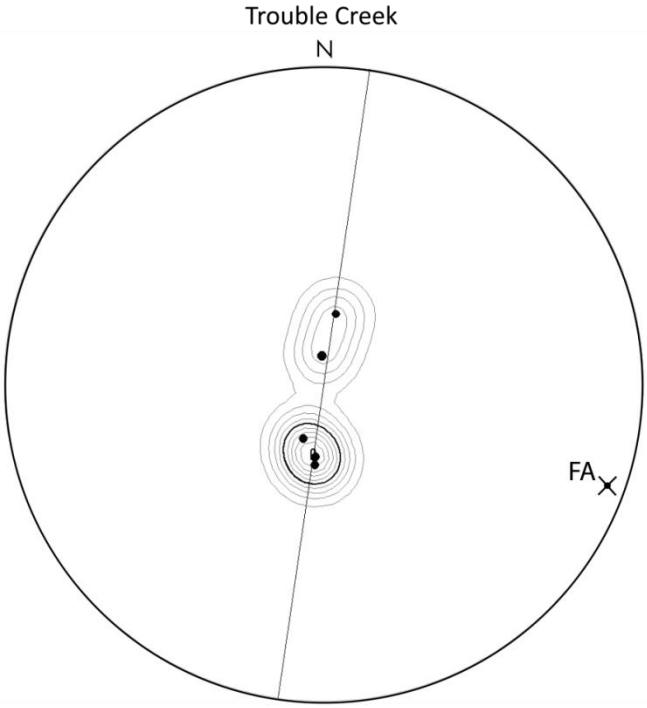

Figure 5.3 Stereographic projection of attitude measurements (poles to bedding) collected along Trouble Creek in the summer of 2010. Fold axis is labeled as FA. Fold axis trends 98.3° and plunges 0.5° E. n=5

5.2.3. Bedding traces

Using the aerial photos, of the Trouble Creek area, I was able to correlate a number of beds on the northern limb with those on the southern limb (Figure 5.4). The bedding displays V patterns in the direction of dip on either side of the hinge and appears to be evenly spaced. This helps to identify that the anticline at Trouble Creek is indeed a gentle, single anticline with little or no displacement by a hinge-parallel fault. To the west of Trouble Creek, beds on the northern limb gradually trend northwestward in the branch zone but then become parallel to the southern Big Bend anticline west of the Chandler River. I traced these beds westward in order to try to correlate between the two branching anticlines.

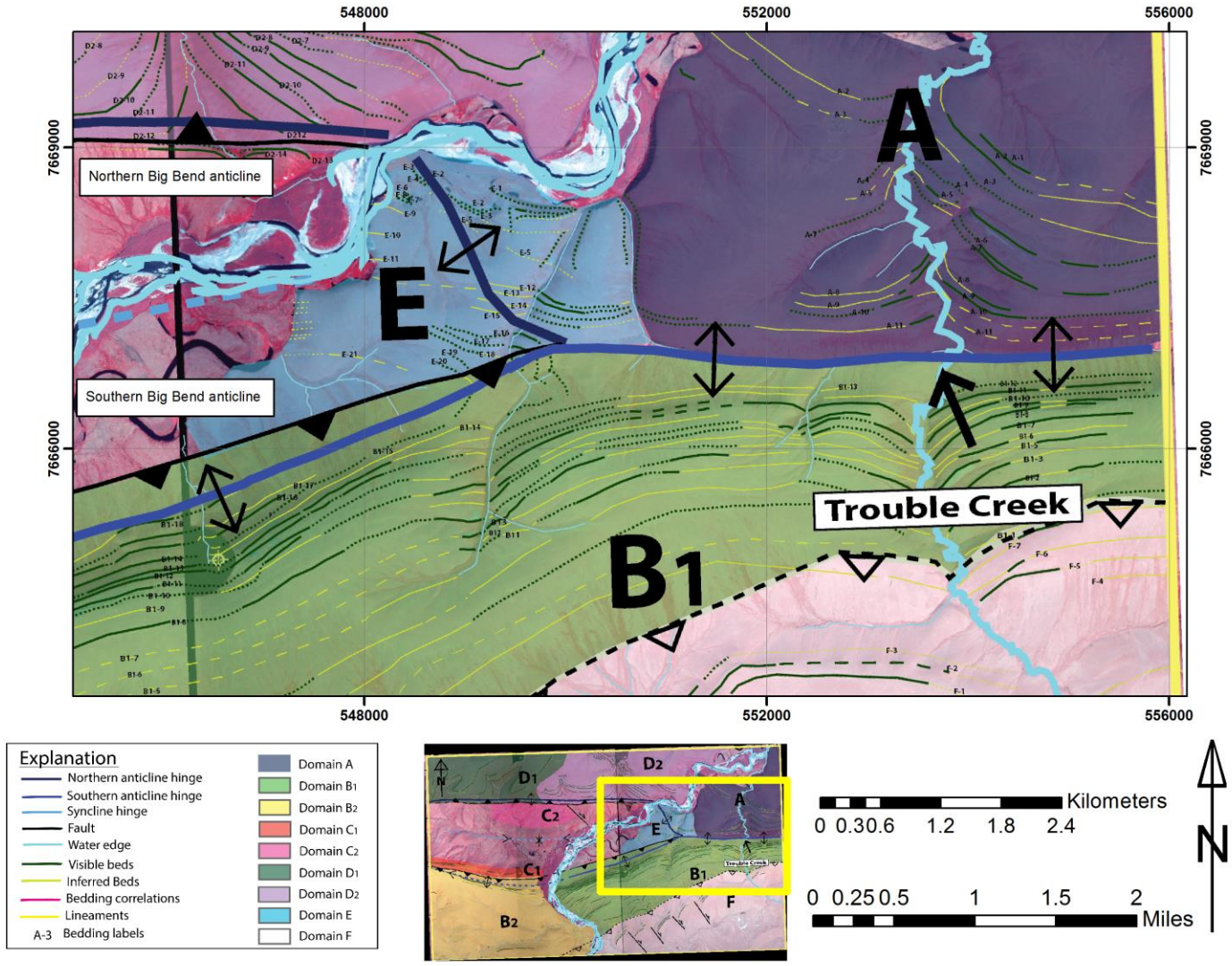

Figure 5.4 Domain map of the Trouble Creek area. Domains A and B1 show bedding traces around Trouble Creek. Beds can be correlated based on elevation and distance from the fold hinge assuming that the fold is fairly symmetrical.

5.3. Southern Big Bend anticline

5.3.1. Field observations

The southern Big Bend anticline was observed both east and west of the Chandler River (Figure 5.1). Most observations were made at outcrops along the river and near abandoned river courses. Observations were also gathered within some larger tributary drainages where outcrops were visible and in a few rare exposures along hill slopes and crests. Much of the visible bedding had collapsed down-slope and so was not useful for attitude measurements. Other areas had no visible bedding, only bedding-parallel rubble zones. In-place bedding is not common; however, I identified enough intact outcrops in order to make a reliable interpretation of the structure as a whole. Reference to locations will be made with respect to the Southern Big Bend west camp and the Southern Big Bend east camp on the banks of the Chandler River (Figure 5. 2). The southern Big Bend anticline contains domains B1, B2 and C1 (Figure 5.2).

Most of the area is underlain by Nanushuk Formation sandstone. The sandstone is usually fine to medium-grained and in 1-10 cm thick beds. Chert nodules, marcasite nodules, cross-bedding, ripples, swales and rip up clasts are visible throughout the outcrops and evidence of bioturbation is present. The beds contain many northwest-southeast and northeast-southwest striking fractures. No other observations were made of these fractures. The fracture pattern at the southern Big Bend east camp was documented as part of a Master's research by Raelene Wentz, and details are presented in her thesis (Wentz, 2014). Rubble is gravel-to-boulder-sized sandstone, with some larger boulders to the south of the camps. Most of the visible bedding is lightly iron stained due to weathering.

I was also able to map areas of very dark silt-rich mud containing sandstone and siltstone fragments on the northern slopes of the southern Big Bend anticline ridge. No visible outcrops of bedding are exposed; however, the material is definitely different and distinguishable from the Nanushuk Formation. This material was found along a tributary drainage to the west of the river, and in thawing, muddy, drainage holes east of the river (Figure 5.1). Based on its highly recessive character and the abundant silt and mud, this is the transition zone between Nanushuk Formation and Torok Formation.

The bedding dips to the south at approximately 15° and is locally well exposed in good, in-place outcrops along the river bank (Figure 5.5). Vegetation cover increases up slope and thus fewer outcrops are present.

Figure 5.5 Southern limb of the southern Big Bend anticline. View to the east of south dipping competent sandstone beds of the Nanushuk Formation. Image is a composite of two photos. Geologist for scale.

Slicken-lines, possible fault gouge, greater erosion and increased vegetation were observed west of the river and near the boundary between Nanushuk sandstone and Torok mudstone. This indicates the location of a fault, but not its direction of movement (Figure 5.1). Direct evidence for a fault was not observed east of the river because of vegetation cover and more gently sloping topography. Instead, more indirect evidence for the continuation of the fault was suggested by the thawing mud pits and the steeper topography on the north slope than the south slope of the southern Big Bend anticline ridge.

5.3.2. Attitude measurements

I combined the attitude measurements for the entire southern Big Bend anticline, excluding the anticline near Trouble Creek, and plotted them on a stereonet (Figure 5.6). These measurements were gathered in the field along the river bank and accompanying drainages. The fold axis trends 259.7° and plunges 0.8° W. Near the river, the trend of this anticline is consistent with the single Trouble Creek anticline as well as other anticlines in the region. This anticline also has very little plunge.

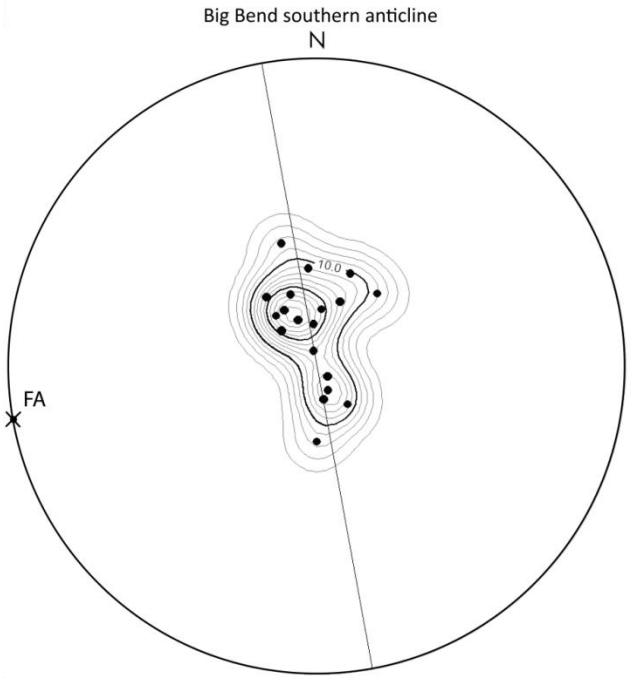

Figure 5.6 Stereographic projection of attitude measurements (poles to bedding) collected near the river from the southern Big Bend anticline in the summer of 2010. Fold axis is labeled as FA. Fold axis trends 259.7° and plunges 0.8° W. n=19

5.3.3. Bedding traces

Bedding was traced using the same method as described in section 4.1. The bed traces trend east-west and are fairly parallel to each other, consistent with other structures in the region. The bedding traces generally correspond with the topography and curve southward across the Chandler River (Figure 5.7). This pattern is likely due to erosion of south dipping beds.

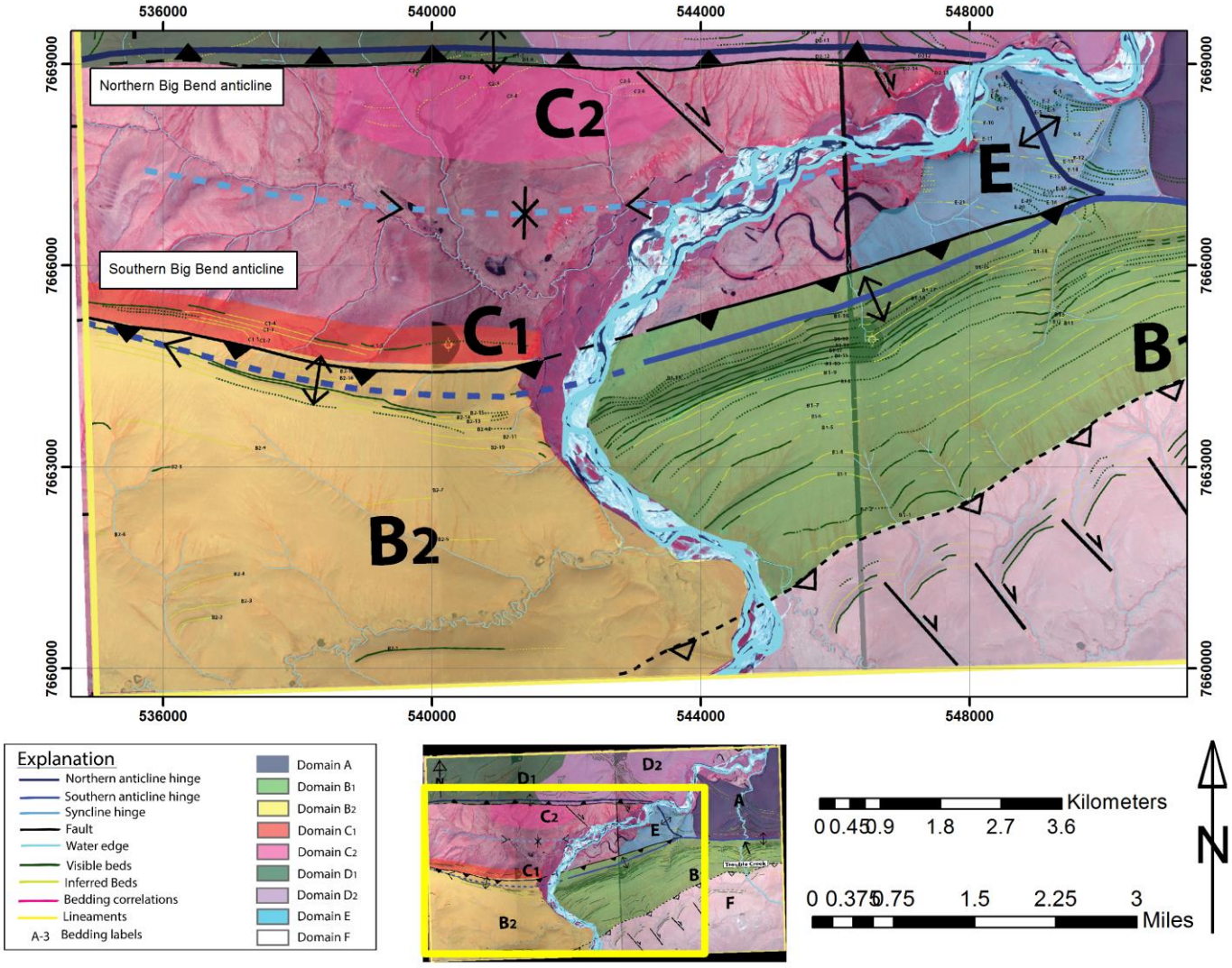

Figure 5.7 Domain map of southern Big Bend anticline. Domains B1, B2 and C1 show bedding traces along the southern Big Bend anticline. Bedding traces were projected across the river in order to correlate bedding on either side of the river.

It was impossible to correlate beds across the river in the southern Big Bend anticline with complete certainty. However, correlations could be inferred between domains B1 and B2 based on bedding orientation, location and spacing. All bedding correlations, both certain and inferred are presented in Appendix H. A few beds were traceable in the southern portion of the aerial photos, better to the east than to the west. Most of these beds could not be correlated across the river due to the large distances between traces. Bedding within domain F is similar to bedding in domain B1 in the aerial photos. However, domain F is separated from domains B1 and B2 due to differences in bedding orientation, thus bedding could not be correlated without a better knowledge of the subsurface structure. Potential scenarios for this change in bedding are discussed more fully in Chapter 6 Interpretations and Discussion.

5.4. Northern Big Bend anticline and Seabee syncline

5.4.1. Field observations

The northern Big Bend anticline was mapped from the Northern Big Bend camp on the western bank of the Chandler River (Figure 5.1). Domains D1, D2 and C1 are included in this area (Figure 5.2). Most mapping was based on outcrops along the river or within tributary drainages. We climbed to the top of Paunagaktuk Bluff (Figure 5.2) in order to map and view surrounding areas. We were also able to travel west-southwest into the syncline between the northern and southern Big Bend anticlines to find the contact between the Nanushuk Formation and the Seabee Formation. Many of the outcrops had in-place bedding, providing good attitude measurements.

The stratigraphy within the area is primarily Nanushuk Formation sandstone, with Seabee Formation within the syncline to the west-southwest (Figure 5.2). No evidence for the presence of Torok Formation was observed in and around the northern Big Bend anticline. The Nanushuk Formation was mapped from the contact with the Seabee Formation northward past the northernmost field observation point to the edge of the study area. At the base of Paunagaktuk Bluff the Nanushuk Formation contains sandstone with sub-rounded grains and 2-3 cm thick beds. Rip up clasts, ripple marks, concretions, bioturbation, thinly bedded coalified layers, cross bedding and convoluted folds caused by currents are all visible within the outcrops. Rubble zones contain large boulders the size of a small adult person. Rubble decreases to gravel size up

section toward the tops of the bluff. Rubble zones were observed on the top of Paunagaktuk Bluff that contain rounded pebbles and conglomerate. This was the only place in the study area where conglomerate was observed. The Nanushuk Formation does contain conglomerate layers near its stratigraphical top (Mull, 1985; Mull et al., 2003).

Seabee Formation was visible in poor outcrops on the ridge above the river, exposed beneath late snow melt, in the low lying area west of the river between the two Big Bend anticlines. Outcrops consist mainly of bentonitic clay with bedding defined locally by layers of very fine mudstone. Interbeds of sandstone contain more matrix than the Nanushuk sandstones. These Seabee sandstone beds contain broken and iron oxidized chert clasts and some coal fragments. Most of the outcrops of Seabee Formation were too disrupted and weathered to obtain reliable attitude measurements but, the general dip of the beds and topography were consistent with their inferred location on the north limb of a gentle syncline.

Evidence for a significant east-west striking fault was observed north of this camp in the form of apparent discordance in bedding traces and corresponding changes in topography and vegetation cover. An area midway up the south-facing slope of the bluff flattens out topographically and contains low grasses such as cotton grass. This was not consistent with the rest of the slope or any other area that was mapped. This flattened area can be traced along the slope of the bluffs to the west visually in the field and on topographic maps and aerial photos. Displacement and slip direction could not be determined with field data alone.

5.4.2. Attitude measurements

Bedding in the Nanushuk Formation within the Paunagaktuk Bluff has a very gentle dip of about 5°N that increases slightly northward to 15° N. South-dipping beds were observed south of the main east-west striking fault, which is consistent with the syncline inferred between the two Big Bend anticlines. Attitude measurements collected on and around the bluff were compiled in a single stereonet (Figure 5.8) and indicate a fold axis with a trend of 87.1° and plunge of 1.0° E. These data include measurements from both north and south of the fault, but fewer measurements were possible near the hinge of the anticline. This may reflect poor exposure near the fault and its proximity to the hinge of the anticline.

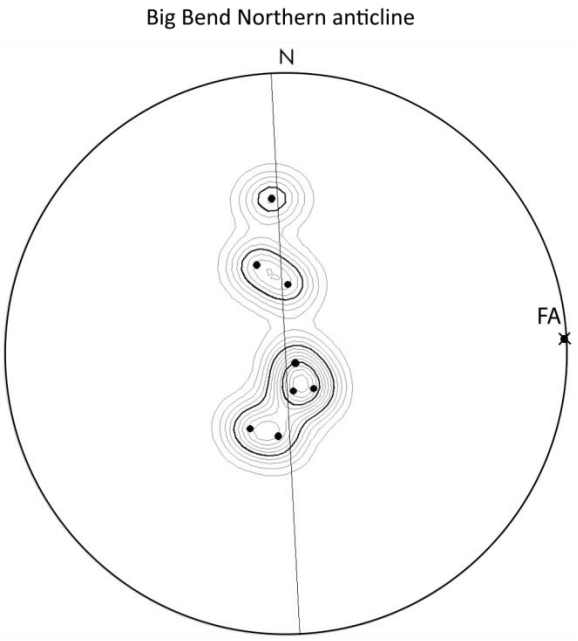

Figure 5.8 Stereographic projections of attitude measurements (poles to bedding) collected from the northern Big Bend anticline in the summer of 2010. Fold axis is labeled as FA. Fold axis trends 87.1° and plunges 1.0° E. n=8

5.4.3. Bedding traces

Bedding was traced using the same method as described in section 4.1. The overall pattern in the area was similar to the southern Big Bend anticline with parallel east-west trending bedding traces (Figure 5.2). Discontinuous exposure across large drainages limited the traceability of the bedding. However, these drainages are helpful in determining bedding dip direction. The bedding in this area was not as consistent and continuous as in the southern Big Bend anticline area. Thus, the bedding north of the fault was grouped into two different domains based on differences in bedding dip and direction.

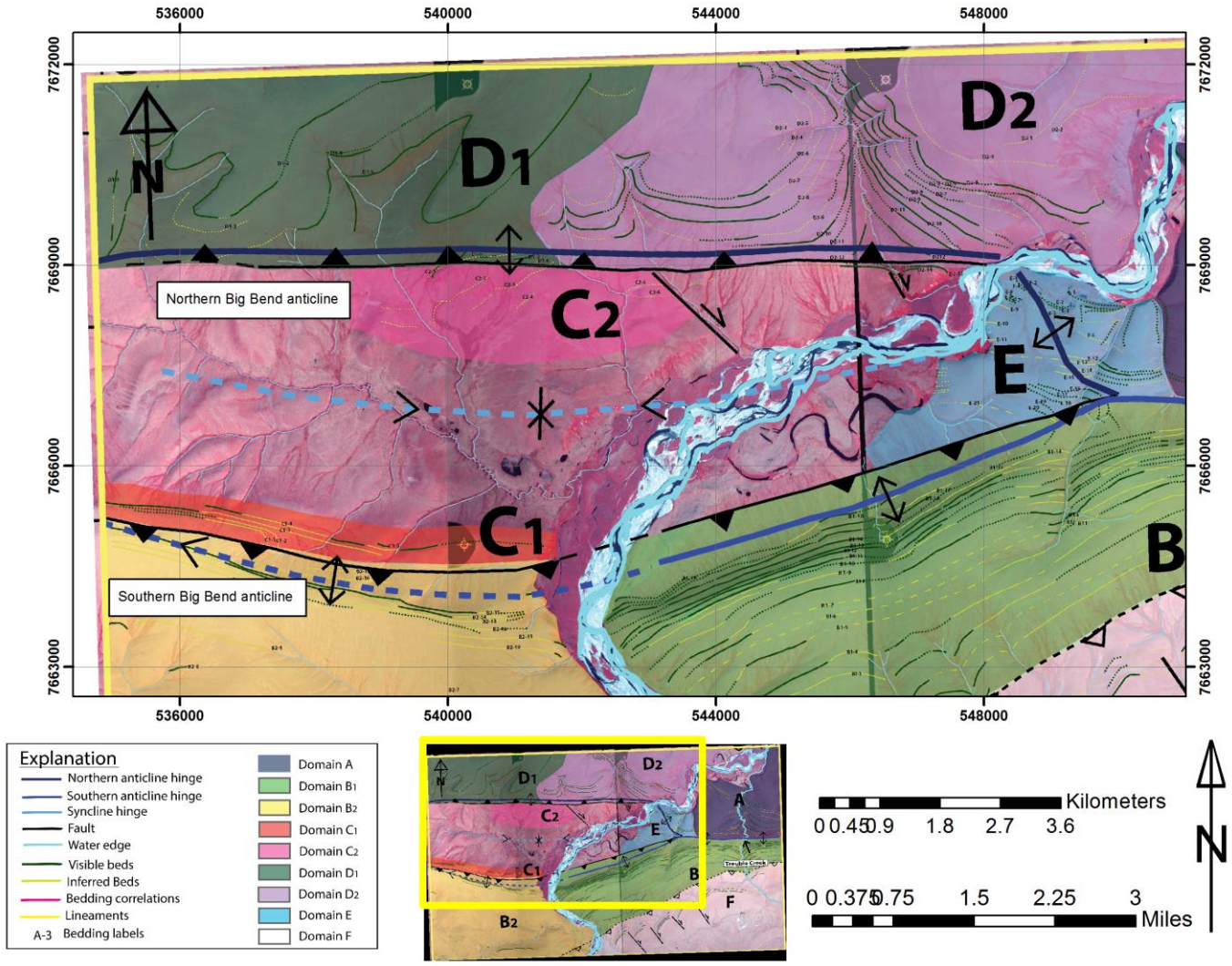

Figure 5.9 Domain map of northern Big Bend anticline. Bedding traces for the northern Big Bend anticline include domains D1, D2 and C2. These traces help to define the structural character of the northern Big Bend anticline and the fault that cuts through it. No correlation of bedding was possible between any of these domains.

Westward, domain D1 exhibits a bedding pattern that suggests a gentle dip to the northwest, implying a change in hinge direction or plunge. We were not able to visit this area on foot, hence all observations are based on aerial photo analysis. Very few beds are visible at the surface and they are widely spaced and follow topography, reflecting the gentle dip and subdued topography. Domain D2, to the east of domain D1, exhibits a bedding pattern that suggests the bedding dips to the north. Numerous, continuous beds are visible. Beds are closer together than in domain D1 and parallel, reflecting their exposure on steep slopes. No evidence of Torok exposure was observed in the field or by air photos as suggested by Mull et al. (2004). Direct correlation between bedding in domains D1 and D2 was not possible from aerial photographs. Observations in the field suggest that beds within domain D1 are a continuation up section of the beds in domain D2. Domain C2 is south of the fault. The beds in domain C2 are few and far between and are mostly inferred based on vegetation patterns. These beds are less visible than up slope in domains D1 and D2 due to gentle slope gradient and poor exposure. Correlation between beds across the fault also was not possible.

5.5. Branch zone

5.5.1. Field observations

Domain E is the branch zone, where the single anticline to the east branches into two to the west (Figure 5.1). This area was visited briefly by helicopter and was viewed from other vantage points in the mapped area, but it was not possible to explore this area thoroughly on the ground because of limited time and access. The area that was visited by helicopter is immediately across the river to the east from the northern Big Bend camp (Figure 5.1).

The bedding at this location dips in a different direction and angle from the bedding within the bluffs across the river to the west. The bedding within the bluffs west of the river dips 15° N-NW, but bedding east of the river dips approximately 30° W-NW. Bedding attitude east of the river also varies within the immediate area, with dip increasing up section by 10°. The outcrop visited appeared to be in-place and allowed for many attitude measurements. Stratigraphy in the area is Nanushuk sandstone, similar to the rock west of the river. The sandstone includes large, partially coalified wood fragments, concretions, rip-ups, fine cross bedding, rippling, and cross laminations. Lineations and gouges in the rocks measure 5+

centimeters and suggest fault movement. These appear to be on bed surfaces but determination of exact orientation is not possible due to slumping beds. However, there was no other evidence of a fault. Displacement visible along fractures seemed to be more prevalent than in other areas within the study. The fracture pattern in the branch zone was summarized in the Master's thesis by Raelene Wentz (Wentz, 2014).

5.5.2. Attitude measurements

Attitude measurements were collected during the brief helicopter reconnaissance stop, across the river to the east of the northern Big Bend camp (Figure 5.2), and plotted on the same stereonet as the measurements taken from the northern Big Bend anticline for comparison (Figure 5.10). Measurements were taken at the base of the hill and at intervals up to the top of the outcrop. The attitudes from the branch zone do not appear to follow the same pattern as the northern anticline. This suggests that the structure at the branch zone is different than the northern anticline, which is consistent with field observations.

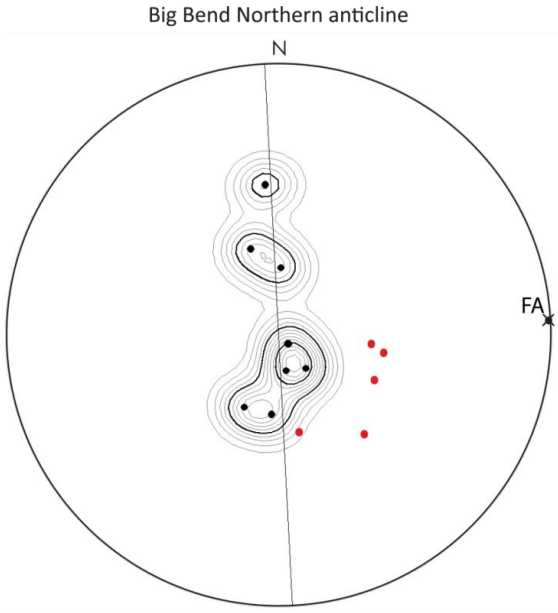

Figure 5.10 Stereographic projection of attitude measurements (poles to bedding) collected from the northern Big Bend anticline (black, n=8) and the branch zone (red, n=5) in the summer of 2010. Fold axis for the northern Big Bend anticline is labeled FA. The branch zone measurements differ from the northern anticline and indicate a change in structure.

5.5.3. Bedding traces

Bedding in the branch zone (domain E) was traced using the same method as described in Chapter 4.1. In the southeastern corner of domain E bedding near the southern Big Bend anticline is easily visible on the aerial photos and has similar characteristics to bedding in domains A and B1 (Figure 5.11). This bedding is parallel, closely spaced, and dips northward. The bedding in the northern part of domain E in the branch zone is not as clear. This bedding is hard to recognize and apparent bedding traces vary abruptly and inconsistently in orientation. This most likely is due to low dip and increased structural complexity. Rough correlations could be made between bedding in the branch zone with domain A and the single anticline at Trouble Creek. Correlations could not be made between bedding in the branch zone and bedding in domain B1.

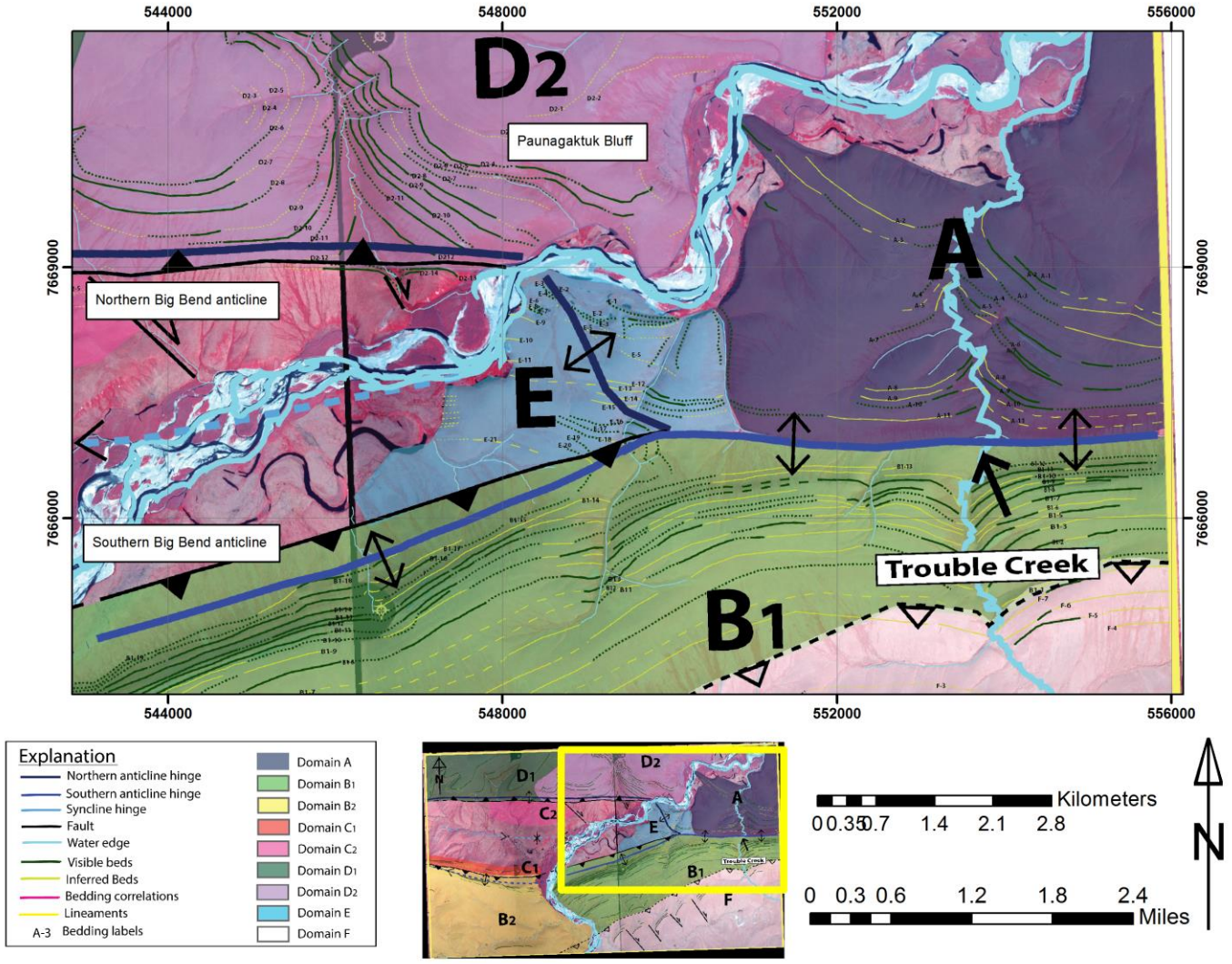

Figure 5.11 Bedding traces in the branch zone, domain E. Bedding is similar to and can be roughly correlated between the southeastern corner of domain E and adjacent bedding in domains A and B1. Bedding cannot be correlated between domains E and D2 due to inconsistencies with bedding characteristics.

5.6. Lineaments

5.6.1. Field Observations

While mapping in the field, I noticed a lineament pattern defined by drainages, with two sets trending northeast and northwest (Figure 5.12). The lineaments show the same trends as the fractures in the area documented by Wentz (2014) (Figure 5.13). The data provided by Wentz (2014) shows the angle between the two fracture sets to be approximately 90°. This is similar to the trend of lineaments observed in the study area.

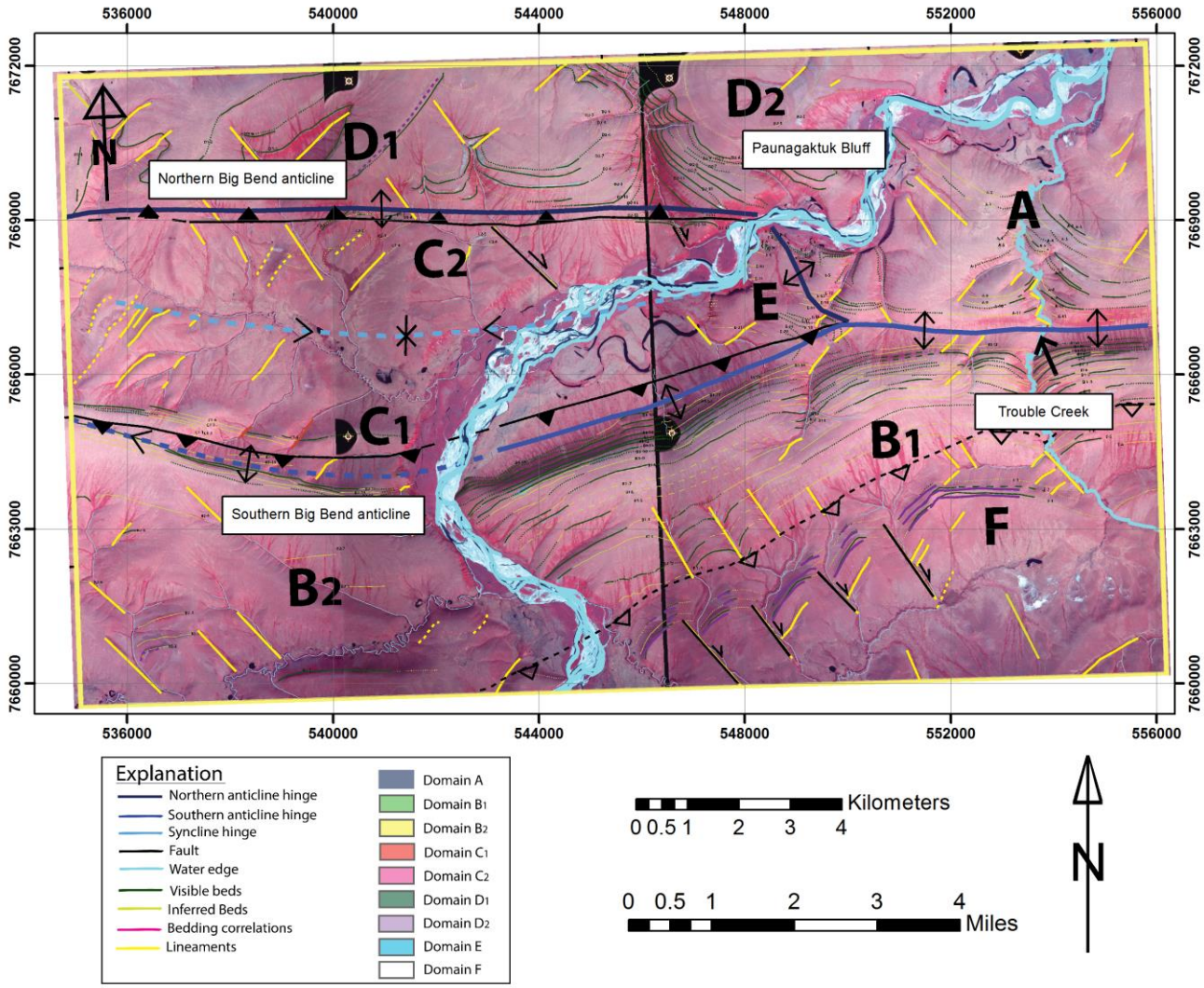

Figure 5.12 Aerial photographs overlain with lineament pattern. Conjugate faults strike northwest-southeast and northeast-southwest. Bedding traced in purple in domain F do not follow trends of other bedding traces in the study area.

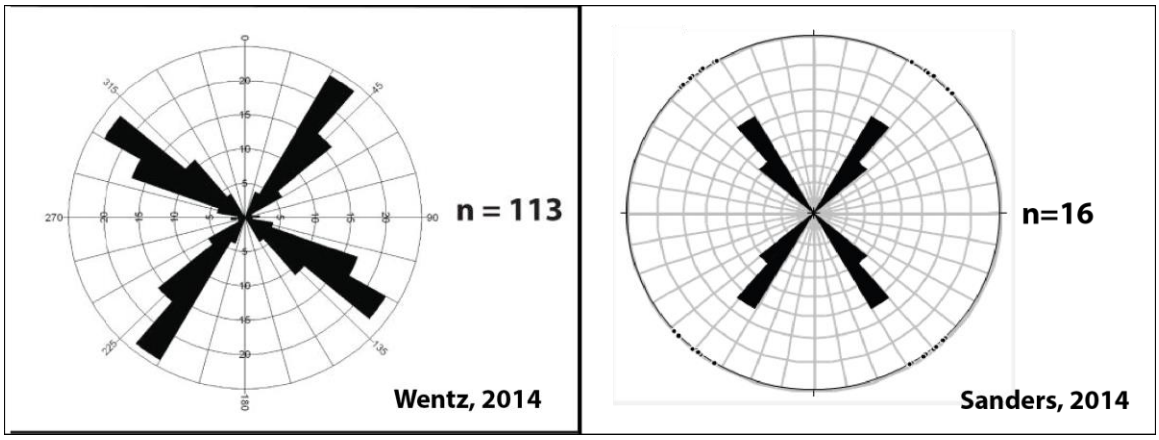

Figure 5.13 Rose diagrams of the southern Big Bend anticline from Wentz (2014) and lineament pattern of the study area as observed in the field and from remote sensing data. Rose diagram of the study area was created on the software Stereonet 7.3.5. This software is produced and maintained by Rick W. Allmendinger (2012).

The most conspicuous set of these structures is in the southeastern part of the area, where bedding appears rotated counterclockwise between faults in a set of north-northwest striking right-lateral faults. The current published interpretation is that they are normal faults (Mull et al., 2004).

This similarity in orientation between fractures and lineaments could be interpreted as indicating that the lineament pattern and the fracture pattern as being genetically related. One possibility is that the lineaments are not normal faults, but are actually strike-slip faults that are related to the local fracture pattern.

5.7. Detachment zone in the southeast corner of the study area

Mull et al. (2004) originally identified a series of normal fault bound blocks in the southeast corner of the study area south of a potential thrust fault. Time in the field did not permit travel to this area however; bedding is clearly defined in the aerial photos (Figure 5.14). The interpreted detachment location was originally mapped on the aerial photographs due to vegetation patterns, and was then further corroborated with the Mull et al. (2004) map and the remote sensing data, as discussed later in this chapter in Remote Sensing (section 5.9). Linear drainages denote the location of the lineaments. At least three blocks are bounded by lineaments and the eastern-most

block has a lineament on its west boundary and appears to have folded but continuous bedding to the east. Within each other block, bedding appears folded near the eastern lineation. Bedding traces in the area show beds that are offset approximately 45° counter clock-wise of horizontal, this is not consistent with other bedding in the study area. These were the only lineament bound blocks, with visible bedding, identified within the study area. Due to the shape and characteristics of the bedding traces, two interpretations of the prevailing structure are possible. The first interpretation is consistent with Mull et al. (2004) and defines the area with normal faults. The curved bedding is a product of erosion on shallow dipping, erosion resistant bedding. An alternative interpretation defines these blocks to be rotated counter clockwise between right-lateral, strike-slip faults above a decollement. The curve in bedding could be interpreted as folding due to block rotation. These were the only structures in the study area with this bedding and lineament pattern. However, I suspect similar structures may be present but not yet identified in the region.

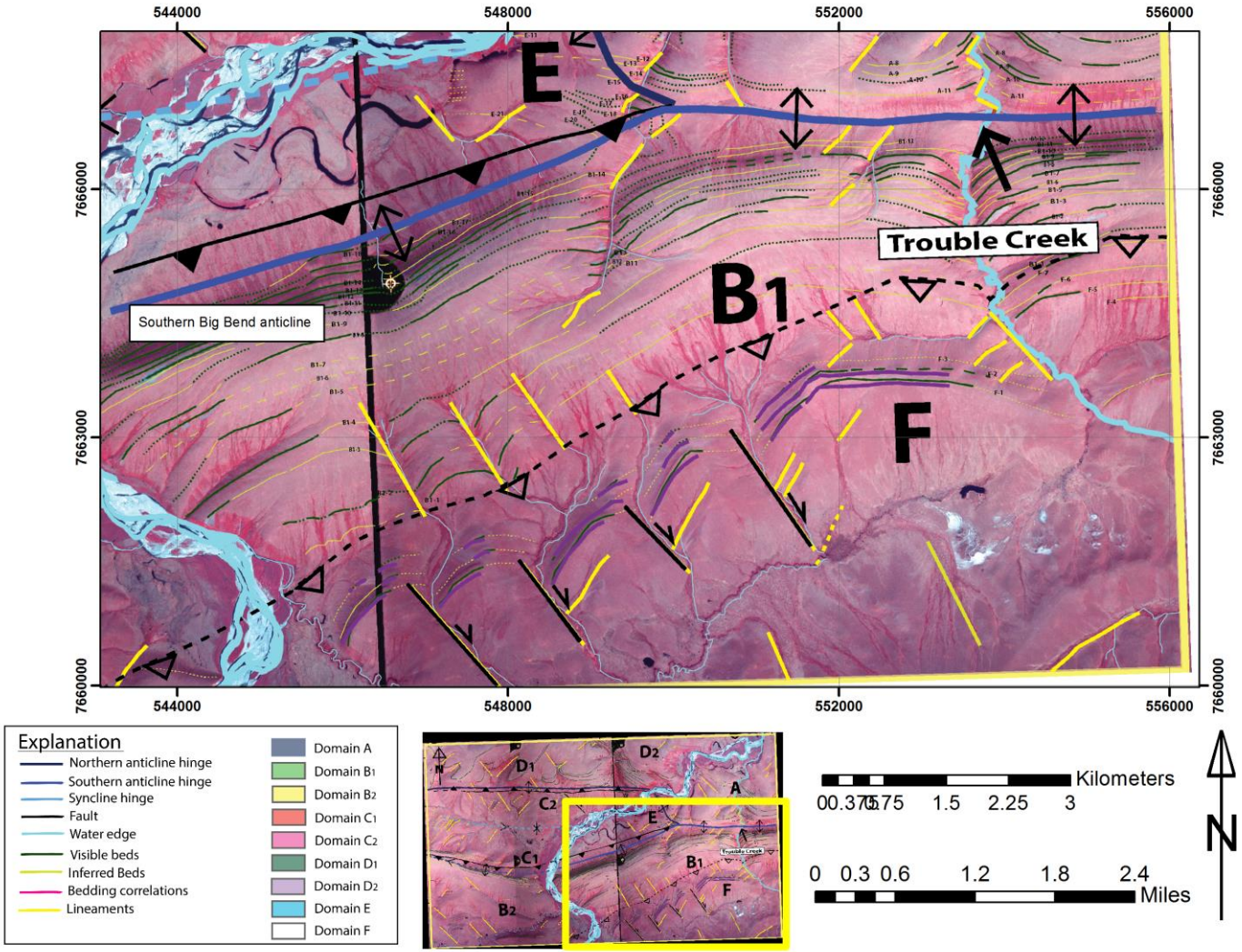

Figure 5.14 Bedding traces of lineament bound blocks and potential detachment zone in the southeastern section of the study area. Location of detachment zone is inferred based on published maps by Mull et al., (2004) and remote sensing data discussed further in Appendix A.

5.8. Atypical anticline

An anticline that is atypical for the area in size and trend was observed in the southwestern part of the study area (domain B2). The gently folded anticline is approximately 15 meters long, 5 meters wide and 2 meters tall (Figure 5.15). The fold is in the Nanushuk Formation with fine-grained sandstone and fist sized or smaller concretions. It trends northeast 55° and plunges 6° east (Figure 4.15). The trend of this anticline has the same orientation as the bedding in the right-lateral, strike-slip fault bound blocks in domain F. The stereographic projection of the attitudes measured on the atypical anticline confirms that its trend is consistent with the orientation of bedding rotated between northwest-striking faults (Figure 5.15). Because of its size, trend and location, I have interpreted this smaller anticline to be related to the deformation that resulted in the lineament bound blocks in the southeastern part of the study area, domain F.

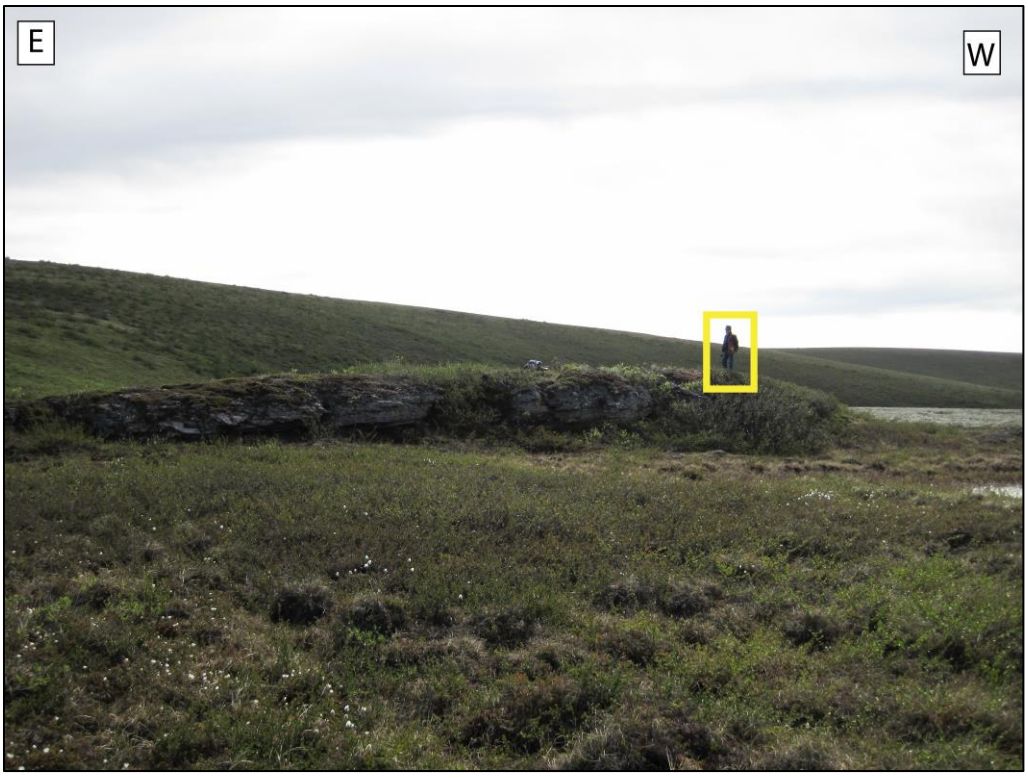

Figure 5.15 Atypical anticline in Nanushuk Formation in the southwestern corner of the study area, south of southern Big Bend anticline west of the river. Anticline is relatively small, approximately 15 meters long, compared to other folds in the area and has a trend of 55° northeast. This trend is not consistent with other folds in the area but is similar to the lineament pattern in the study area. View to the southwest. Geologist for scale.

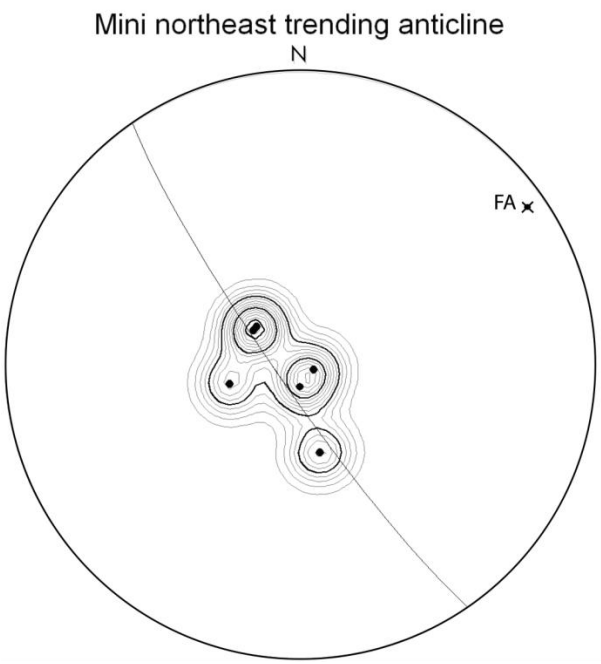

Figure 5.16 Stereographic projection of attitude measurements (poles to bedding) collected from atypical small anticline in the southwest portion of the study area. Fold axis is labeled FA. The fold axis trends 55.3° northeast, plunges 6.3° east and is similar in trend with the orientation of bedding between northwest-striking faults. n=6

5.9. Satellite Data

Satellite data analysis was used to gather more information about the study area. Due to limited amounts of time and access in the field, remote sensing data proved very helpful for planning field work as well as expanding and verifying observations made in the field. Appendix A, contains background information, methods, data, results and interpretations of all satellite data. Only two of the images processed, that are the most crucial to the results, will be discussed in this chapter.

5.9.1. Landsat 5 Thematic Mapper (TM)

Optical data, such as those acquired by Landsat, are often used for surficial geologic mapping. A Landsat 5 TM image was processed to generate a vegetation index as vegetation can signal a change in soil moisture, soil availability or nutrient content. This vegetation index

(Figure 5.17) shows differences in vegetation in potential fault locations. Increases in vegetation in a linear pattern, following fault traces, can be observed in the south limb of the northern Big Bend anticline, the north limb of the southern Big Bend anticline and north of the lineament bound blocks in the southeast corner of the study area.

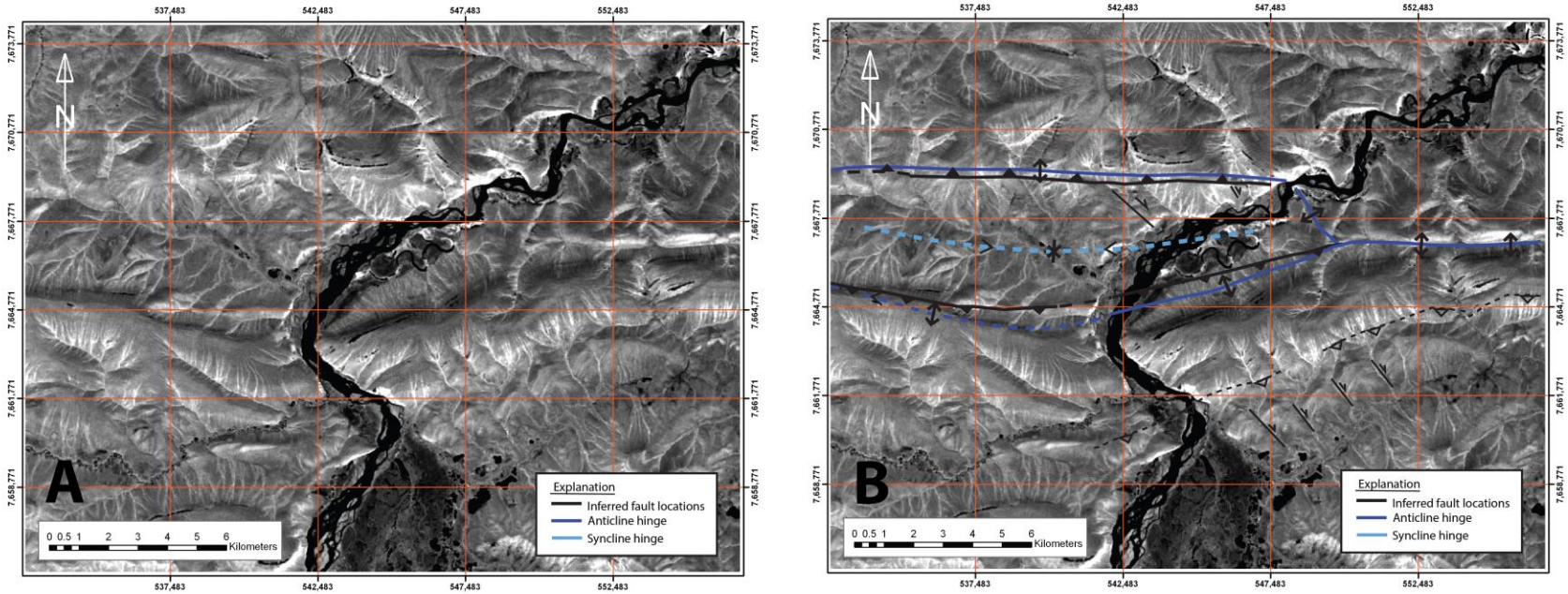

Figure 5.17 Vegetation index of Landsat 5 TM. Uninterpreted (A) and interpreted (B). Variations in vegetation density help to identify differences in erosion due to underlying lithology, soil moisture content and nutrient content. Linear patterns can indicate fault traces.

5.9.2. Synthetic Aperture Radar (SAR)

Advanced Land Observation System's Phased Array L-Band Synthetic Aperture Radar (ALOS PALSAR) data combined with European Remote Sensing (ERS-2) satellite data is helpful in observing fault traces that may not be visible on the surface as PALSAR data has the potential to penetrate the groundcover and the first few inches of soil. In this image (Figure 5.87), a dark lineament associated with the backthrust in the south limb of the northern Big Bend anticline is seen continuing through the branch zone and toward Trouble Creek. No evidence was found in the field or with aerial photos that this fault continued this far east.

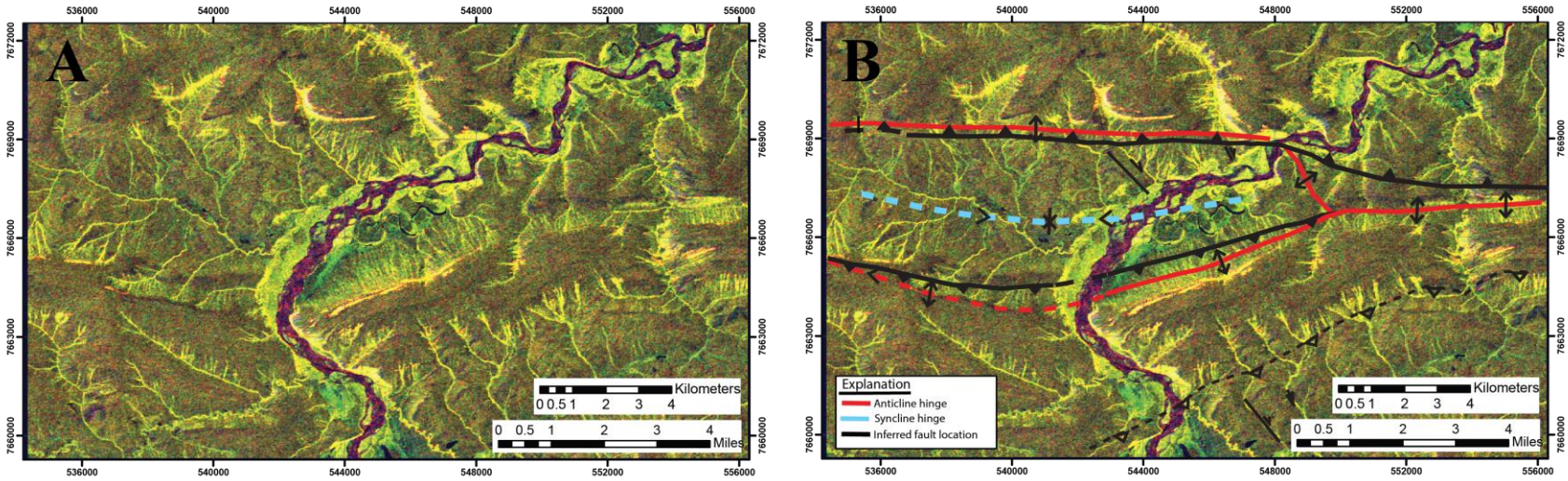

Figure 5.18 Combined PALSAR and ERS-2 data in an FCC composed of HV polarized bands from two different date PALSAR and one ERS-2 image. Uninterpreted (A) and interpreted (B). Clear, moving water is green. Gravel and eroded areas are light with some magenta. Green is resistant rock. The thrust faults are seen here as darker lineaments. Some bedding traces are also dark but are not as laterally continuous or dark as the interpreted faults.

5.10. Summary of field, air photo and remote sensing observations

When the map information from each domain is combined, the general structural pattern within the area becomes apparent (Figure 5.19). Seabee Formation is present between the north and south Big Bend anticlines, indicating the location of a syncline. Nanushuk Formation is present throughout the rest of the study area with exposures of Torok Formation only along the northern slope of the southern Big Bend anticline. Beds could be reliably correlated between the northern and southern limbs of the Trouble Creek anticline and along the southern Big Bend anticline. Correlations in bedding could not be made between the northern and southern Big Bend anticlines due to discontinuities in visible bedding and offset across faults.

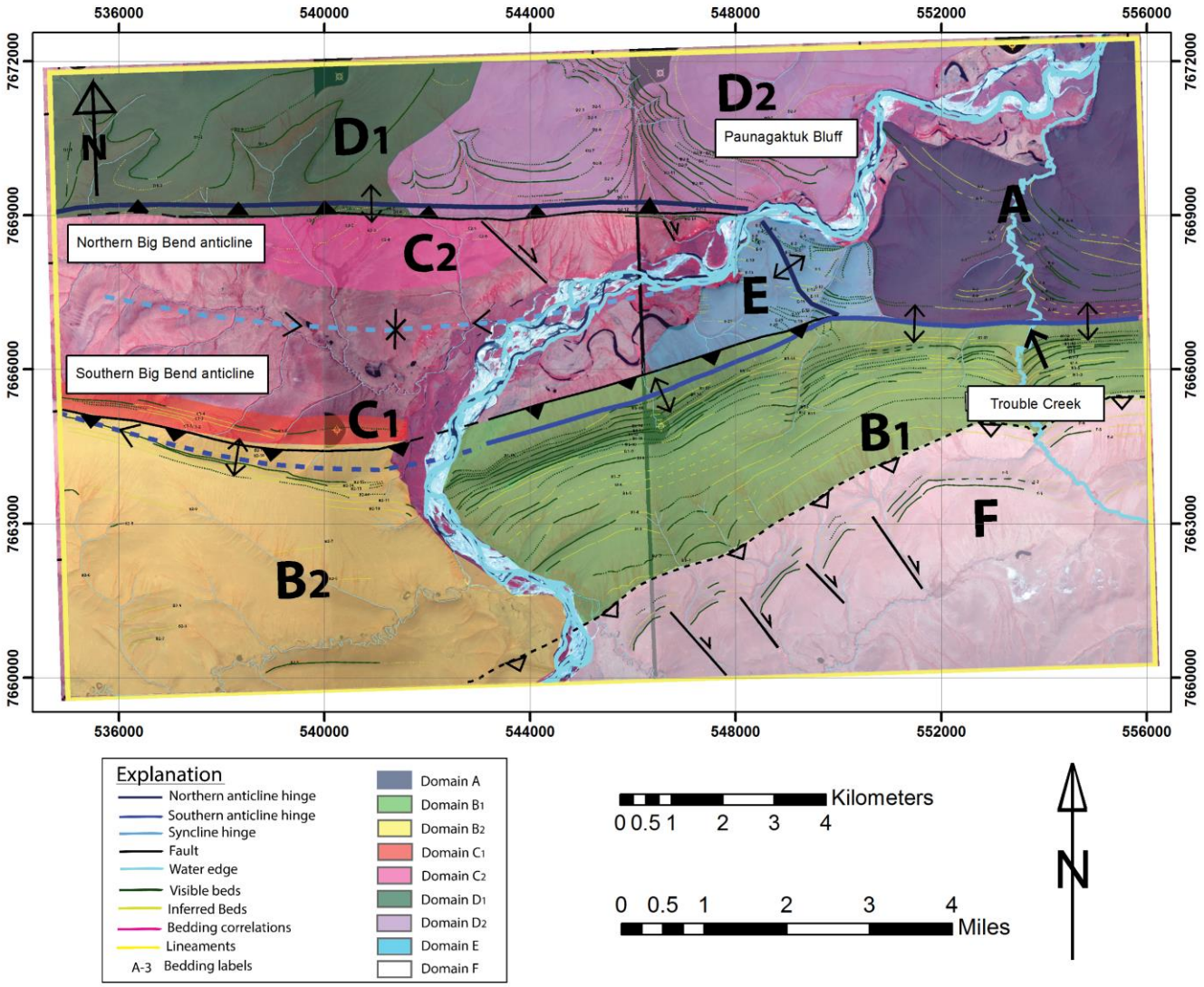

Figure 5.19 Bedding traces and domains of the study area and preferred structural interpretation.

The single anticline that is present at Trouble Creek branches into two separate anticlines to the west. Evidence for major east-west striking faults is present in the southern limb of the northern Big Bend anticline and in the northern limb of the southern Big Bend anticline. Strike-slip faults are present, observed in the field in the southern limb of the northern Big Bend anticline and interpreted in air photos of the lineament bound blocks in domain F in the southeast corner of the study area. The strike-slip faults are parallel to the dominant fracture sets of the area. Bedding traces indicate that the anticlines trend east-west except in the branch zone. A compilation of all the attitude measurements from the Trouble Creek, southern Big Bend and northern Big Bend anticlines confirms that the anticlines trend east-west and were likely formed at the same time and due to the same deformation processes (Figure 5.20).

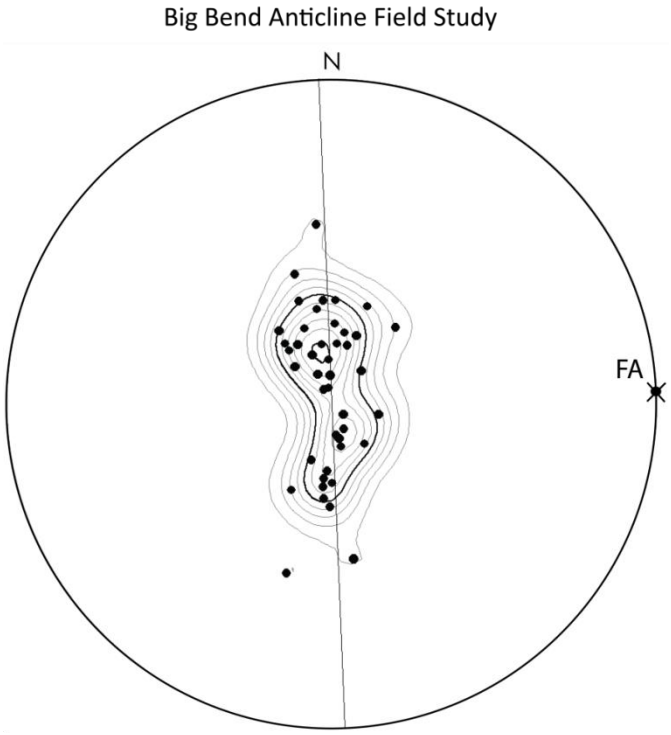

Figure 5.20 Stereographic projection of combined attitude measurements (poles to bedding) collected from the northern and southern Big Bend and Trouble Creek anticlines in the summer of 2010. Fold axis is labeled as FA. The fold axis trends 86.9°, and plunges 0.8° E. n=44

5.10.1. Construction of cross sections

Three north-to-south cross sections were constructed (Figure 5.21). The cross sections were oriented this way because most structures in the region trend east to west, indicating north-south contraction. Hence, a north-south cross section will show true stratigraphic thickness and structural geometry which can be used to determine the amount of shortening. Unit thicknesses are based on data from the Seabee, Big Bend and Grandstand wells (Figure 5.22) (Nelson et al., 2005). A table of unit thicknesses from these wells, acquired from Alaska Geologic Materials Center Data Report No. 284, is included in Appendix I. Topographic profiles used in the cross sections were obtained from the ASTER GDEM data in order to reflect the most recent and accurate topographic information.

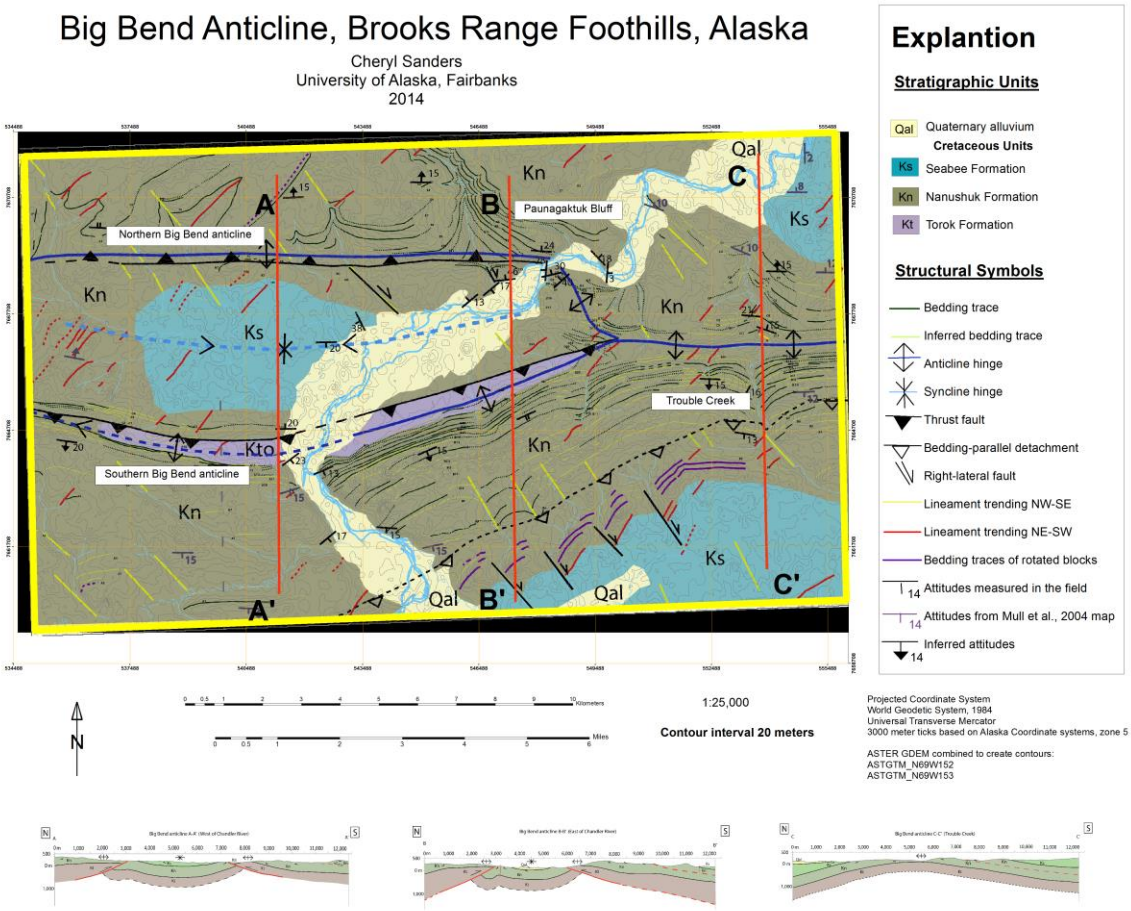

Figure 5.21 Map of the study area with cross section locations. Cross section A-A' crosses the two branches of the Big Bend anticline and the thrust faults that cut through them. Cross section B-B' crosses both anticlines at the center of the study area on the east side of the Chandler River. Cross section C-C' crosses the single anticline at Trouble Creek.

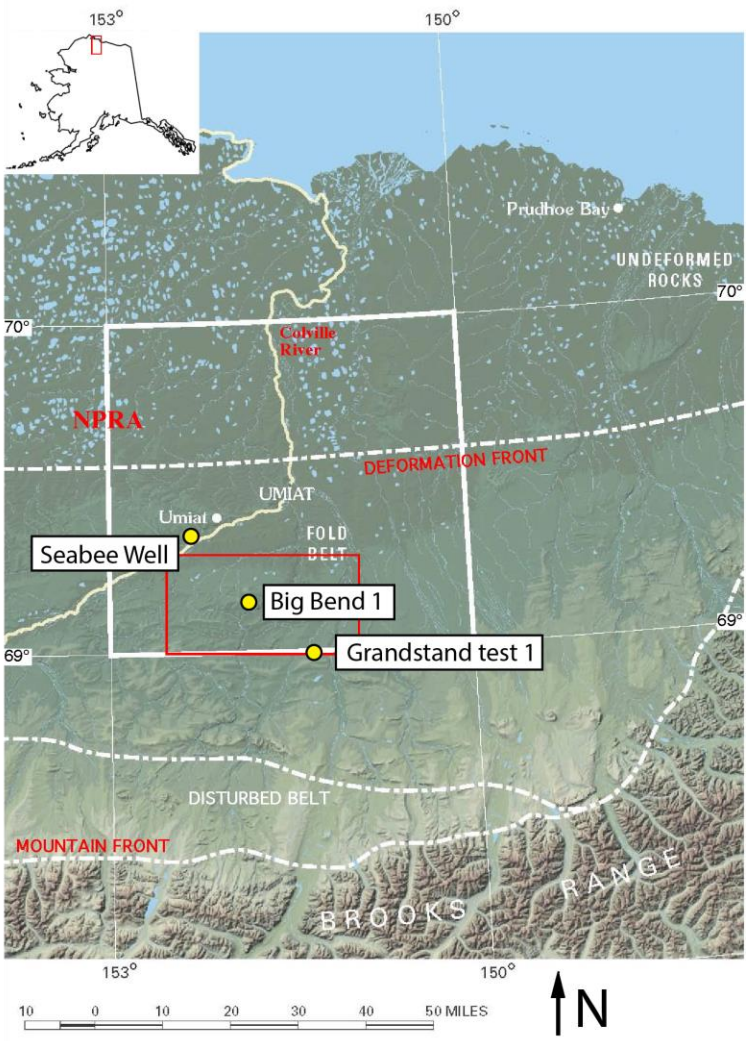

Figure 5.22 Well locations. Wells used for unit thickness. Modified from Mull et al., 2004 and Nelson et al., 2005.

5.10.1.1. Projection of surface information

All projections into the subsurface are based on attitude measurements collected in the field in the summer of 2010 and unit contact locations determined in the field or from the aerial photographs and satellite data. Attitude measurements from the map published by Mull et al. (2004) were used to provide supplemental attitudes for areas that I did not visit. Cross section A-A' is located in the western part of the study area and crosses both branches of the Big Bend anticline, the Seabee syncline, the forethrust and the backthrust. Cross section B-B' is located in

the center of the study area, mostly east of the Chandler River, and crosses the two branches of the Big Bend anticline as well as the thrust faults cutting them. Cross section B-B' is around 3 km west of the branch zone within mapped areas with attitude measurements. Cross section C-C' crosses the single anticline at Trouble Creek.

Cross section C-C' is discussed first because it has the simplest geometry. The remaining cross sections are discussed according to increasing complexity.

Cross section C-C' displays a single gentle anticline (Figure 5.23). Nanushuk Formation was the only unit observed in the field near Trouble Creek so the depth of Torok Formation is inferred. The contacts of Seabee Formation and the Quaternary alluvium are from Mull et al. (2004).

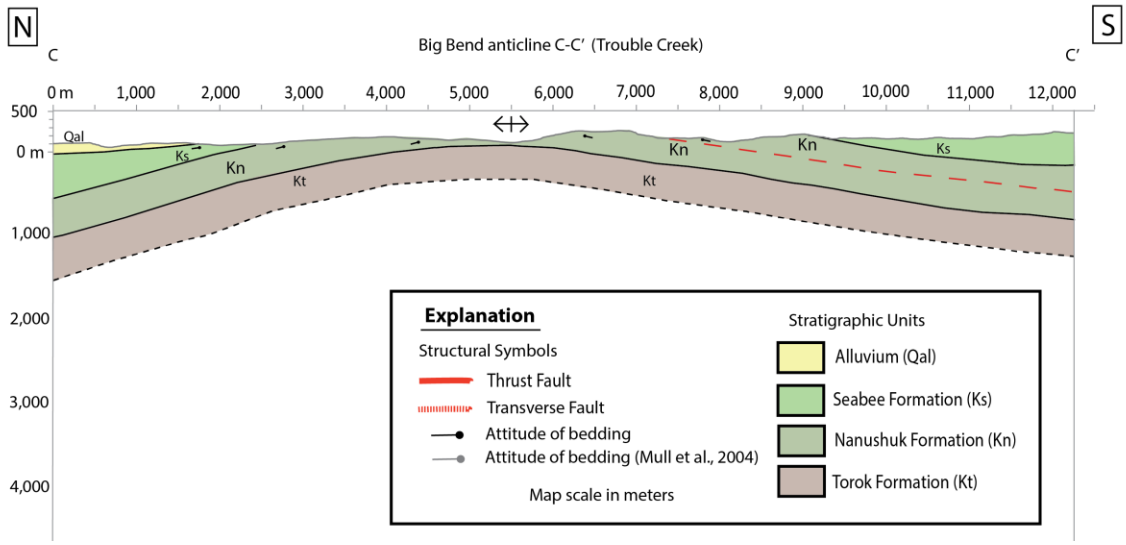

Figure 5.23 Cross section C-C' across the Trouble Creek anticline. Cross section shows one gently dipping anticline. No vertical exaggeration. There is a possibility the backthrust fault through the northern anticline extends this far as suggested by PALSAR and ERS-2 data.

From the surface there appears to be one anticline with a broad, flat top, which is most likely the case farther east of Trouble Creek. Bedding towards the north dips approximately 15° north. Bedding toward the south dips approximately 15° south near the anticline hinge and then starts to level out farther south into a syncline south of the study area. The PALSAR and ERS-2 data (Figure 5.18) suggest that the northern fault extends east-southeast toward the southern Big Bend anticline near Trouble Creek. It is highly uncertain that the backthrust extends this far east, but it

is structurally plausible. The exact geometry of the backthrust is not known as it was not observed in the field at this location. The detachment zone in the south limb of the anticline was not observed in the field either and is inferred from satellite data. It is possible that thrust displacement along the detachment zone increases in this area as the Nanushuk Formation appears thicker here than elsewhere in the study area based on bedding dip and unit contacts. Another possible explanation for this thickened stratigraphy will be discussed in Chapter 6.8 (Cross section restoration).

Cross section B-B' displays the north and south Big Bend anticlines and the thrust faults that cut through them in the Torok Formation through Seabee Formation (Figure 5.24). Quaternary alluvium is mapped along the line of section in the syncline between the two anticlines, but Seabee Formation is exposed in the syncline to the west. Seabee Formation is exposed in the south limb of the south anticline above Nanushuk Formation. Nanushuk Formation is resistant to erosion and so topographically expresses the anticlines, but is covered by Quaternary alluvium in the syncline and by Seabee Formation in the south limb of the south anticline. Torok Formation is inferred beneath the Nanushuk sandstone. The exact geometry of the upper contact of the Torok Formation is unknown but is discussed in more detail with cross section A-A'.

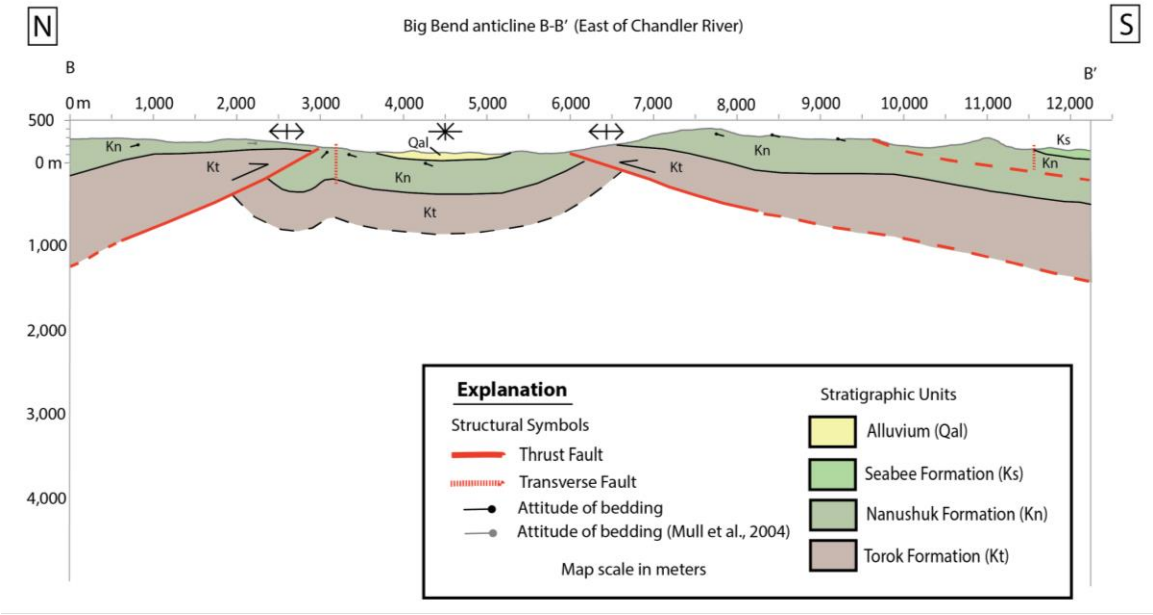

Figure 5.24 Cross section B-B' across the Big Bend anticlines east of the Chandler River. Cross section shows a backthrust that cuts through the southern limb of the northern anticline and a forethrust that cuts through the northern limb of the southern anticline, with a gentle, flat-bottomed syncline in between. A detachment zone is shown in the southern limb of the south anticline, but it is unknown if there is significant thrust displacement on this detachment. No vertical exaggeration.

The northern anticline has a wide and very gentle flat top. A backthrust cuts the southern limb of the northern anticline just south of the hinge. Immediately south of the backthrust, variations in dip suggest a small anticline, perhaps the result of folding preceding thrust breakthrough. The backthrust is not exposed, so its dip and displacement are inferred. The southern Big Bend anticline is a gentle anticline cut by a forethrust just north of its hinge. Evidence of the forethrust was only exposed in a drainage west of the river, so dip and displacement are inferred. Increased slope angle on the north limb along with numerous thawing mud pits of fine grained silt and mud suggest the Nanushuk-Torok contact.

Cross section A-A' crosses the two Big Bend anticlines and the Seabee syncline to the west of the Chandler River (Figure 5.25). The structures of the area are very similar to those in cross section B-B'. Cross section A-A' shows a very gentle northern anticline cut by a backthrust. The dip and amount of displacement along this fault are unknown. Displacement is inferred based on the thickness of Nanushuk exposed north of the fault and the location of the Seabee

contact south of the fault. Seabee Formation is present across most of the syncline with only narrow exposures of Nanushuk sandstone observed near each thrust fault. This helped to define the geometry of the gentle, flat-bottomed syncline. The relatively small fold south of the backthrust is still evident here but is gentler and may die out completely farther west. The southern anticline has slightly steeper limb dips then the northern anticline and is cut by a forethrust in its northern limb. The amount of displacement and dip of this fault are also inferred. Bedding appears to flatten south of the anticline. The detachment zone is mapped to the south but appears to have little or no displacement in this area based on unit thicknesses according to regional well log data.

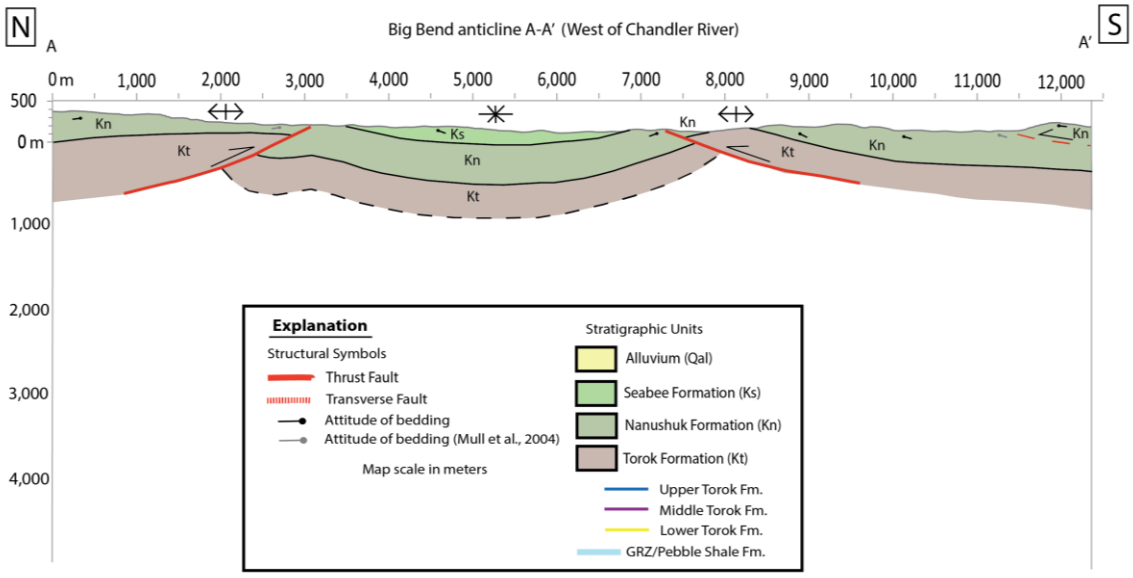

Figure 5.25 Cross section A-A' across the Big Bend anticlines west of the Chandler River. Mapped surface features include two gentle anticlines with a flat-bottomed syncline in between. The southern anticline is cut by a forethrust through the northern limb and the northern anticline is cut by a backthrust in the southern limb. Fault directions can be inferred however, dip angles are unknown. A detachment zone is shown in the southern limb of the south anticline, but it is unknown if there is significant thrust displacement on this detachment.

Chapter 6 Interpretation and Discussion

6.1. Introduction

Once I had compiled and analyzed all of the surface data, I interpreted the surface structure and extrapolated it into the subsurface. My structural interpretations of the surface fold and fault geometry are shown in map form (Figures 6.1, Supplemental Map file: M.1). Very little information about the subsurface of the Big Bend area has been made public, thus all interpretations presented here are based on surface information and structural trends. Seismic data (courtesy of Renaissance Alaska) from Umiat anticline, 30 km north of Big Bend, also proved to be helpful as an analog for interpreting the subsurface structure of the Torok Formation. The cross sections and seismic data were then used to create a geometrically and kinematically valid cross section restoration (section 6.8 Cross Section Restoration).

The westward branching of the Big Bend anticline adds a complexity that has not been addressed in much other research and makes comparing this region to other fold-and-thrust belts difficult. The Niger Delta is a gravitationally driven base-of-slope fold-and-thrust belt, but it is a good analog for fold geometry that is well documented with seismic data. The mechanical stratigraphy of the region adds to the complexity of the area and so a new model for the Brooks Range foothills fold-and-thrust belt is discussed at the end of this chapter.

6.2. Structural interpretations of folds and faults

I compared my field data and remote sensing analyses against the two published geologic maps of the area: Detterman et al. (1963, 1:125,000 scale, Figure 6.2 and Appendix E) and Mull et al. (2004, 1:250,000, Figure 2.2). I present two structural interpretations that are viable based on my analysis of the field and remote sensing data (Figures 6.1 and 6.2; Supplemental Map files: M.1 Preferred and M.2 Alternate). My preferred model updates the stratigraphic contacts and structural interpretations from those that were previously published.

6.2.1. Model A: preferred model

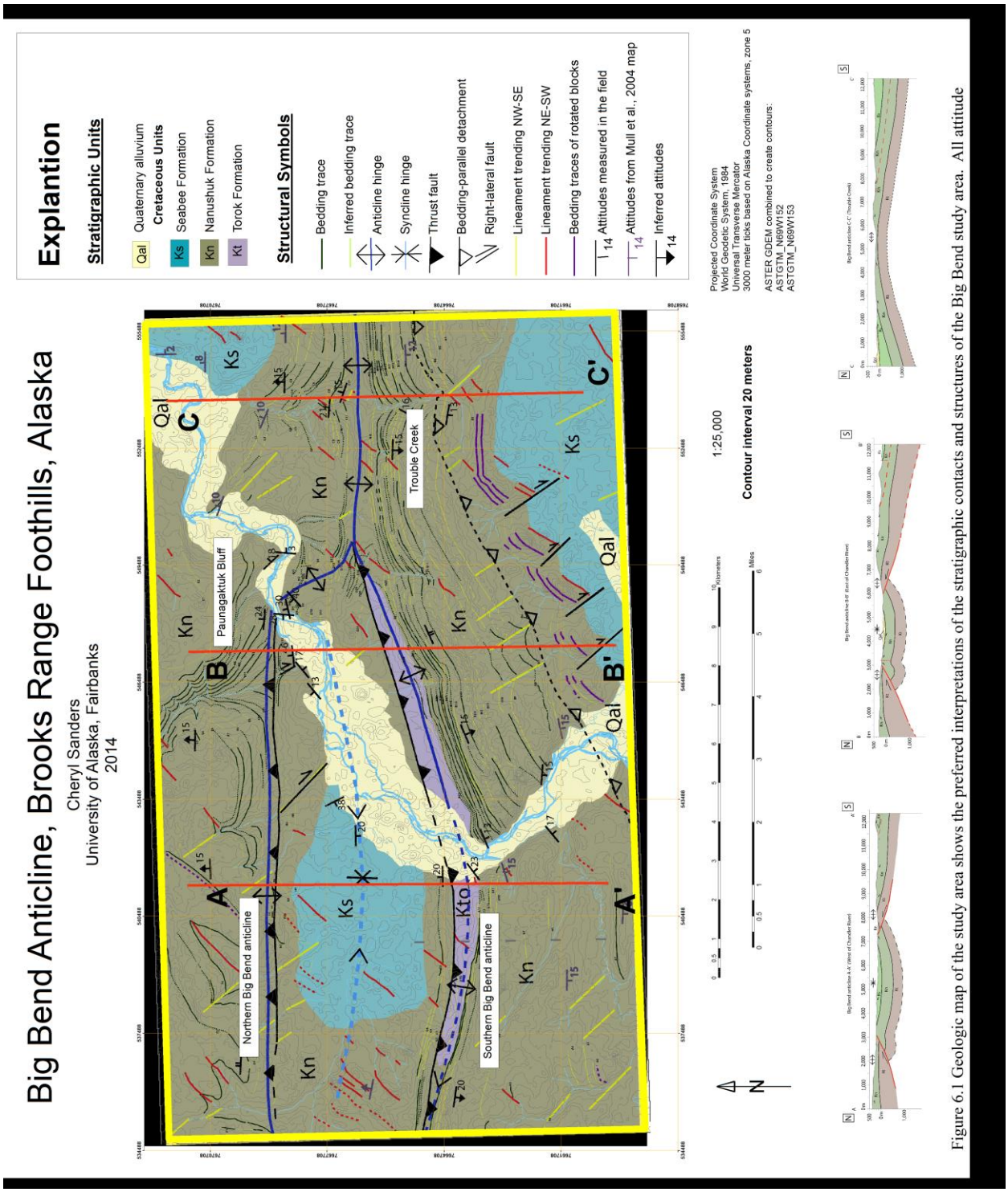

Figure 6.1 Geologic map of the study area shows the preferred interpretations of the stratigraphic contacts and structures of the Big Bend study area. All attitude

The preferred map (Figure 6.1) was made based on field observations, attitude measurements, stereographic projections, and bedding and lineament traces from aerial platform and satellite

remote sensing analysis. The domain maps discussed throughout Chapter 5 (Observations and Results), were helpful for determining localized structures and then identifying stratigraphic and structural trends throughout the study area. Some attitude information was used from the map by Mull et al. (2004) to help fill in information in areas that I was unable to visit.

My preferred interpretation includes two gentle parallel anticlines that merge eastward into one gentle anticline. The southern Big Bend anticline is cut by a forethrust in its north limb with displacement sufficient to expose the Torok Formation. The forethrust continues out of the study area to the west. The northern Big Bend anticline is cut by a backthrust in its south limb. A very gentle northwest-southeast trending anticline connects the two east trending anticlines at the branch zone, and a single anticline continues east from there. This bridging anticline and the forethrust terminate at the same location along the southern Big Bend anticline. I interpret the blocks of bedding in the southeast corner of the map to be bounded by northwest-striking right-lateral strike-slip faults. Other similar strike-slip faults are present throughout the study area and strike both northwest and northeast consistent with the local fracture pattern (Figure 6.1). My interpretations are based on aerial platform and satellite data since data from the field is limited or nonexistent. I interpret the northern limit of rotated bedding traces to mark the surface trace of a bedding parallel detachment zone above which rotation occurred. The dip and displacement of this detachment zone are unknown, but it likely follows an incompetent stratigraphic interval. This interpretation is based on satellite data analysis and an apparent increased unit thickness based on surface projections.

My stratigraphic and structural interpretations differ from those of Detterman et al. (1963) (Figure 6.2). The main stratigraphic difference between my interpretation and that of Detterman et al. (1963) is that I do not show Torok Formation within the south limb of the southern Big Bend anticline. Their map also shows that the Seabee Formation in the syncline between the two anticlines extends to the backthrust fault to the north and to the forethrust to the south, whereas I do not.

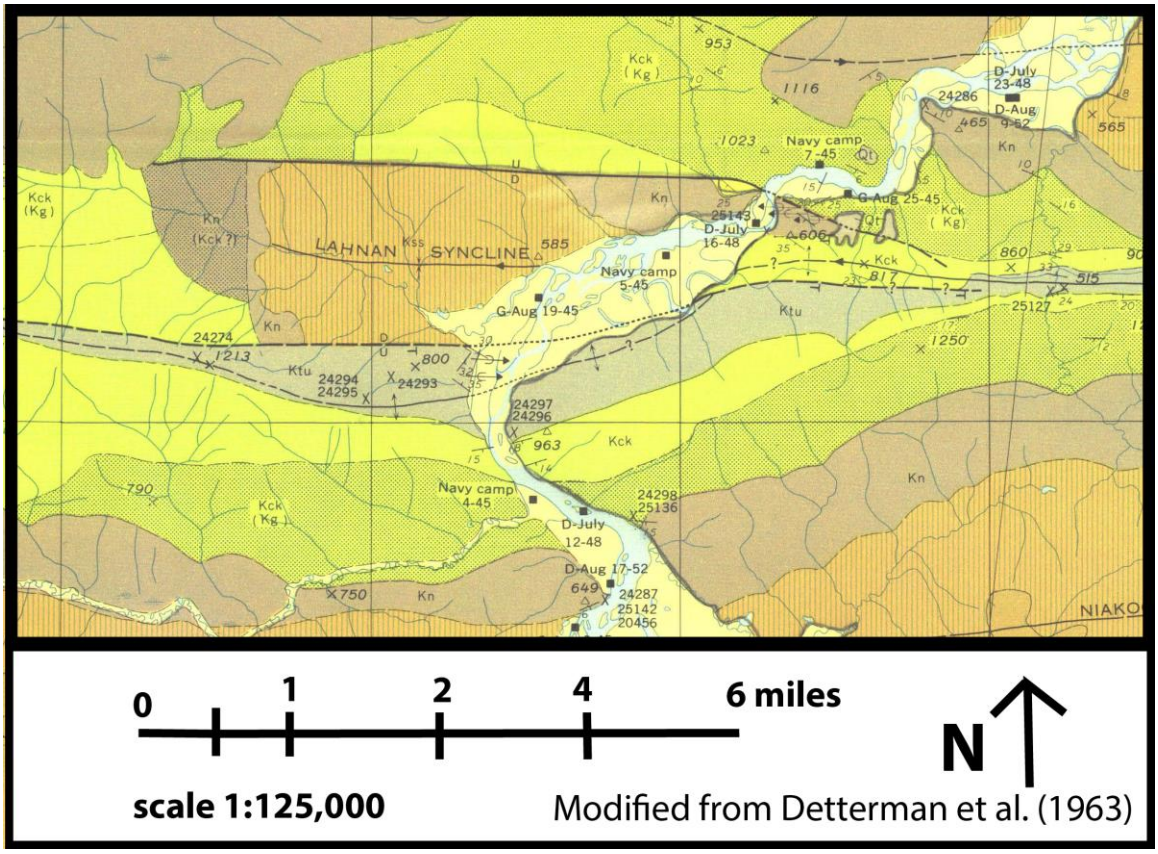

Figure 6.2 Big Bend anticline area as interpreted by Detterman et al., (1963). Main differences between the preferred interpretations and this map is the extent that Torok Formation is mapped in the southern Big Bend anticline and that Seabee Formation is bound to the north and south by normal faults.

The preferred and Detterman et al., (1963) interpretations show significant structural differences throughout the study area (Figure 6.2). The Detterman et al. (1963) map does not show the strike-slip faults, right-lateral strike-slip bound blocks, detachment zone or the bridging anticline in the branch zone. Most importantly, their map also does not include the northern Big Bend anticline. The southern Big Bend anticline is mapped similarly in both interpretations to the west and near the Chandler River. However, Detterman et al. (1963) showed the southern anticline terminating eastward at the forethrust and the anticline at Trouble Creek continuing westward north of the forethrust almost to the Chandler River. They showed the northern backthrust as a very high angle fault with unspecified dip directions.

The Mull et al. (2004) map (Figure 6.3) is more similar to my interpretation but still shows some important differences. The Mull et al. (2004) and Detterman et al. (1963) maps both differ

from my map in that they show the Seabee Formation extending northward against the backthrust and southward against the forethrust. My map differs from that of Mull et al. (2004) in the exact location of unit contacts for the Seabee and Nanushuk Formations in the southwest corner of the study area. The biggest stratigraphic differences are in the location of the Torok Formation and are directly related to the structural interpretation in this study. Mull et al. (2004) mapped Torok in drainages north of the backthrust, but I interpreted the rocks in this area to be too high in the Nanushuk for Torok to be exposed. In the southern Big Bend anticline, Mull et al. (2004) also mapped different contacts between the Nanushuk and Torok formations south of the forethrust than I did.

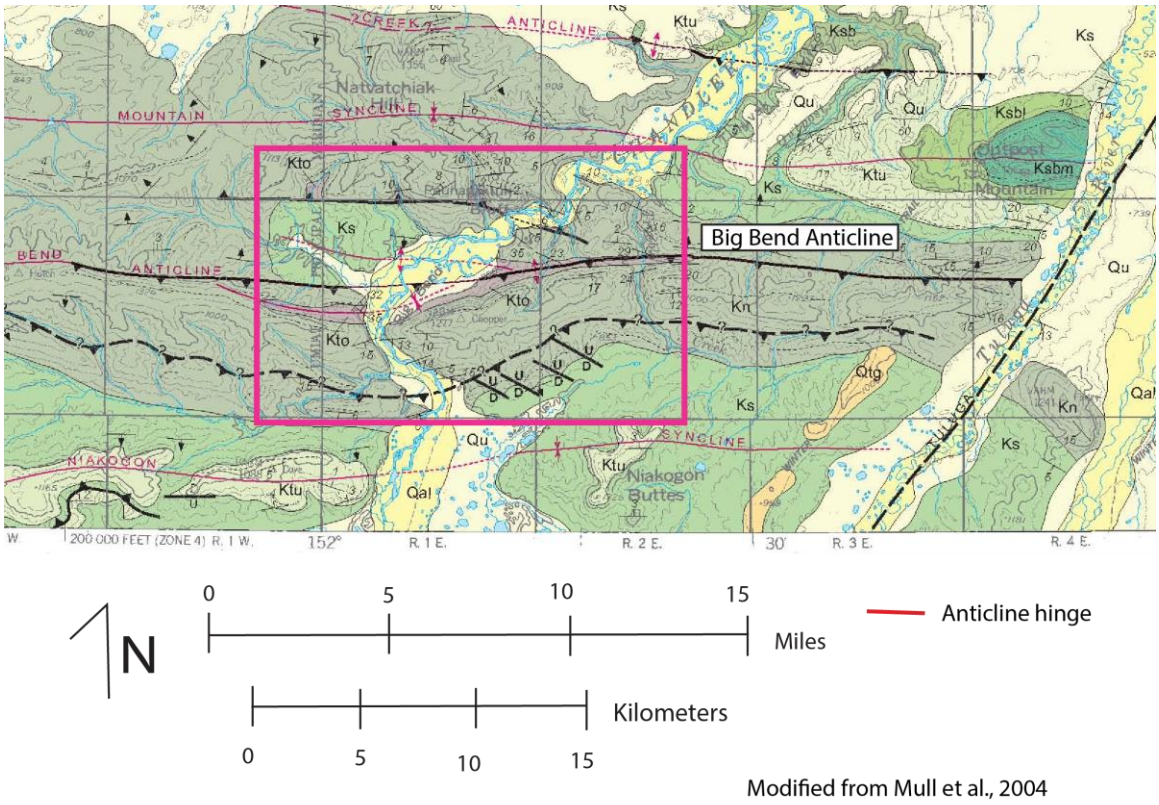

Figure 6.3 Mull et al. (2004) map of the study area. Main differences between this map and the preferred interpretation for this research include mapped unit contacts for Seabee and Torok Formation and lack of the northern Big Bend anticline and bridging anticline in the branch zone.

Mull et al. (2004) showed more structural detail than Detterman et al. (1963), but there are still significant differences between the Mull et al. (2004) map and my own interpretation. The most important difference is that their map does not show the northern Big Bend anticline and the

bridging anticline. There are slight differences in the exact locations of the southern Big Bend anticline and the forethrust. Mull et al. (2004) showed Torok in the core of a syncline south of the forethrust and Seabee in the core of an anticline north of the forethrust. Based on the stratigraphic relations, the fold symbols were probably inadvertently switched on the Mull et al. (2004) map, and should have shown an anticline to the south and a syncline to the north as on my map and the Detterman et al. (1963) map. Mull et al. (2004) showed the detachment zone in the southern part of the area as a laterally extensive thrust fault and interpreted the northwest-striking faults in the southeast part of the area as dip-slip faults. The most significant structural difference is that Mull et al. (2004) showed the forethrust continuing far east of Trouble Creek whereas I interpret it to terminate eastward at the branch zone.

My observations provided little basis to determine the relative timing of structures, so I can only infer the structural evolution of the area based on the distribution and character of the structures. Three east-west trending anticlines dominate the structure of the area, one to the east and two to the west. The eastern anticline trends between the western anticlines, so they may all have originated separately. Alternatively, the southern and eastern anticlines may have been a single anticline with a gentle bend along trend.

Local shortening is probably greater to the west because exposure of Torok in the south anticline and Seabee in the syncline indicates greater structural relief and because both western anticlines are cut by thrust faults (Figure 6.4). As shortening increased and, perhaps, the eastern anticline propagated westward and the western anticlines propagated eastward, they overlapped in the branch zone. The complex non-cylindrical folding in this area resulted from continued shortening. Both the forethrust and backthrust cut through anticline limbs, suggesting that they post-date formation of the anticlines. The thrust faults may have propagated westward to accommodate continued shortening to the west, but no faulting occurred to the east either because shortening was less there or because continued shortening did not require faulting in the single simple anticline.

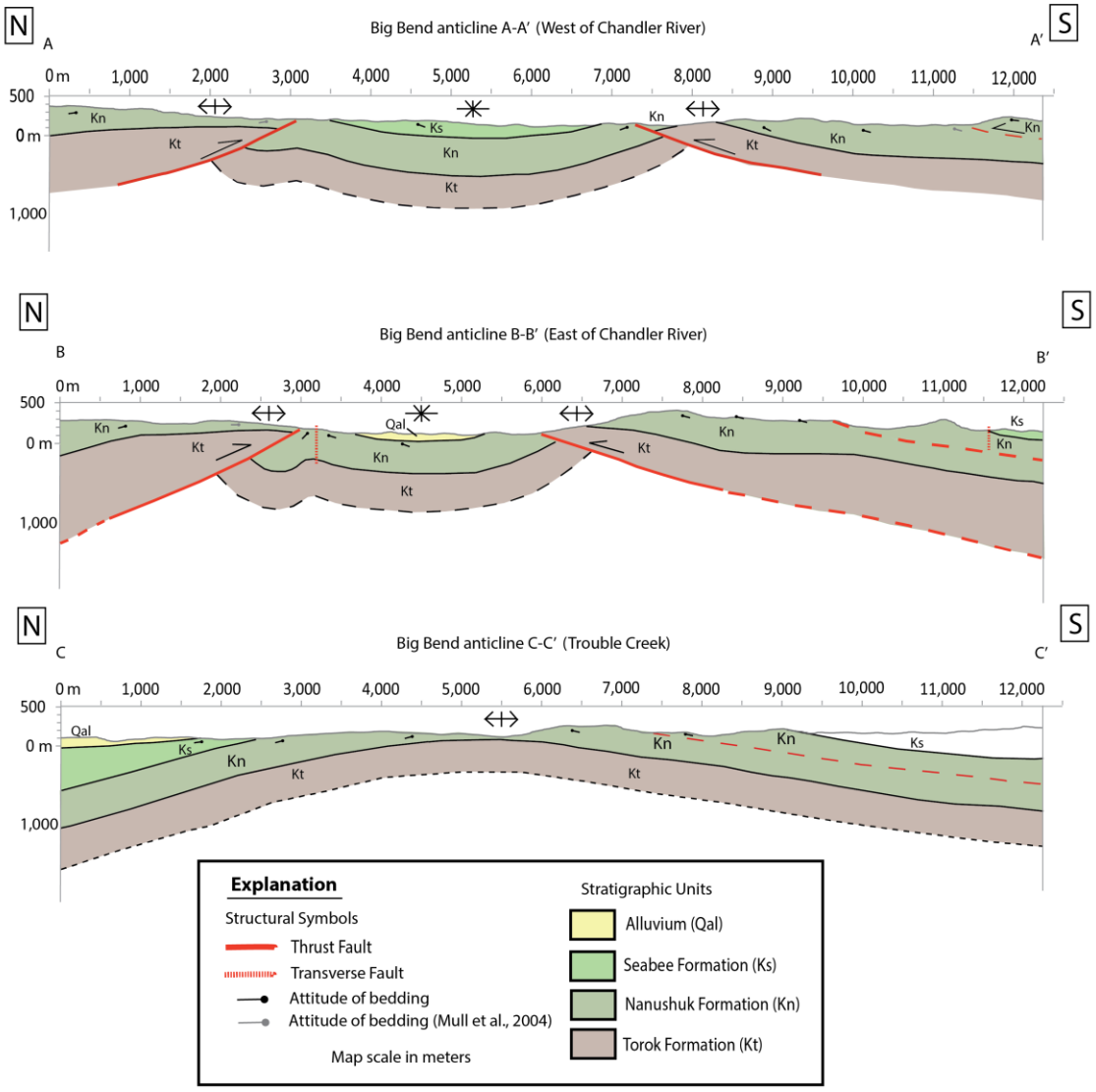

Figure 6.4 Surface projection cross sections of the study area. Cross section locations are located on preferred interpretation in Figure 6.1. The westernmost cross section, A-A', cuts through the northern and southern Big Bend anticlines. It shows displacement along a backthrust in the southern limb of the northern anticline and a forethrust in the northern limb of the southern anticline with a syncline exposing Seabee Formation in the middle. Cross section B-B' is similar to A-A', but it is closer to the branch zone and thus appears more concentrated. The easternmost cross section, C-C', shows a single gentle anticline without breakthrough thrust faults. All three cross sections include a potential detachment thrust to the south that may help to explain the thickened Nanushuk Formation in that area.

The local strike-slip faults and regional folding and thrust faulting are consistent with north-south shortening. The strike-slip faults and thrust faults are unlikely to have formed under the same local stress conditions. Thrusting and strike-slip faulting may have occurred at different

times as a result of regional changes in stress conditions or local changes in stress state within the folds may have allowed formation of the strike-slip faults. The NE-SW and NW-SE conjugate fractures developed prior to the main stages of fold-and-thrust deformation and are not likely to have formed during thrusting (Wentz, 2014).

6.2.2. Model B: alternative model

The alternative interpretation (Figure 6.5) is identical to the preferred interpretation except that the forethrust continues to the east beyond Trouble Creek as shown by Mull et al. (2004) map. The backthrust continues to the east toward Trouble Creek in a similar location to the high angle normal fault shown on the Detterman et al. (1963) map. The backthrust is closely related to the northern Big Bend anticline hinge so the hinge is extended east beyond Trouble Creek. Remote sensing data suggest that the backthrust may continue to the east across the river toward Trouble Creek. Fault displacement east of the branch zone is probably very small and likely dies out eastward, and I found no evidence that the northern anticline continues east of the branch zone. This is not my preferred model because I found no field evidence for a thrust throughout the Trouble Creek anticline area. The eastward continuation of the northern backthrust in the northern part of this area is based on limited remote sensing evidence. Any thrust displacement in this area is relatively small based on the dip and traces of bedding in the field and on the aerial photos. Significant displacement would have been identified during correlation of the bedding between the north and south limb of the Trouble Creek anticline.

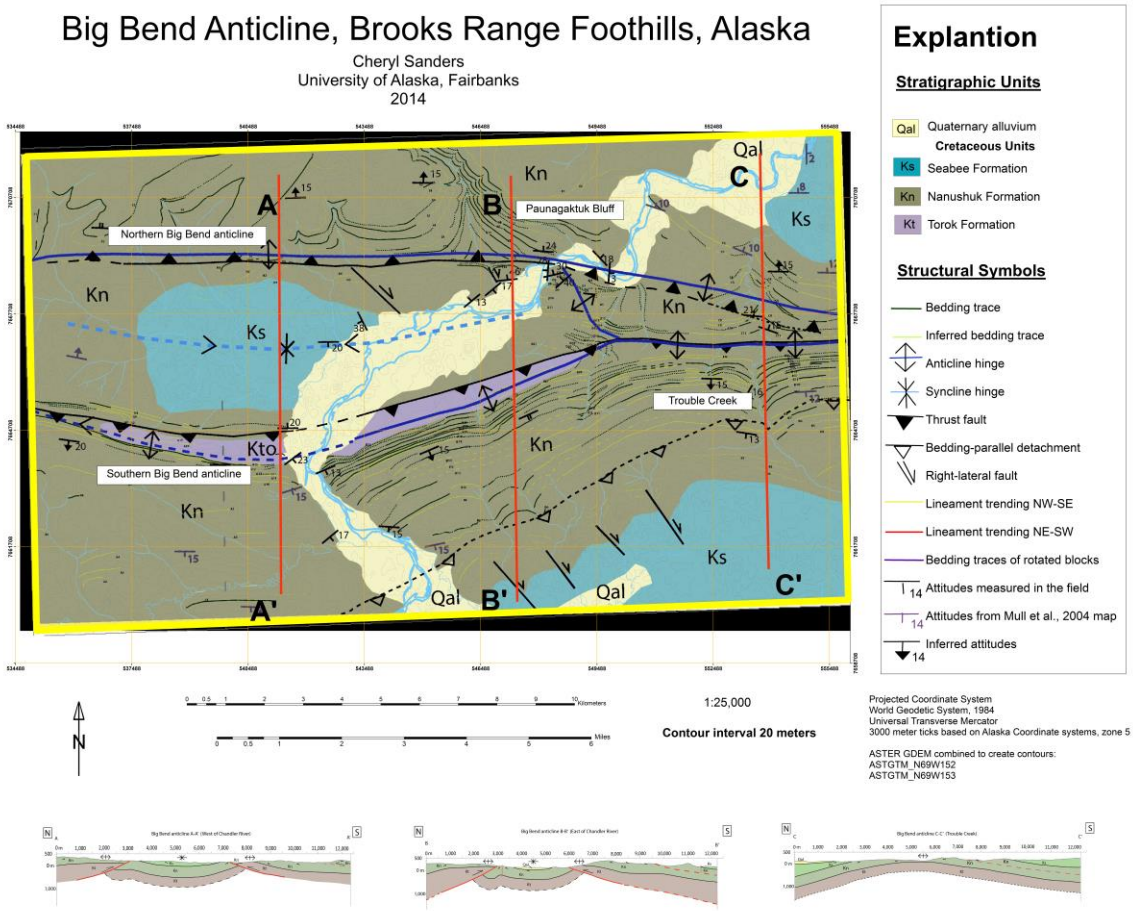

Figure 6.5 Geologic map of the study area with an alternative structural interpretation. This interpretation is identical to the preferred interpretation except for the continuation of the forethrust, northern anticline hinge and backthrust to the east past Trouble Creek

6.3. Torok deformation at Big Bend anticlines and analogous Umiat anticline

The Torok Formation was only very poorly exposed at the surface at a few locations. Thus, understanding its stratigraphy and structure from field observations alone was impossible. Regional observations suggest that the anticlines defined by the Nanushuk Formation at the surface formed by structural thickening within the underlying Torok Formation (Kirschner and Rycerski, 1988; Moore et al., 2004; Wallace, 2009; Wallace et al., 2011). No publicly available seismic data could be obtained for the Big Bend area, so I applied another approach.

The Umiat anticline is closer to the deformation front than the Big Bend anticline (Figure 2.2), but is an analogous anticline with the best available seismic and well data in the region. Umiat anticline is similar to the Big Bend anticlines in its stratigraphy, geometry and kinematic history and is part of the same fold-and-thrust belt. Renaissance Alaska provided three dimensional seismic data for Umiat anticline. I interpreted bedding reflectors, folds, and faults in a representative line from the north-northeast to the south-southwest across the Umiat anticline perpendicular to its axis (Figure 6.6).

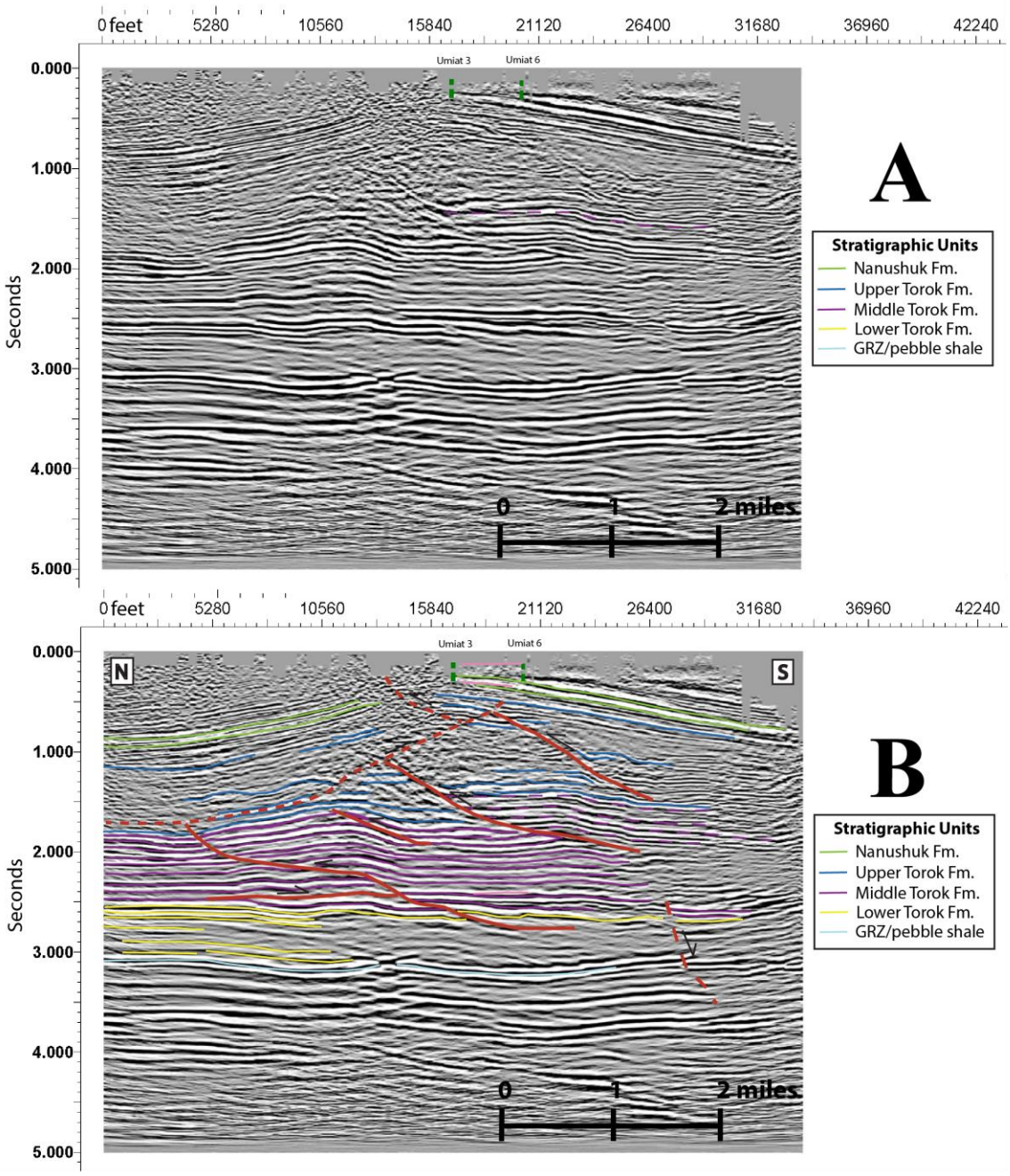

Figure 6.6 Seismic reflection line from Umiat anticline. Uninterpreted line above, interpreted line below. The competent Nanushuk Formation overlies the incompetent Torok Formation. Torok is separated into three structurally and seismically distinct units. Seismic reflectors are visible but poorly defined within the upper Torok, and are deformed by faulting. Middle Torok has well defined seismic reflectors that are deformed by faulting and folding. Lower Torok has very poorly defined seismic reflectors that display only minor faulting. Most of the visible contraction is within the upper and middle Torok.

Seismic reflections were correlated to stratigraphic units using NPRA (National Petroleum Reserve-Alaska) well logs and seismic data (Miller et al., 2000). Interpreted tops of Nanushuk, Torok, and GRZ (gamma ray zone)/pebble shale are displayed on the interpreted seismic section. The seismic data show a gentle anticline in the Nanushuk Formation with a series of faults and folds beneath it (Figure 6.6). A seismically noisy area precludes meaningful interpretation at the crest of the anticline.

The Nanushuk Formation was interpreted on both sides of the anticline by comparing stratigraphically identified reflectors on the south side with those on the north side. Reflectors in the Nanushuk Formation show a very gentle fold. Reflectors in the lower portion of the Nanushuk are visible and easily recognizable. Up section and closer to the surface, the reflectors become hard to follow due to the high level of noise in the data. The Torok Formation was divided into three seismically distinct intervals based on reflection characteristics and geometry. This is easiest to see when the line interpretation is viewed without the seismic reflection data (Figure 6.7). The lower Torok Formation displays relatively parallel and flat reflectors. Traces on the north side of the anticline are visible and easily recognizable, but the reflectors on the south side are hard to follow and there is too much noise for interpretation. This interval shows no folding and only a few fault traces. The middle Torok Formation has reflectors that are easily visible. These reflectors are closely spaced and parallel and provide good definition of the structure. The middle Torok displays thrust faults that vary in dip, defining ramps and flats. The thrusts are imbricated with the lowest to the north and the highest to the south, but they do not appear to originate from the same basal detachment. The lack of visible faulting within the lower Torok Formation suggests that the basal detachment is near its top. The upper Torok Formation shows only a few widely spaced and discontinuous reflectors across the line. This is the hardest interval to interpret due to the lack of traceable reflectors but it is also the most important because this is where the faults that reach the surface appear to originate. A backthrust is identifiable in the upper Torok Formation, but its exact location, dip and displacement are unclear (Figure 6.6B). Previously, two forethrusts are mapped here (Molenaar, 1982). The noisy area at the crest of the anticline also makes it unclear whether any of the seismically defined faults reach the surface.

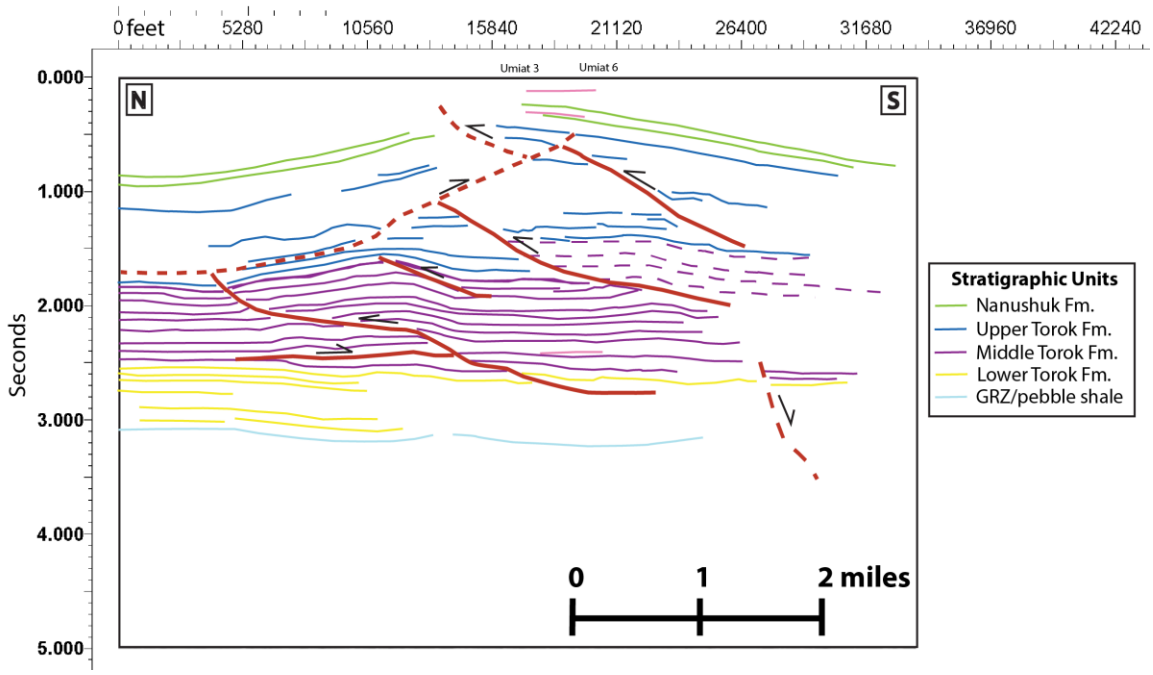

Figure 6.7 Line-only interpretation of the Umiat anticline seismic reflection line. Only major faults are shown to define the general geometry of the structure. The distinct character of the three Torok units is more easily seen without the seismic data.

The seismic data supports previous interpretations (Moore et al., 2004; Wallace, 2009; Wallace et al., 2011) that the foothills folds formed above a low-taper triangle zone (Jones, 1982; McMechan, 1985) or a passive-roof duplex (Banks and Warburton, 1986; Wallace, 1993). An idealized model of a triangle zone by Jones, (1982) is easily modified to fit closely with the Umiat seismic interpretation and the structures at Big Bend anticline (Figure 6.8). In this model, the basal detachment is above the Kingak Shale, the pebble shale unit, and the lowermost Torok Formation. The middle part of the Torok Formation is imbricated above the basal detachment to form a forward vergent duplex thrust system. Another detachment within the upper Torok Formation is the upper backthrust detachment of a passive-roof duplex. Culminations within the duplex form the cores of the anticlines above the upper detachment. The passive-roof detachment and the basal detachment converge at the leading edge of the triangle zone.

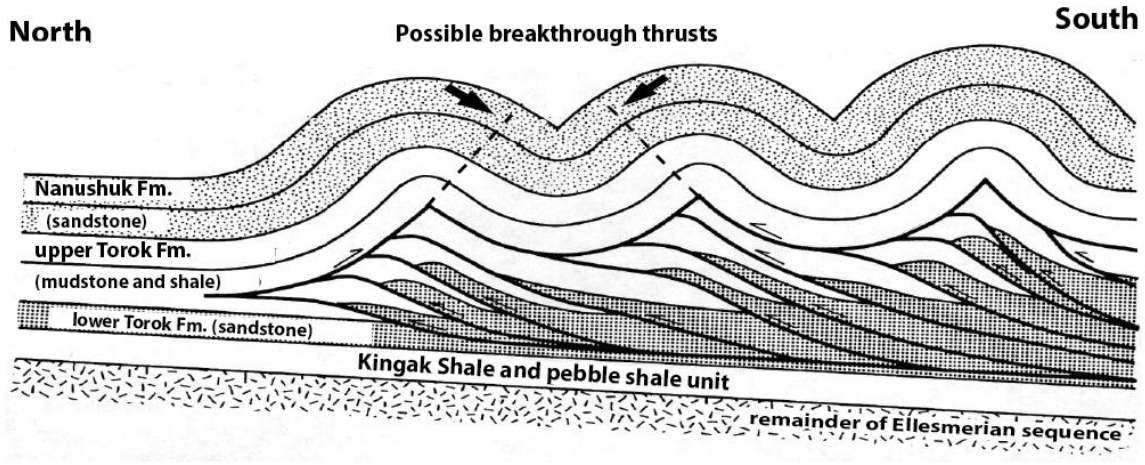

Figure 6.8 Model of Brooks Range foothills fold geometry. Syncline in the study area has a more flat-bottomed shape than shown here. Modified from Jones, 1982.

This model fits well with my Umiat anticline seismic interpretation because that interpretation shows stacking of forward-vergent thrust faults in the Torok Formation that account for the anticline in the overlying Nanushuk Formation. The folds at Umiat and Big Bend differ in detail from this model, as is addressed in the section on the restoration of cross section A-A' and in Chapter 6.7: Discussion.

6.4. Incorporation of seismic data into Big Bend interpretation

Subsurface deformation of the Torok Shale at Big Bend anticline is illustrated in cross section A-A' Subsurface Deformation (Figure 6.9) based on interpretation of seismic data from the Umiat anticline. In this cross section the Torok Formation is divided into the same units identified seismically at Umiat anticline: upper, middle, and lower Torok Formation. As seen at Umiat, shortening is accommodated mostly within the upper and middle Torok with the lower Torok unit and underlying stratigraphy showing very little, if any, deformation.

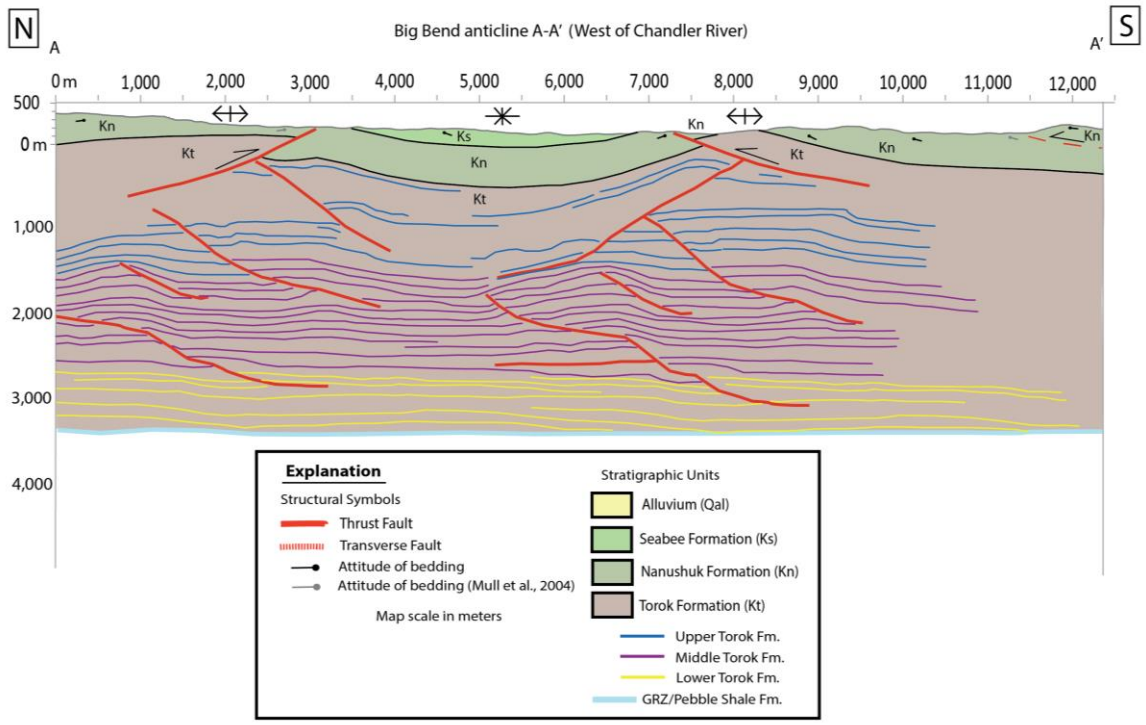

Figure 6.9 Cross section A-A' projected to depth across the Big Bend anticlines west of the Chandler River. Subsurface interpretations are inferred based on interpretation of seismic data from Umiat anticline. Vertical exaggeration is only approximately zero because the seismic is in time not depth. Mapped surface features include two gentle anticlines with a flat-bottomed syncline in between. The southern anticline is cut by a forethrust through the northern limb and the northern anticline is cut by a backthrust in the southern limb. These two thrust faults and their dips are consistent with the Umiat seismic interpretation. In the subsurface the Torok Formation is divided into three distinct units. The upper and middle units accommodate most of the shortening on forethrusts and backthrusts. The lower unit has some faulting and thickening, but probably is the main basal detachment horizon.

6.5. Origin of folds in the study area

The Big Bend folds are near the leading edge of the foothills fold-and-thrust belt, which is the northernmost part of the Brooks Range orogen (Kirschner and Rycerski., 1988; Moore et al., 2004; Wallace, 2009; Wallace et al., 2011). The nature of the folds at Big Bend are dependent on the mechanical stratigraphy of the units and the zones of detachment. A relatively competent unit, the Nanushuk Formation, is bounded above and below by two incompetent units, the Seabee and Torok formations. As shortening occurred, the Torok Formation shale thickened by stacking and internal folding of horses in a duplex. Basal detachment is within shale in the lowermost

Torok Formation and the roof detachment is in slope clinoform shale beneath the transition to topset Nanushuk Formation sandstone (Mull et al., 2003; Houseknecht and Schenk, 2005; Houseknecht et al., 2009). The duplex formed in more competent sand-rich toe-of-slope deposits in the middle Torok Formation. The roof detachment allowed the overlying Nanushuk and Seabee Formations to fold in response to thickening of the underlying Torok. Nanushuk sandstone formed gentle, wide anticlines and synclines over variations in relief on the thickened Torok. The Big Bend anticlines are approximately concentric folds. The syncline between the anticlines is also an approximately parallel fold but has a wide, flat bottom, which probably reflects either minimal or uniform shortening in the Torok of the flat-lying part of the syncline.

The model by Homza and Wallace (1995) represents the study area best with Nanushuk Formation as the competent layer that deforms with parallel gentle folds (Figure 3.2). The Torok Formation is the underlying incompetent layer deformed with structural thickening and disharmonic folding. This model assumes that the competent layer maintains pre-folded thickness and bed length and the incompetent layer changes thickness and bed length as deformation progresses.

6.6. Origins of the branching fold at Big Bend

Based on stereoplot analysis and regional structural trends, the folds in the study area formed at the same time and due to similar stress. The exact nature of their deformation remains largely unknown. It is unclear how the northern Big Bend anticline and the southern Big Bend anticline are connected without a clear understanding of the structure in the branch zone. Based on folds and faults of the area, I interpret more shortening was accommodated to the west of the branch point due to the fact there are two fold and two thrust faults. To the east of the branch point there is only a gentle fold without evidence of thrust displacement.

Based on these observations two main interpretations of the area are possible. The southern fold, including the Trouble Creek anticline, could have started to form and as contraction increased the northern fold branched out to accommodate more shortening to the west. Or, more likely, all three folds started to form independently of each other and as contraction increased they extended into each other. I prefer the second interpretation based on the bends in the current anticlines and the perpendicular nature of the branching anticline to other folds in the region,.

Considerably more data from the field on time of folding, amount of contractions and subsurface structures would be required to verify this.

6.7. Origins of thrust faults in the study area

The thrust faults in the area are poorly exposed or inferred in the subsurface, so their origins are uncertain. The forethrust and backthrust mapped in the Nanushuk Formation both cut across the steeper limbs of anticlines and have relatively small displacement. These characteristics, combined with interpretation that the Nanushuk folds are detachment folds, suggests that the thrusts formed as "break-thrust folds" (Fischer et al., 1992) or by breakthrough of detachment folds (Wallace and Homza., 2004). These thrusts may be directly related to folding and to thickening within the Torok Formation assuming that the structure of the Torok at Big Bend is similar to the structure of the Torok at Umiat. I interpret the forethrust to connect to the forward thrusting within the Torok either directly from one of the horses or from the roof detachment. I interpret the backthrust to be connected to the passive roof detachment.

No information about the faults in the Torok is available from the study area, so my subsurface interpretation is based entirely on the Umiat seismic interpretation. Assuming the Umiat analog, Torok contains horses in a duplex with displacement on each horse of approximately 100 m or less. I interpret the horses to have formed in middle Torok Formation and the lower part of upper Torok Formation.

6.8. Origin of strike-slip faults in the study area

Linear drainages brought to light a fault and/or fracture controlled pattern in the area (Figure 6.10). Further investigation showed that some of the lineaments had displacement and showed evidence for faulting. Some of the lineaments in the southeast corner of the study area are mapped as normal faults by Mull et al., 2004. I interpret these to be northwest-striking faults with apparent right-lateral offset, but the exact amount and nature of displacement is unknown. I interpreted these faults to bound blocks that have been rotated above a detachment surface but that the bounding faults are related to other right-lateral faults of the area. Their strike and sense

of displacement support this idea. These faults likely formed at the same time as the other strike slip faults in the area.

I was able to map a few strike-slip faults in the study area but I suspect more transverse faults were either not visible at the surface or were not recognized. It is unclear when these strike slip faults formed relative to the folds and thrust faults.

Wentz (2014) identified a set of conjugate shear fractures with northwest and northeast strikes, similar in trend with the strike-slip faults that I observed. This overall fracture and fault pattern is consistent with north-south contraction, as are the folds and thrust faults in the area. However, the transverse faults and thrust faults probably did not form at the same time because the intermediate axis of principal stress ($\sigma 2$) is expected to be vertical for strike-skip faults, while it is expected to be horizontal for folds and thrust faults (Price and Cosgrove, 1990). Wentz (2014) interpreted the conjugate fractures to predate thrust faulting in the area.

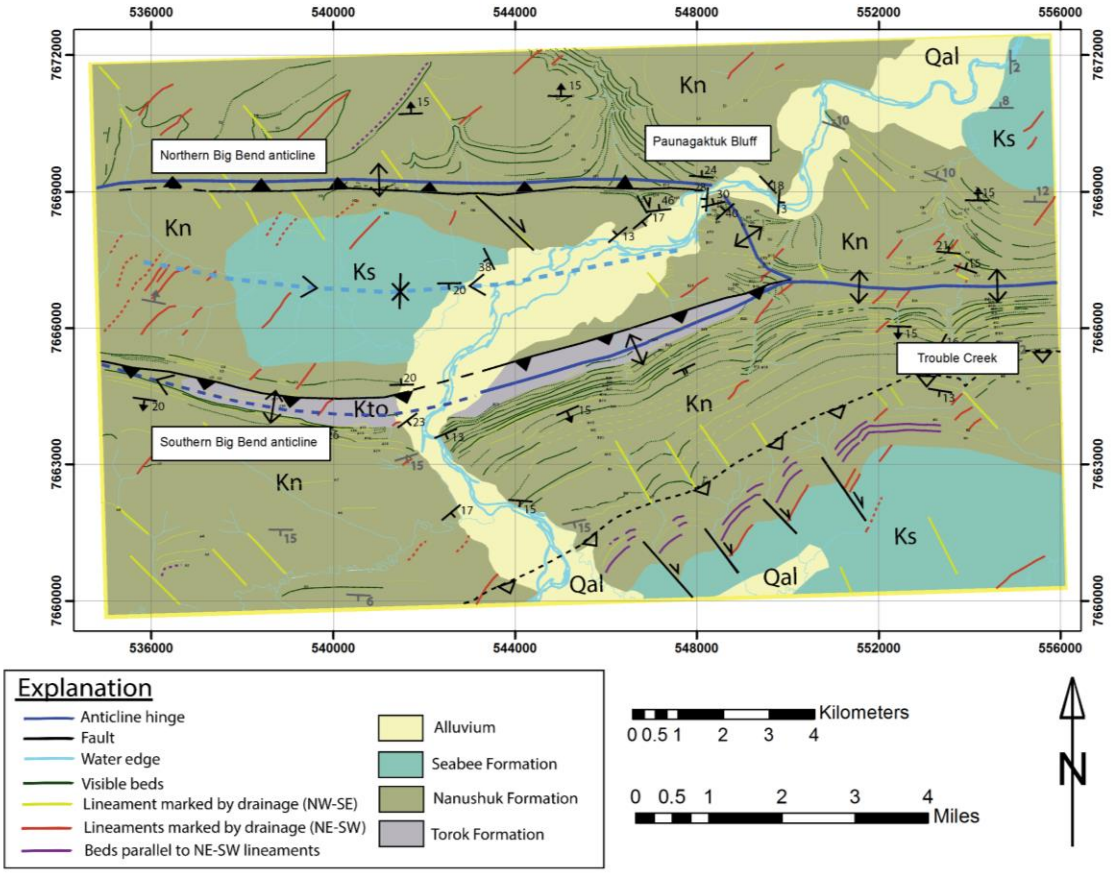

Figure 6.10 Geologic map with preferred structural interpretation and lineament pattern. Lineaments were mapped from drainage patterns and local bedding offset patterns such as in the southeastern corner of the study area. Lineaments follow similar trends as fracture sets identified in the Master's study by Raelene Wentz (2014).

6.9. Cross section restoration

A kinematically viable restorable cross section of A-A' was created in order to more fully understand how deformation of the Torok Formation relates to deformation of the overlying Nanushuk Formation. The model was originally made by hand by combining the surface cross section A-A and the Umiat seismic interpretation (Figure 6.9) using a light table. The modified Jones, 1982 model (Figure 6.8) was helpful in defining horse shape, size and area. Horses in the duplex were drawn to provide the necessary structural relief beneath the anticlines and with a fault geometry generally consistent with the seismic interpretation. The image was then digitized (Figure 6.11). Most of the horses are the same size and area; however horses 7 and 9 are exactly

half the size and area of the other horses. This reproduces the similar but thinner horses identified on the Umiat seismic line. It is important to emphasize that this is an idealized model and is not based on seismic data from the study area.

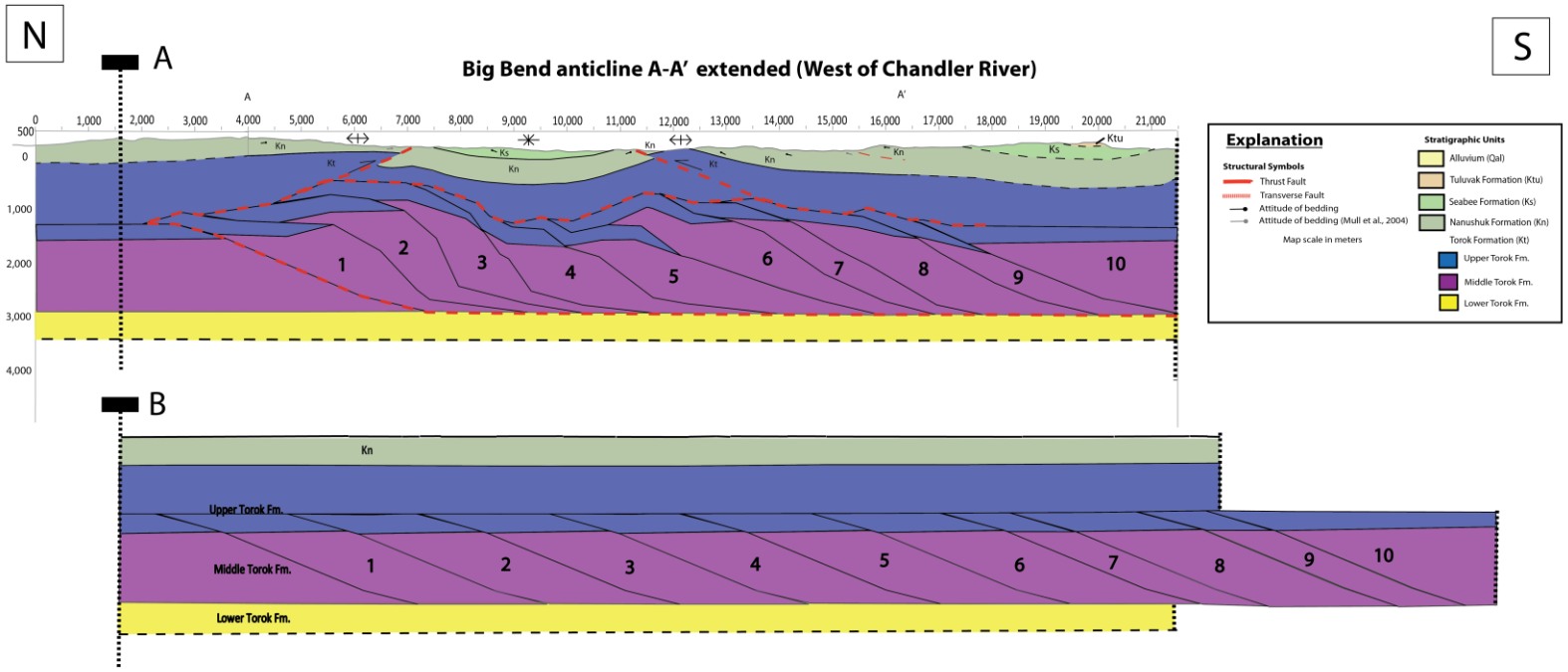

Figure 6.11 Deformed (A, above) and restored (B, below) cross sections of A-A' that show a passive-roof duplex interpretations for the structure of the area. Folds in uppermost Torok and Nanushuk are separated by a roof thrust from horses in underlying Torok. Pin near left end of sections represents the northern point from which deformation in the study area was restored. Differences in length at different stratigraphic levels in the restoredsection indicate estimated differences in approximate amount of shortening. There is a large disparity in shortening between the competent Nanushuk Formation and the incompetent Torok Formation.

A pin was set at the northern end of the cross section in order to establish the northern limit of deformation addressed in the cross section. All shortening is measured from this northern pin. The size and shape of the horses were modeled from the horses interpreted in the Umiat seismic line. Their shape is similar to a rhombus and is used because it mimics the shape of the faults interpreted in the seismic data while still being fairly convenient to manipulate while maintaining constant area and perimeter of each horse. The dip of the faults is also modeled from the seismic interpretation. Coincidently, the fault dip is approximately 15°, which is similar to the measured dip of bedding at the surface. Other assumptions include a basal detachment above the lower Torok Formation and a roof detachment in the upper Torok Formation, with each horse being confined between these detachments.

To create this model, 0.1 inch graph paper and a light table were used. This method allowed manipulation of the horse blocks while maintaining consistent perimeters and area. The base for the restorations was the topographic profile and surface projection from cross section A-A' that included the interpretation to depth from the Umiat seismic data (Figure 6.9). Horse size and shape were created using the faults identified in the interpreted Umiat seismic as slip surfaces. Once the size and rhombohedral shape of horses was identified, this pattern was repeated such that all the space between the basal and roof detachments was filled. All of the side lengths and area of each rhombus was kept constant. Two horses (7 and 9) had to be half the area of the other horses due to spatial constraints. Horses were numbered in increasing order away from the pin. Once the deformed model was complete, restoration could occur by sliding horses back to original stratigraphic position along bounding fault planes.

This model does raise some problems as it currently stands. The sub-surface part is based on seismic data from an anticline 30 km north that was interpreted in time, not depth. This model's stratigraphic features and geologic structures are under the Big Bend anticlines but it is not a true reproduction of exactly what is under Big Bend anticlines. Also, the complete thickness of upper Torok Formation is not accounted for in the model because the whole of upper Torok is not contained within the horses, it is cut by the roof detachment. The model also does not account for thickening in the Nanushuk Formation.

The restoration proved to be very interesting and suggests differences in unit shortening that correlate with differences in structural style. The faults and folds were restored to a state prior to deformation (Figure 6.11B). The Umiat seismic data (Figure 6.7) indicate that most of the

structural relief in the Umiat anticline formed above the lower Torok Formation, so I assumed this interval to be unfaulted. Approximately 6.5 km of shortening is accommodated by horses in the middle and upper Torok Formation. Approximately 1 km of shortening is accommodated by folding and faulting in the remaining upper Torok and Nanushuk Formation. The difference in shortening between the two intervals is 5.5 km. This identifies a pressing question: why is there a difference in shortening and how is it accounted for?

The most likely explanation for this difference is that it reflects differences in mechanical stratigraphy between the Nanushuk and Torok Formations. Torok Formation is relatively finer-grained and thinner bedded compared to the Nanushuk sandstone and is thus more susceptible to shorter-wavelength folding and closer-spaced faulting. This explains the multiple internally folded horses within the Torok interbedded shale and fine-grained sandstone. Thicker-bedded, coarser-grained Nanushuk sandstone, being much more competent, would accommodate the same shortening differently. It would be expected to form longer-wavelength folds and more widely spaced faults. It is also very plausible that the competent Nanushuk Formation thickened by layer-parallel shortening before or during folding and faulting. Unit thickening can allow for large amounts of shortening that are only detectable on a very small scale and may not be readily observed in the field. Another possible contributor to the difference in shortening could be related to triangle zone geometry. The roof-thrust has a backthrust sense of motion, so some shortening above the roof thrust (in Nanushuk) may be accommodated in structures outside of the cross section to the south (and hence not accounted for by the reconstruction). Both and/or either explanations could explain the wide difference in shortening between the Nanushuk and Torok Formations in the study area and may be applicable to other areas in the region.

6.10. Discussion

6.10.1. Niger Delta analog for the foothills fold-and-thrust belt

The Niger Delta is a base-of-slope fold and thrust belt that provides good seismic images of folds analogous to those in the Big Bend area. This analog is useful for understanding fold and fault geometry above a decollement in shale. A seismic reflection line (Figure 6.12) shows three gentle detachment anticlines with forethrusts and backthrusts that cut through their limbs. The anticlines are separated by much-wider flat-bottomed synclines. The anticlines and faults are

formed in a competent interval above a flat-lying incompetent decollement unit. The Niger Delta fold-and-thrust belt differs from the Brooks Range foothills because it is a base-of-slope fold-and-thrust belt where contraction was driven by downslope gravitational sliding along the detachment as opposed to orogenic contraction driven by convergent tectonics.

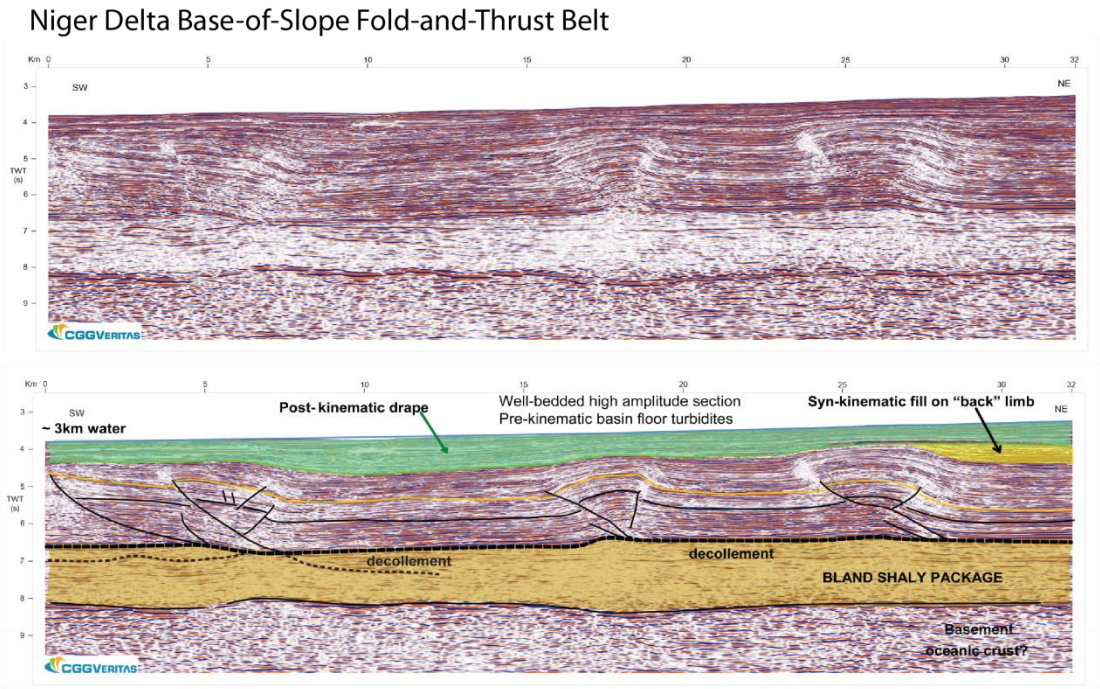

Figure 6.12 Seismic reflection line from Niger Delta fold-and-thrust belt. Top image: Uninterpreted line from Virtual Seismic Atlas, Torvela, 2009. Bottom image: Interpreted line from Virtual Seismic Atlas, (Cullen, 2009).

6.10.2. Geometric-kinematic model for the Brooks Range northern foothills

As discussed in section 3.4 and 6.3, a model by Jones (1982, Figure 6.13) for formation of detachment folds above a low-taper triangle zone fits well with the Brooks Range foothills folds (Wallace, 2009; Wallace et al., 2011). However, this model is highly idealized. The syncline in the study area is more flat bottomed and the true shape of the anticlines from the study area is not well represented. I modified the Jones (1982) model to better characterize the area based on my surface projected cross sections (Figures 5.22-24) and my interpretation of the Umiat seismic line

(Figures 6.6-7). This model (Figure 6.14) displays the gentle anticlines separated by flat-bottomed synclines. The folds are formed above thickened Torok Formation. The Torok is divided into lower, middle and upper mechanical units. Middle Torok has accommodated thickening by folds and thrust faults above a basal detachment at the top of lower Torok. A vaguely defined upper detachment in upper Torok separates thickened Torok below from folded Nanushuk above. Together, these structures form a low-taper triangle zone (Jones, 1982; McMechan, 1985).

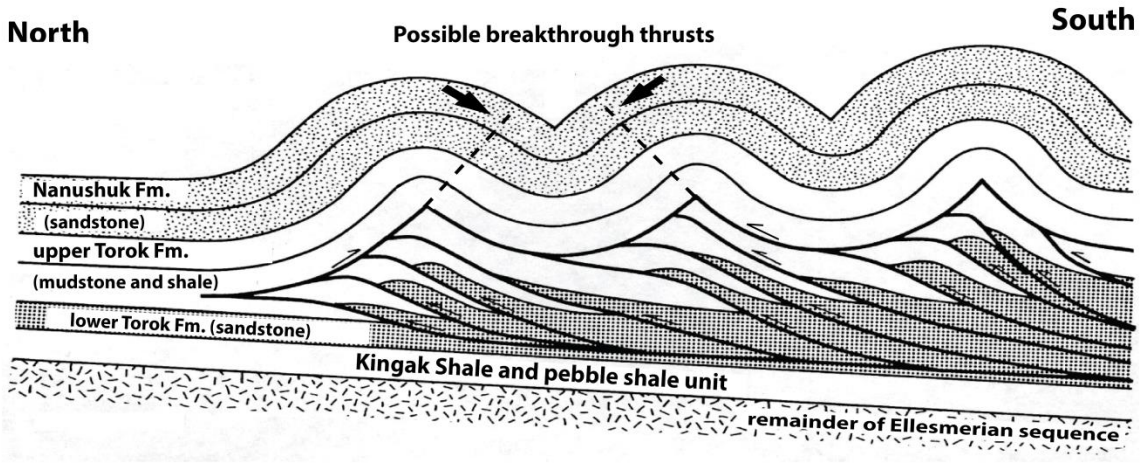

Figure 6.13 Model for the Brooks Range foothills adapted from Jones (1982). Anticlines and synclines are both concentric folds, with circular outer arcs and cuspate hinges in their cores. Faults dip at approximately 45°.

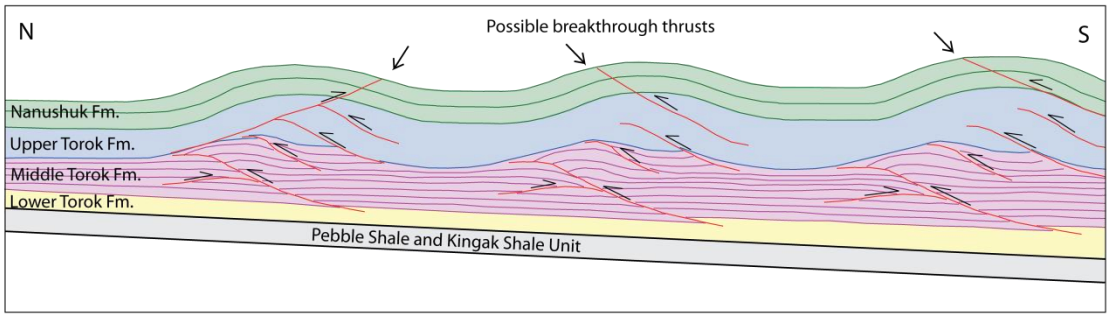

Figure 6.14 New model for the Brooks Range foothills folds based on field observations in the Big Bend area and interpretation of seismic data from the Umiat anticline.

I modified the Jones (1982) model first by stretching it horizontally to show wider flat-bottomed synclines and gentler anticlines in Nanushuk. I used the Umiat seismic interpretation to represent the Torok deformation more realistically. I then used this to infer how thrust faults might cut through the anticline limbs. The updated model should provide a more accurate representation of the geometry and kinematics of the structures and will be helpful for understanding the structure in other parts of the Brooks Range foothills fold-and-thrust belt. This model may also be helpful in understanding the structure and evolution of similar fold-and-thrust belts throughout the world.

Chapter 7 Conclusions

7.1 Generalized conclusions of the thesis

This research resulted in a more detailed understanding of the distribution of the local stratigraphy and of the structural geometry of the Big Bend area. A single, gentle anticline observed at Trouble Creek branches westward into two parallel, east-west trending gentle anticlines separated by a syncline. Small-displacement forethrusts and backthrusts cut through limbs of the anticlines west of the branch zone. A forethrust cuts through the north limb of the southern Big Bend anticline and terminates eastward in the branch zone. A backthrust cuts through the south limb of the northern Big Bend anticline. Observations in the field suggest this fault terminates to the west of the branch zone. However, remote sensing data suggest the backthrust could possibly continue eastward past the branch zone with small displacement, but terminate west of Trouble Creek.

Significant thrusts are restricted to the area west of the branch zone. This suggests that branching of the anticlines played a role in the origin of the thrusts. A very gentle northwest trending anticline connects the two larger anticlines in the branch zone. The branch zone contains complex fold trends and plunges that are not consistent with the east-west trending structures of the area.

Small-displacement conjugate strike-slip faults can be identified throughout the area by displacements in bedding and drainage patterns. The conjugate strike-slip faults and the dominant local fracture set have similar orientations and likely formed concurrently. These strike NE-SW and NW-SE and are located on both north and south dipping anticline limbs. The orientation and shear-sense are consistent with the direction of fold and thrust contraction. The strike-slip faults are interpreted as having formed before the thrust faults in the area. The lineament bound blocks in the southeast corner of the study area are interpreted to be connected to these conjugate strike-slip faults. The most likely explanation for these blocks based on the evidence I observed is that they are bounded by strike-slip faults and are underlain by a low angle detachment with an unknown displacement. This detachment may or may not help to account for the thickened Nanushuk Formation in the southern part of the study area. No extensional structures were observed or interpreted in the study area.

Structural cross sections were constructed from study area surface cross sections combined with interpretation of subsurface data from Umiat anticline to the north of the study area, which provides a useful analog to the subsurface structure in the Big Bend area. Gentle anticlines separated by flat bottom synclines in competent Nanushuk Formation sandstone formed over Torok thickened by more closely spaced north vergent folds and thrust faults. Collectively these structures form a low-taper triangle zone. Seismic data from the Umiat anticline area shows the Torok Formation to have three seismically and structurally distinct intervals. Basal detachment occurs within the lower Torok Formation. Folding and imbrication of horses are present within the middle to upper Torok Formation. A passive-roof detachment exists within the upper Torok, allowing for gentle folds in the overlying upper Torok and Nanushuk formations. The roof-thrust is a backthrust with displacement within the upper Torok Formation. The low taper between the basal and roof detachments allows the breakthrough of the folded roof sequence by either forethrusts or backthrusts.

The cross section restoration suggests shortening in the Torok duplex is greater than in the overlying folds and breakthrough thrusts. Shortening is not fully accommodated by breakthrough thrusts because map relations don't allow enough shortening. Differences in shortening of the overlying Nanushuk could be accommodated by layer-parallel shortening and/or structures above the roof thrust to the south of the cross section.

The results of this research are potentially beneficial to the oil and gas industry because of their relevance to oil and gas exploration in the region. Exploration is currently occurring near Umiat. An understanding of the subsurface structures is helpful in determining the extent and geometry of the hydrocarbon traps. Several hydrocarbon traps are known to exist in anticlines near Umiat (e.g., E. Umiat, Gubik, Wolf Creek) (Kumar et al., 2002). As oil and gas prices increase and the supply of North American oil and gas decreases it likely will be economical to produce from the Umiat area. The first well drilled by Linc Energy was completed during the winter of 2013-2014 with more projected for the following year (Linc Energy, 2012). This research will be beneficial to the public interest as it provides a more detailed geologic map than what is available currently and so will help in making land-use decisions. From a broader scientific perspective, it addresses the geometry and evolution of a type of thrust-related fold that is important in the frontal part of fold-and-thrust belts worldwide, as well as in base-of-slope deformed belts such as the deep Gulf of Mexico and Niger Delta.

7.2 Recommendations for further study

More information and a deeper understanding of the local and regional geology are beneficial for any studied area, including the Big Bend anticline area. Some of the questions that this research was not able to answer include.

1. What is the exact nature of the structure in the branch zone?
2. What accounts for the apparent differences in shortening between Torok and its bounding units?
3. What was the burial depth during fold-and-thrust deformation?
4. How did deformation progress?
5. How exactly do the fractures and strike-slip faults relate to each other, and how and when did they form?
6. What is the surface location and dip of the detachment zone beneath the right-lateral strike-slip faulted blocks?
7. How does this detachment zone fit into the kinematics of the area?

There are many holes to fill in the progress towards understanding this area fully. More time in the field to visit certain areas of interest, such as the branch zone and the southeast detachment location, would obviously be beneficial. However, thermochronological analysis and seismic data from the area would also be very informative.

References

Ahlbrandt, T.S., A. C. Huffman, J.E. Fox, and I. Pasternack, 1979, Depositional framework and reservoir-quality studies of selected Nanushuk Group outcrops, North Slope, Alaska, *in* T. S. Ahlbrandt, ed., Preliminary geologic, petrologic and paleontologic results of the study of Nanushuk Group rocks, North Slope, Alaska: USGS Circular 794, p. 14-31.

Amer, R., Kusky, T., Reinert, P.C., Ghulam, A., 2009, Image processing and analysis using Landsat ETM^{+} imagery for lithological mapping Fawakhir, Central Eastern Desert of Egypt, *in* Proceedings, American Society for Photogrammetry and Remote Sensing Annual Conference, Baltimore, March 2009: Maryland

Atkinson, P.K., and Wallace, W.K., 2003, Competent unit thickness variation in detachment folds in the Northeastern Brooks Range, Alaska: geometric analysis and conceptual model: Journal of Structural Geology, v. 25, p. 1751-1771

Banks, C.J., and Warburton, J., 1986, "Passive-roof" duplex geometry in the frontal structures of the Kirthar and Sulaiman mountain belts, Pakistan: Journal of Structural Geology, v. 8, p. 229-237.

Bird, K.J., and Molenaar, C.M., 1992, The North Slope foreland basin, Alaska, *in* Leckie, D.A., and Macqueen, R.W., eds., Foreland basins and foldbelts: American Association of Petroleum Geologists Memoir 55, p. 363–393.

Cullen, A., 2009, Fold and thrust belt, Hedberg exercise: DW Nigeria Interpretation: http://see-atlas.leeds.ac.uk:8080/homePages/interpretedLine.jsp?resourceId=0900006480014b40 (June 2014)

Davis, D.M., and Engelder, T., 1985, The role of salt in fold-and-thrust belts: Tectonophysics, v. 119, p. 67-88

Detterman, R.L., Bickel, R.S., and Gryc, G., 1963, Geology of the Chandler River region, Alaska: U.S. Geological Survey Professional Paper 303-E, p. 223-324, 16 plates including map sheet, scale 1:125,000.

Eastman, J.R., 2001, Guide to GIS and image processing, Volume 1: Worcester, Massachusetts, Clark Labs, Manual.

Epard, J.L., and Groshong, R.H. Jr, 1995, Kinematic model of detachment folding including limb rotation, fixed hinges and layer-parallel strain: Tectonophysics, v. 247, p. 85-103

Erickson, S.G., 1996, Influence of mechanical stratigraphy on folding vs faulting: Journal of Structural Geology, v. 18, n. 4, p. 443-450

Fischer, M.P., Woodward, N.B., Mitchell, M.M., 1992, The kinematics of break-thrust folds: Journal of Structural Geology, v. 14, no. 4, p. 451-460

Goff, D.F., 1990, Mechanics of thrust-ramp spacing [Ph.D. dissertation]: Collage Station, Texas A&M University

Homza, T.X., and Wallace, W.K., 1995, Geometric and kinematic models for detachment folds with fixed and variable detachment depths: Journal of Structural Geology, v. 17, no. 4, p. 475-588.

Homza, T.X., and Wallace, W.K., 1997, Detachment folds with fixed hinges and variable detachment depth, northeastern Brooks Range, Alaska: Journal of Structural Geology, v. 19, nos. 3-4, p. 337-354.

Houseknecht, D.W. & Schenk, C.J., 2005, Sedimentology and sequence stratigraphy of the Cretaceous Nanushuk, Seabee, and Tuluvak Formations exposed on Umiat Mountain, north-central Alaska: US Geol. Survey Prof. Paper, 1709–B.

Houseknecht, D. W., Bird, K. J. and Schenk, C. J., 2009, Seismic analysis of clinoform depositional sequences and shelf-margin trajectories in Lower Cretaceous (Albian) strata, Alaska North Slope. Basin Research, 21: 644–654. doi: 10.1111/j.1365-2117.2008.00392.x

Jamison, W.J., 1987, Geometric analysis of fold development in overthrust terranes: Journal of Structural Geology, v. 9, p. 207-219

Johnson, A.M., 1980, Folding and faulting of strain-hardening sedimentary rocks: Tectonophysics, v. 62, p. 251-278

Jones, P.B., 1982, Oil and gas beneath east-dipping underthrust faults in the Alberta foothills, in Powers, R.B., ed., Geological studies of the Cordilleran thrust belt, Volume 1, Rocky Mountain Association of Geologists, Denver, Colorado, p. 61-74.

Kirschner, C.E., and Rycerski, B.A., 1988, Petroleum potential of representative stratigraphic and structural elements in the National Petroleum Reserve in Alaska: Chapter 9, in Gryc, G., ed., Geology and Exploration of the National Petroleum Reserve in Alaska, 1974 to 1982: U.S. Geological Survey Professional Paper 1399, p. 191-208, 2 plates. Kumar, N., Bird, K.J., Nelson, P.H., Grow, J.A., and Evans, K.R., 2002, A digital atlas of hydrocarbon accumulations within and adjacent to the National Petroleum Reserve—Alaska (NPRA): U.S. Geological Survey Open-File Report 02-71, 80 p.

Kumar, N., Bird, K.J., Nelson, P.H., Grow, J.A., and Evans, K.R., 2002, A digital atlas of hydrocarbon accumulations within and adjacent to the National Petroleum Reserve-Alaska (NPRA): U.S. Geological Survey Open-File Report 02-71

Lillesand, T.M., Kiefer, R.W., and Chipman, J.W., 2008, Remote Sensing and Image Interpretation: John Wiley & Sons, Inc.

Linc Energy, 2012, Fueling our Future: www.lincenergyumiat.com (June 2014)

McMechan, M.E., 1985, Low-taper triangle-zone geometry: An interpretation of the Rocky Mountain foothills, Pine Pass-Peace River area, British Columbia: Bulletin of Canadian Petroleum Geology, v. 33, no 1, p, 31-38.

Miller, J.J., Agena, W.F., Lee, M.W., Zihlman, F.N., Grow, J.A., Taylor, D.J., Killgore, Michele, and Oliver, H.L., 2000, Regional seismic lines reprocessed using post-stack processing techniques: National Petroleum Reserve-Alaska (NPRA): U.S. Geological Survey Open File Report 00-286

Mitra, S., 2003, A unified kinematic model for the evolution of detachment folds: Journal of Structural Geology, v. 25, p. 1659-1673

Molenaar, C.M., 1982, Umiat field, an oil accumulation in a thrust-faulted anticline, North Slope of Alaska: Powers, R.B., ed., Geologic studies of the Cordilleran thrust belt, Rocky Mountain Association of Geologists, p. 537-548.

Molenaar, C. M., 1985, Subsurface correlations and depositional history of the Nanushuk Group and related strata, North Slope, Alaska, *in* A. C. Huffman, Jr., ed., Geology of Nanushuk Group and related rocks, North Slope, Alaska: USGS Bulletin 1614, p. 37-59.

Molenaar, C. M., 1988, Depositional history and seismic stratigraphy of Lower Cretaceous rocks in the National Petroleum Reserve in Alaska and adjacent areas, *in* G. Gryc, ed., Geology and exploration of the National Petroleum Reserve in Alaska, 1974 to 1982; USGS Professional Paper 1399, p. 593-621.

Molenaar, C.M., R.M. Egbert, and L.F. Krystinik, Depositional facies, petrography, and reservoir potential of the Fortress Mountain Formation (Lower Cretaceous), central North Slope, Alaska: Geology and exploration of the National Petroleum Reserve in Alaska, 1974 to 1982, edited by G. Gryc, pp. 257-279, U.S. Geological Survey Professional Paper 1399, 1988.

Moore, T.E., Wallace, W.K., Bird, K.J., Karl, S.M., Mull, C.G., and Dillon, J.T., 1994, Chapter 3: Geology of northern Alaska, in Plafker, G., and Berg, H.C., eds., The geology of Alaska: The Geology of North America, Geological Society of America, Boulder, Colorado, v. G1, p. 49-140.

Moore, T.E., Potter, C.J., O'Sullivan, P.B., Shelton, K.L., and Underwood, M.B., 2004, Two stages of deformation and fluid migration in the west-central Brooks Range fold and thrust belt, northern Alaska, *in* Swennen, R., Roure, F., and Granath, J.W., eds., Deformation, fluid flow, and reservoir appraisal in foreland fold and thrust belts: American Association of Petroleum Geologists Hedberg series, no. 1, p. 157–186.

Mull, C.G., 1985, Cretaceous tectonics, depositional cycles, and the Nanushuk Group, Brooks Range and the Arctic Slope, Alaska, in Huffman, A.C., Jr., ed., Geology of the Nanushuk Group and related rocks, North Slope, Alaska: U.S. Geological Survey Bulletin 1614, p. 7–36.

Mull, C.G., Houseknecht, D.W., and Bird, K.J., 2003, Revised Cretaceous and Tertiary stratigraphic nomenclature in the Colville Basin, northern Alaska: U.S. Geological Survey Professional Paper 1673, 51 p.

Mull, C.G., Houseknecht, D.W., Pessel, G.H., and Garrity, C.P., 2004, Geologic map of the Umiat quadrangle, Alaska: U.S. Geological Survey Scientific Investigations Map 2817-A, scale 1:250,000, 1 sheet.

Nelson, P.H., Bird, K.J., Houseknecht, D.W., Potter, C.J., Moore, T.E., 2005, Potential tight gas resources in a frontier province-Jurassic through Tertiary strata beneath the Brooks Range foothills, Arctic Alaska: U.S. Geological Survey Open-File Report 2006-1172

O'Sullivan, P.B., 1996, Late Mesozoic and Cenozoic thermo-tectonic evolution of the North Slope foreland basin, Alaska, *in* Johnson, M.J., and Howell, D.G., eds., Thermal evolution of sedimentary basins in Alaska: U.S. Geological Survey Bulletin 2142, p. 45–79.

O'Sullivan, P.B., Murphy, J.M., and Blythe, A.E., 1997, Late Mesozoic and Cenozoic thermotectonic evolution of the Central Brooks Range and adjacent North Slope Foreland Basin, Alaska: Including fission track results from the Trans-Alaska Crustal Transect (TACT): Journal of Geophysical Research, v. 102, p. 20,821-20,845.

Poblet, J., and McClay, K., 1996, Geometry and kinematics of single-layer detachment folds: American Association of Petroleum Geologists Bulletin, v. 80, p. 1085-1109.

Price, N.J., and Cosgrove, J.W., 1990, Analysis of geological structures, Cambridge University Press, 502 p.

Shimer, G.T., McCarthy, P.J., Hanks, C.L., 2014, Sedimentology, stratigraphy and reservoir properties of an unconventional, shallow, frozen petroleum reservoir in the Cretaceous Nanushuk Formation at Umiat field, North Slope, Alaska: American Association of Petroleum Geologists, v. 98, p. 631-661

Torvela, T., 2009, Fold and thrust belt, Hedberg exercise: DW Nigeria Regional Project: http://see-atlas.leeds.ac.uk:8080/homePages/generic.jsp?resourceId=0900006480014288 (June 2014)

Wallace, W.K., 1993, Detachment folds and a passive-roof duplex: Examples from the northeastern Brooks Range, Alaska, *in* Solie, D.N., and Tannian, eds., Short notes on Alaskan geology 1993: Alaska Division of Geological and Geophysical Surveys Geologic Report 113, p. 81-99.

Wallace, W.K., 2009, Mechanical stratigraphy and the structural geometry and evolution of the central and eastern foothills of the Brooks Range, northern Alaska, *in* Hanks, C.L., ed., Unraveling the timing of fluid migration and trap formation in the Brooks Range foothills: A key to discovering hydrocarbons: National Energy Technology Laboratory, Department of Energy, Final report for DOE award DE-FC26-06NT41248, Chapter 2, 34 p.

Wallace, W.K., and Homza, T.X., 2004, Detachment folds versus fault-propagation folds, and their truncation by thrust faults, *in* McClay, K.R., editor, Thrust tectonics and petroleum systems: American Association of Petroleum Geologists Memoir 82, p. 324-355.

Wallace, W.K., Duncan, A.S., Finzel, E.S., and Sanders, C., 2011, Geometry and evolution of folds in the central Brooks Range foothills, in Hanks, C.L., ed., Producing light oil from a frozen reservoir: Reservoir and fluid characterization of Umiat field, National Petroleum Reserve, Alaska: Department of Energy, Annual report for DOE award DE-FC26-08NT0005641, Chapter 5, 40 p.

Wentz, R., 2014, Fracture characteristics and distribution in Cretaceous rocks near the Umiat anticline, North Slope of Alaska [Master's thesis]: Fairbanks, University of Alaska

Wiltschko, D.V. and Chapple, W.M., 1977, Flow of weak rocks in Appalachian Plateau folds: Bulletin of American Association of Petroleum Geologists, v. 61, p. 653-670

Woodward, N.B., and Rutherford, E., 1989, Structural lithic units in external orogenic zones: Tectonophysics, v. 158, p. 247-267

Unknown, 1999, TOC/rock-eval pyrolysis geochemical data for 26 Alaska North Slope wells: Alaska Division of Geological & Geophysical Surveys Geologic Materials Center Data Report 284, 51 p. doi:10.14509/19132

Publications resulting from this work:

Sanders, C. M., Wallace, W.K., May 2011, Structural Geometry of the Big Bend Anticline, Brooks Range Foothills, Alaska. 86th Annual Meeting of the Pacific Section, American Association of Petroleum Geologists, Anchorage, Alaska, Abstracts, p. 84.

Appendix A Remote Sensing Data and Results

A.1. Methods/workflow

Satellite data is used in this study to look for trends in the overall study area that may not be apparent on the ground level or in aerial photographs alone. Optical and Synthetic Aperture Radar (SAR) data are used to identify geologic structures and bedding traces. Satellite images can be overlain on any digital elevation model such as the ASTER GDEM (Advanced Spaceborne Thermal Emission and Reflection Radiometer Global Digital Elevation Map) data to be viewed in 3-D in order to analyze reflectance values with topographic information. Most of the satellite data analysis was done after field work was completed, thus allowing for some ground based information to aid satellite image analysis. This became very helpful when locating and mapping the extent of geologic structures and stratigraphic unit contacts using remote sensing data.

Optical images are from Landsat 5 Thematic Mapper (TM) and SAR images are from Advanced Land Observation System's Phased Array L-Band Synthetic Aperture Radar (ALOS PALSAR) in the dual fine resolution mode. Exact image identification numbers and acquisition dates are in appendix B. The optical and SAR imagery was enhanced with various filters and indices to show lineaments and variations in lithology. Visual analyses were performed on all images to locate stratigraphic features and geologic structures by observing patterns in vegetation growth, lithology, and drainages. In the research process, other analysis techniques were also tried but proved not to be helpful toward this research. This chapter discusses only the images that were useful for the research. The data that was not used is in appendix C, accompanied by an explanation. All images are created at a scale of 1:100,000, images are scaled to fit in the text of this thesis. All of the images presented here were originally created or projected to the coordinate system of WGS 1984 UTM zone 5. Spatial reference linear unit is in meters.

Software used in processing the images for this research included:

1. ERDAS Imagine 9.3 for optical image processing and analysis
2. ESRI ArcGIS 8.0 and ESRI ArcGIS 10 for compilation of final remote sensing images and final maps (use of ArcMap and ArcScene)
3. Alaska Satellite Facility (ASF) MapReady 2.3 for initial processing and terrain correction of PALSAR images

A.2. Basic of Satellite Data Analysis

In this study, Optical and SAR images are use. Optical images include Landsat 5 TM bands and ASTER GDEM that are collected in the visual and near, mid and thermal infrared portions of the electromagnetic spectrum. PALSAR data are in the L-band with horizontal (HH) and vertical (HV) polarization in the microwave region of the electromagnetic spectrum at 1-2 GHz. One of the uses of PALSAR, with its long wavelength, is for mapping land surfaces, particularly geologic structures. One big advantage of PALSAR data is that it is largely unobstructed by clouds. Most of the images used for this research were collected in the summer and early fall when the study area is essentially devoid of snow cover. The short length of acquisition opportunities limits the number of image options, however suitable images were found for each sensor type.

Optical images are often displayed as a red, green, blue (RGB) image with different spectral bands or combinations of bands displayed in each color. SAR images may also be displayed this way as typically each image has a number of bands or layers stacked together to make the complete image. Each band represents a different wavelength range and thus represents different image types (Table 5.1). A normal or true color optical image, such as a conventional photograph, is displayed with TM bands 3, 2 and 1 displayed in RGB respectively. A false color composite (FCC) is any combination of bands other than 321. As an example, this research uses a standard FCC of 432 which means the image is a false color composite with bands 4 in red, 3 in green and 2 in blue.

Table A.1 Thematic Mapper Spectral Bands table describes the purpose and use of each band of the Landsat 5 TM data. The bands used for this research include: 1,2,3,4, and 7. Bands 5 and 6 were analyzed but were not as useful. Modified from Lillesand et al., 2008.

Table 5.1 Thematic Mapper Spectral Bands

Band	Wavelength (μm)	Nominal Spectral Location	Principal Applications
1	0.45-0.52	Blue	Designed for water body penetration, useful for coastal water mapping. Also useful for soil/vegetation discrimination, forest-type mapping, and cultural feature identification
2	0.52-0.60	Green	Designed to measure green reflectance peak of vegetation for vegetation discrimination and vigor assessment. Also useful for cultural feature identification.
3	0.63-0.69	Red	Designed to sense in a chlorophyll absorption region aiding in plant species differentiation. Also useful for cultural feature identification.
4	0.76-0.90	Near IR	Useful for determining vegetation types, vigor, and biomass content, for delineating water bodies, and for soil moisture discrimination.
5	1.55-1.75	Mid IR	Indicative of vegetation moisture content and soil moisture. Also useful for differentiation of snow from clouds.
6[a]	10.4-12.5	Thermal IR	Useful in vegetation stress analysis, soil moisture discrimination, and thermal mapping applications.
7[a]	2.08-2.35	Mid IR	Useful for discrimination of mineral and rock types. Also sensitive to vegetation moisture content.

[a] Bands 6 and 7 are out of wavelength sequence because band 7 was added to the TM late in the original system design process

Spectral band ratios or indices are another analysis performed on optical images. Certain spectral band ratios or indices enhance certain types of lithology or vegetation. Others highlight differences in texture due to sediment size. Predetermined indices can be very helpful when dealing with large or multiple data sets that need to be analyzed in a timely manner. The last analysis performed on optical data for this research is called a principal component analysis. A principal component analysis allows the data to be compressed such that common statistical components can be viewed as their own bands (Amer et al., 2009). This analysis allows the researcher to view and analyze different components of the image in order to identify specific characteristics about each component. As an example principal components may help to distinguish between fine grained sediment deposited near a river bed and fine grained sediment within a swampy basin. This method can take the seven layers associated with Landsat images

and compress the most common components down to three or four bands so that the variability between components can be optimally analyzed (Lillesand et al., 2008).

The long wavelength of PALSAR images allows the waves to penetrate through the surface vegetation. This is a very useful tool in looking at the surface lithology of an area. The L-band operates in the 1-2 GHz range. Surface features that may not show up on other optical data, such as faults or lithological boundaries, are more likely to be visible in L-band data. The downside of such deep penetration into the vegetation and soil or sediment layer is that the presence of liquid water can disrupt the returning signal. In areas with lots of standing water or high precipitation levels, L-band data may not be as useful as other SAR data. This is especially true in swampy, boggy terrain.

A.3. ASTER GDEM

The ASTER GDEM images provide a topographic base that can be compared to published topographic maps of the area. The topographic maps used for this research were created in 1955 using aerial photographs, whereas the ASTER GDEM images were collected after 2000. The ASTER GDEM data were provided by NASA and METI (the Ministry of Economy, Trade and Industry of Japan) and are at a 30 meter spatial resolution. The data were collected between March 2000 and August 2008 in cooperation with the Japan-US ASTER Science Team. A sample of the topographic maps created for this research can be found in appendix D.

Two ASTER GDEM images had to be combined in a mosaic because of an image boundary in the study area. The ASTER GDEM topographic information was used to create 3-D images of the area in ArcScene. Other images were draped over the 3-D topography in order to better identify and visualize lithological boundaries and locations of structures such as faults or fold hinges. The best image drapes came from the processed Landsat 5 TM images. These draped images helped to delineate structures that were then mapped on the TM images as described in the next section.

A shaded relief image, or “hillshade”, was derived from the ASTER GDEM (Figure A.1). The hillshade provides a view of the topography with most of the ridges and major drainages

visible. The brightest areas are ridge tops, which are fairly flat, making them highly reflective. The dark areas have steep slopes that are not as reflective. These help define drainage areas. There is very little distinction of the actual river location. An apparent increased level of noise in the image could be due to the type of vegetation covering the area.

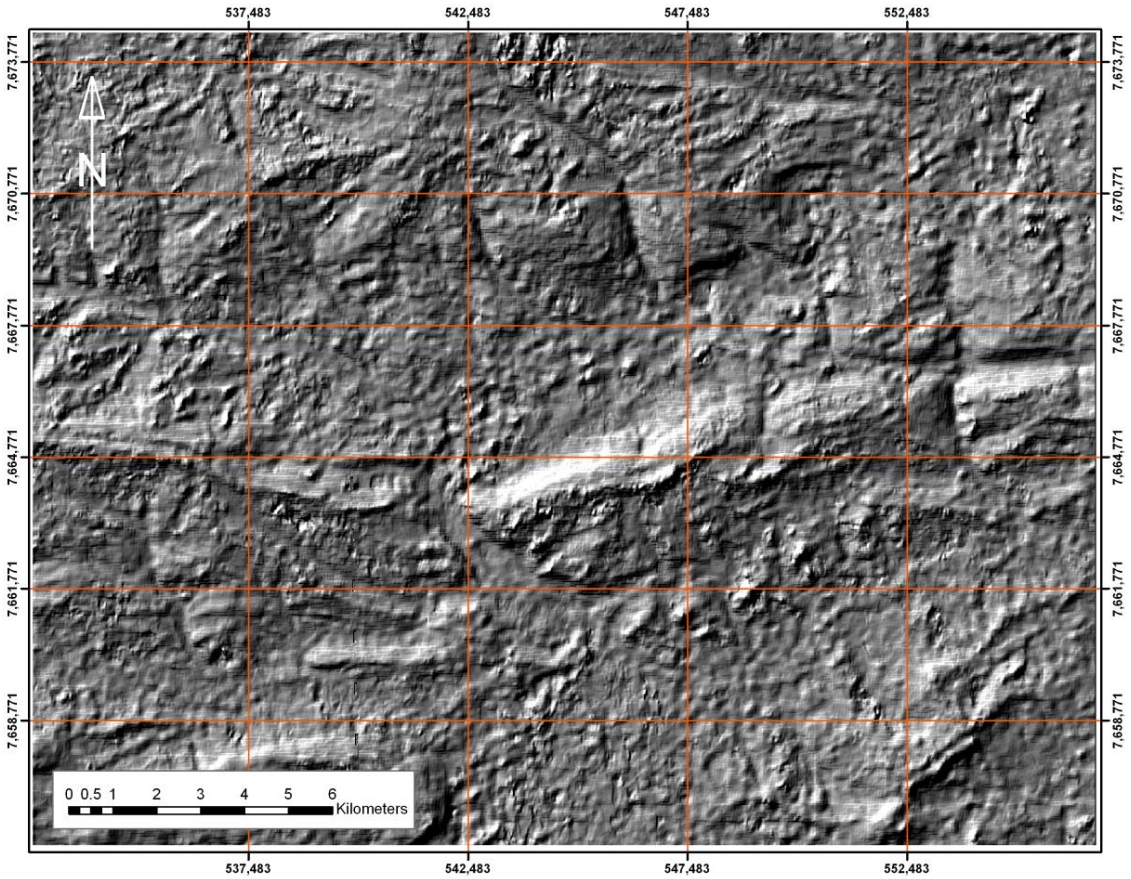

Figure A.1 Hillshade derived from ASTER GDEM to show topography. Ridges and some drainages are visible. Scale is set at 1:100,000.

The ASTER GDEM was also used to create the contour lines used as the base for the final geologic map (Figure A.2). I decided that it was important to use the ASTER GDEM contour lines since the most recent published topographic information was over 50 years old. A comparison between the old and new information showed that there were some slight differences, mostly due to changes in drainage patterns. The contour interval for the base map

was set at 20 meters. The base level contour was set at 140 meters above sea level to keep it consistent with the 1955 topographic maps.

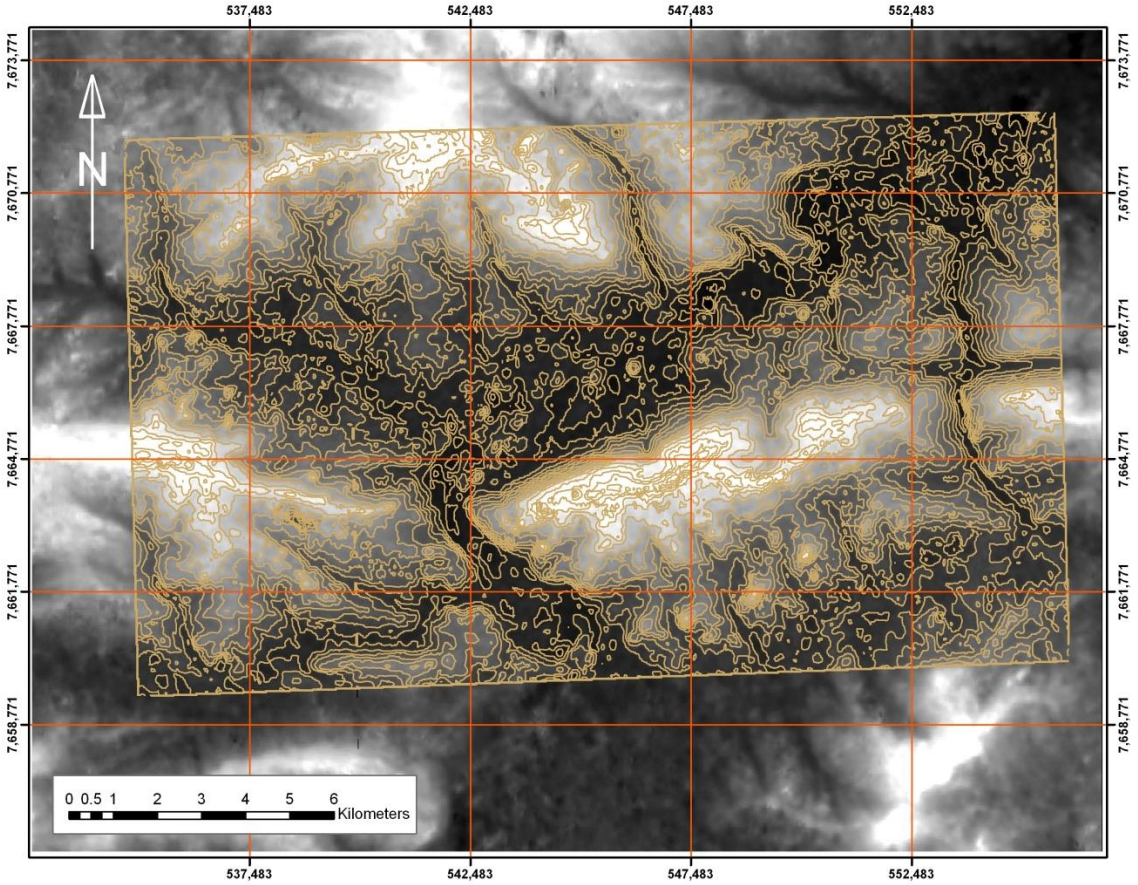

Figure A.2 Twenty meter contour interval map derived from ASTER DEM above a base at one hundred forty meters above sea level, as determined from the published topographic map. These contours are used on the geologic map made for this research.

A.4. Landsat 5 TM: analysis and how it relates to the study area

Optical data, such as Landsat data, can be very informative for surficial geological mapping. For this research, Landsat 5 TM help to define lithology, drainage patterns, erosion patterns, hill slope, bedding dip, vegetation characteristics and water features. The image used for this research was taken in August 2009 because it was acquired on a clear day. It has a thirty meter

spatial resolution, three bands in visual wavelengths and four bands in the infrared region of the spectrum. This allows for a wide range of FCCs and indices to process for mineral, clay and vegetation content. A principal component analysis was also performed.

Some of the images processed and presented in this thesis have colored boxes denoting important areas. The yellow box in the northern part of the image in Figure A.3 encloses the part of Paunagaktuk Bluff where bedding is most visible. The green box in the eastern part of the image surrounds Trouble Creek where it cuts through the eastern part of the Big Bend anticline. The orange box encompasses the southern limb and hinge of the southern Big Bend anticline. The light blue box surrounds the lineament bound blocks in the southeastern corner of the image. Lineament patterns are visible on some images and have been drawn on the images to help the reader see the pattern. Interpretations of the geologic structure are shown for all processed images for geologic reference and spatial reference between images. Uninterpreted images are also included for comparison.

An FCC with bands 4,3, and 2 is a standard composite for identifying differences in lithologic units based on vegetation characteristics (Figure A.3). Vegetation shows in red, with more densely vegetated areas being darker. Green shows unconsolidated fine grained sediment. Cyan shows bedding and other exposed rock. The north dipping bedding of Paunagaktuk Bluff is within the yellow box. Dip direction of bedding follows the rule of V's in the major drainage in the eastern side of the yellow box. The green box shows the bedding dipping in opposite directions, indicating that the anticline hinge is perpendicular to Trouble Creek. The orange box shows the bedding that is visible in the southern Big Bend anticline. Drainage patterns show up well in this image as dark red linear features. Drainages typically have a higher density of vegetation due to the increased soil available from erosion and the abundant water for plant growth. The light blue box in the southeastern corner surrounds lineament bound blocks interpreted to be separated by right-lateral faults. The direction of slip and rotation can be determined by the offset of the bedding within the blocks.

A generalized structural interpretation for the area is shown with anticline hinges in dark blue and faults in black. The anticline hinge locations were determined based on bedding dip direction. The fault in the northern part of the study area was determined based on an increase in vegetation in an east-west linear zone of recessive topography parallel to the northern anticline hinge. The dashed fault to the south of the southern anticline was determined based on the

northern boundary of the lineament bound blocks and associated changes in the drainage patterns. This fault is thought to be the detachment zone that allowed for strike-slip movement of the block. Direction and amount of displacement of the faults cannot be determined from satellite information.

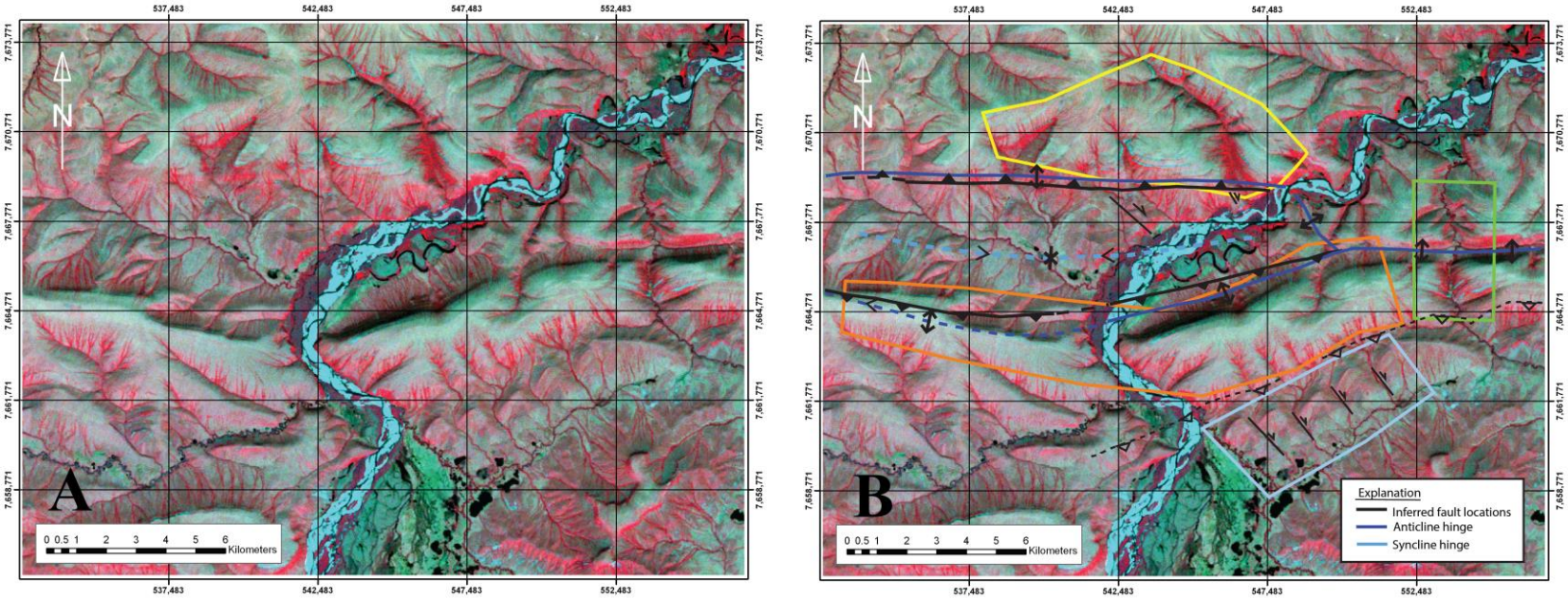

Figure A.3 FCC 432 of Landsat 5 TM, uninterpreted image (A, left) and with structures and location boxes included (B, right). This image shows exposed rock in cyan and increasing amounts of vegetation in red. The vegetation is densest near drainages making the drainage pattern in the image stand out. The yellow box in the top of the study area is around the beds visible in the northern limb and crest of the northern Big Bend anticline. Bedding strike and dip direction is evident from the bedding pattern along the drainages. The green box in the east of the study area is around the Trouble Creek area. Bedding dip direction is clear and can be used to determine the anticline hinge. The orange box in the center of the study area shows the location of the southern Big Bend anticline. Bedding strike and dip direction can be determined from bedding patterns in the drainages. The blue box in the southeast corner of the study area surrounds lineament bound blocks separated by right-lateral faults. Rotation direction can be determined from the visible bedding that forms the ridges near the north of each block. The location of the northern fault was determined from a linear vegetation pattern. The detachment in the south limb of the southern Big Bend anticline was determined based on changes in vegetation patterns. Hinge locations were chosen based on bedding dips and topography when the image was draped over the ASTER GDEM.

An FCC with bands 7,4, and 3 is another standard combination for viewing variations in surface lithology based on vegetation physiognomies (Figure A.4). In this image, well exposed rocks and bedding show as magenta. Clear, moving water is blue and standing water is black. Gravel and areas with low vegetation such as ridge tops are purple. Areas devoid of vegetation are the brightest purple. Areas with increased or dense vegetation are green. These areas tend to show in drainages and areas with known clay-rich lithology, thus an increase in soil moisture may account for the denser vegetation.

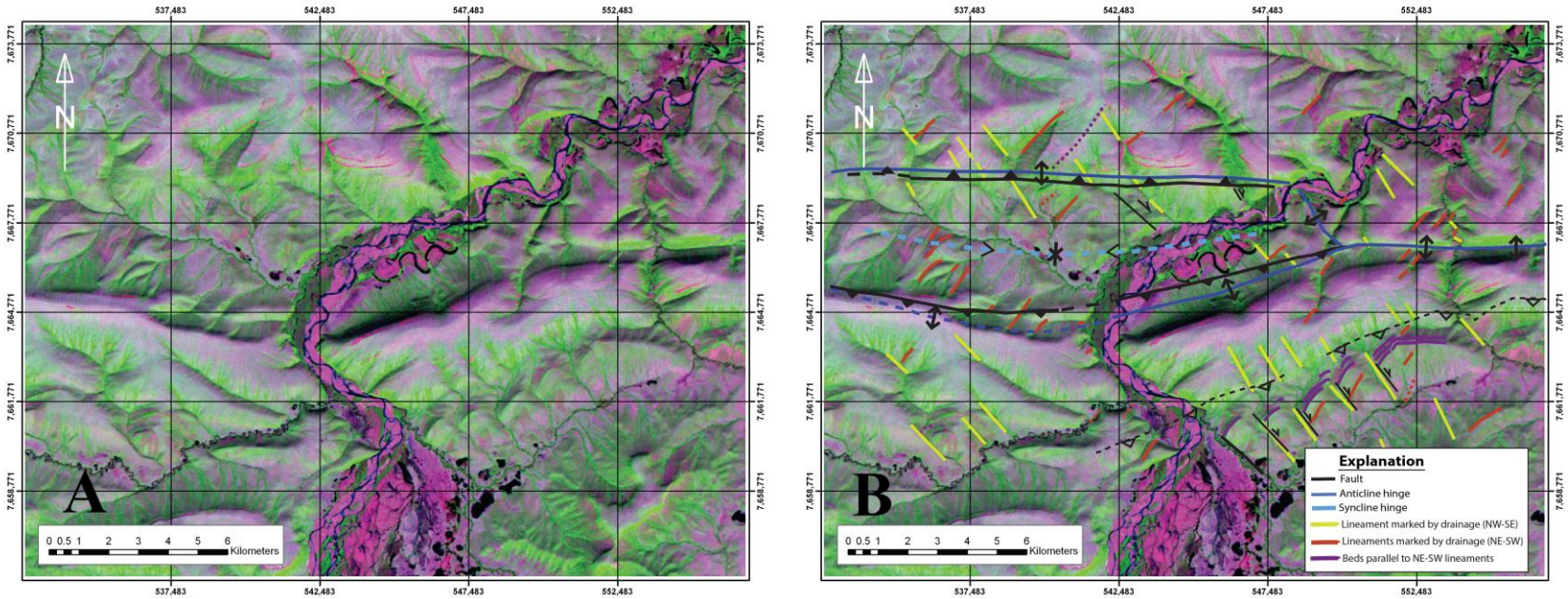

Figure A.4 FCC 743 of Landsat 5 TM, uninterpreted image (A, left) and interpreted image showing lineament patterns and the northern fault (B, right). Lineaments are marked by drainages that are straight and sub-parallel or by discontinuity of bedding on the same trend. The lineaments marked in yellow (NW-SE) and red (NE-SW) have similar trends to the dominant sets in the local fracture pattern. NW-SE lineaments help to identify the lineament bound blocks in the southeast corner of the study area. The northern fault shows as a bright green strip, on the uninterpreted image, due to the increase in vegetation density possibly due to an increase in water or soil along the fault trace. Hinge locations are for reference.

Drainage areas show up very well in this image and seem to highlight the lineament pattern first identified on the topographic maps. By emphasizing the drainage areas that are more linear than other drainages, a general northwest-southeast and northeast-southwest pattern of trends emerged. This was especially true near the lineament bound blocks in the southeast corner of the study area. The drainages separating these blocks are linear and follow the northwest-southeast trend. The offset in the bedding shows apparent right-lateral strike-slip motion along these lineaments.

The most interesting aspect of this image is the location of the northern fault that cuts through the southern limb of the northern Big Bend anticline. The FCC 743 image shows a linear pattern of dense vegetation midway up the slope of Paunagaktuk Bluff. This feature trends east-west parallel with the anticline hinge and is a continuation of an area with visible fault offset identified during field work. The increase in vegetation may be due to an increase in moisture due to breaks in the rock or due to an increase in soil, both consistent with a fault trace. It is unlikely that a change in drainage pattern created this increase in vegetation because it transects southward trending drainages.

Two different indices (Lillesand et al., 2008) were generated from the Landsat 5 TM image: the ferrous minerals index and the vegetation index. The ferrous minerals index was used to identify differences in lithology and erosion patterns. Differences in lithology would be helpful for determining lithologic boundaries. More recessive units such as the Seabee and Torok Formations would have a different erosion pattern than more resistant Nanushuk Formation. The vegetation index highlights differences in vegetation such as type, density, water saturation and chlorophyll concentration. Anomalous changes in vegetation can be the result of changes in geologic structure especially in areas without cultural influences.

The ferrous mineral index is projected in shades of grey (Figure A.5). Very light areas are gravel, fine grained sediment or exposed rocks. Dark areas show low mineral reflectance values, such as areas covered by water or dense vegetation. Areas of traceable bedding are outlined by the yellow, green and orange boxes. The light color of the exposed rocks contrasts with the darker, vegetated areas between the beds making it easy to distinguish the number and location of beds. The exposed bedding traces are helpful when using the rule of V's to determine bedding dip and ultimately the location of the anticline hinges. Areas of medium reflectance values with

some lighter spots are located between the yellow and orange boxes and south of the orange box. These areas are mapped as Seabee Formation in previous work by Mull et al., (2004) and from my field work. These lighter areas are due to the clay rich nature of Seabee Formation. The very bright areas along the river are due to gravel bars. In the southern part of the study area, near the river, the light areas are due to sediment that has been carried downriver and deposited as the river shifted its bed. This sediment is within and under low marshes and swamps created on top of old river beds.

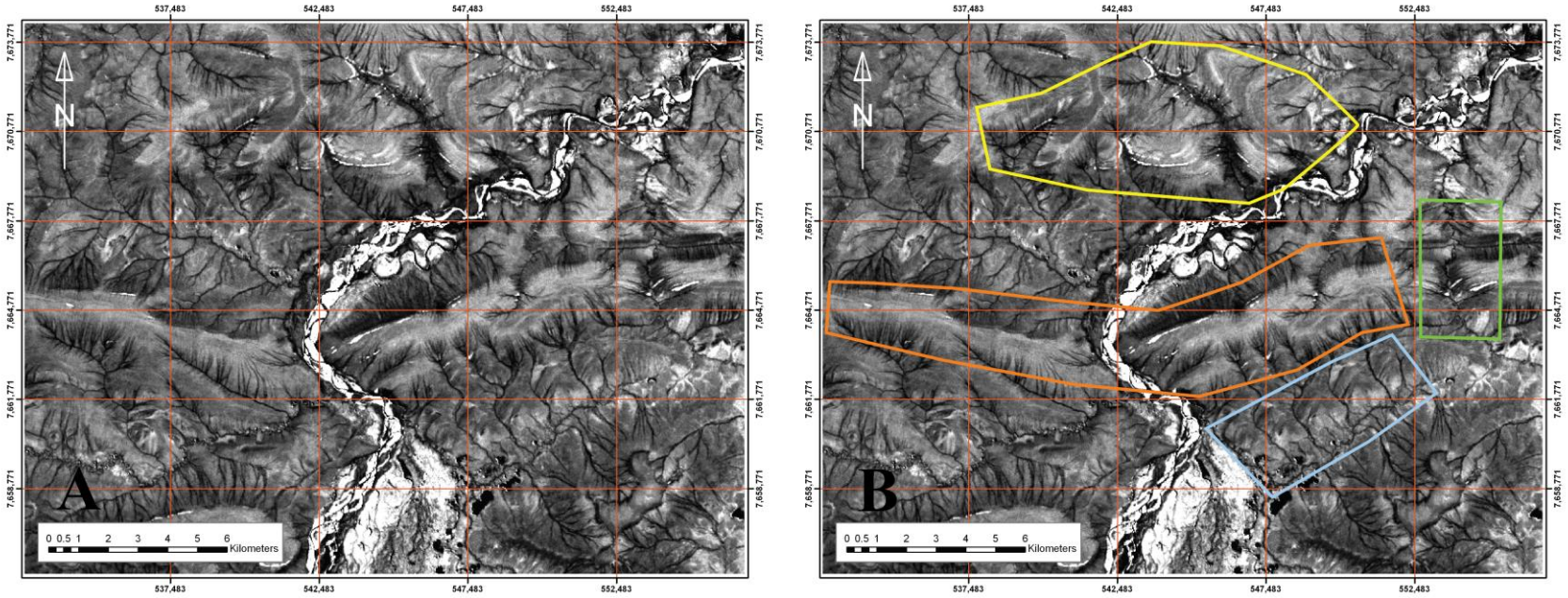

Figure A.5 Images made using the ferrous minerals index on Landsat 5 TM (TM band 3/TM band 1) with a sharpening filter, uninterpreted (A, left) and with location boxes (B, right). This image helps to identify drainages, exposed rocks and bedding trace. The drainages, along with most of the water associated with the river, are very dark due to a lack of minerals in the water. All exposed rocks, either as outcrop, rubble zones or unconsolidated sediment, show up with a very light color. The beds in the yellow, green and orange boxes can be traced to help identify the dip direction of beds and shape of the geologic structures. Lighter areas around the river are due to an increase in reflectance value and are the result of gravel bars and sediment carried downslope and deposited in marshy/swampy areas near the river.

Northern latitudes typically show notable differences in vegetation between south facing and north facing slopes. Changes in vegetation can also signal a change in soil moisture, soil availability, or nutrient content. The vegetation index produced from the Landsat 5 TM (Figure A.6) shows many of these anomalies. As expected, more soil and soil moisture are present in the drainage areas. These appear brighter on the image, with the densest vegetation growing in areas with the most soil and moisture. Water and exposed rocks, including river gravels, have the strongest absorption and appear dark. The traces of bedding are identifiable in this image as thin dark lineaments within the hills of the northern and southern anticlines.

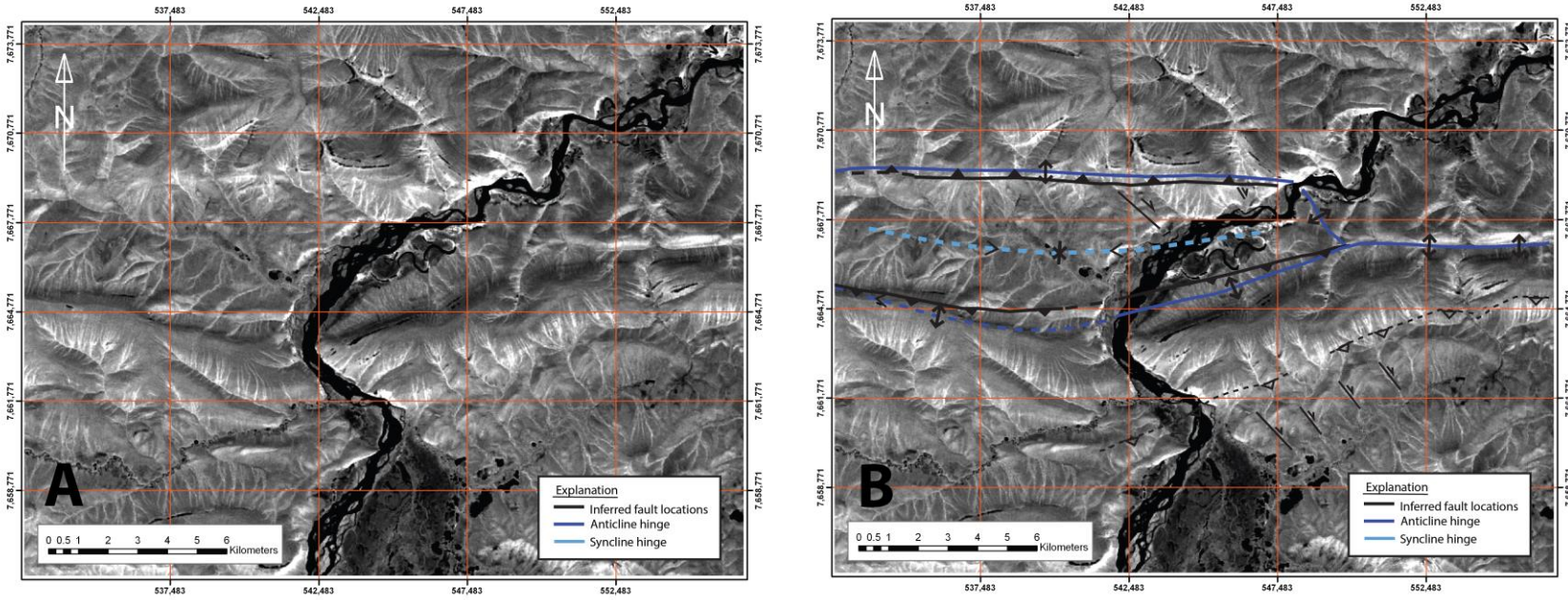

Figure A.6 Vegetation index of Landsat 5 TM; uninterpreted (A) on the left and with structural interpreted (B) on the right. This image shows differences in vegetation. Taller and denser vegetation near the drainages shows with a light color. Moving or free standing water is dark, almost black. The river, ponds and swampy areas are all dark. Outcrops, rubble and unconsolidated sediment also show as a dark color. Differences in vegetation can be seen on different limbs of the southern Big Bend anticline, as discussed further in the text. The northern fault is also visible as an increase in vegetation.

In the southern Big Bend anticline in particular, but also seen in the northern Big Bend anticline, the south facing slope has a higher percentage of brighter digital values and thus more vegetation. This may partially be due to the fact that water draining down the south facing slope of the southern Big Bend anticline flows along the dip of bedding so the slope is more conducive to plant growth. Water on the northern slope drains across bedding, which increases erosion but seems to hinder vegetation growth as can be seen by the increase in dark areas on the north facing slope. The difference in vegetation could also be due to the fact that these south facing slopes receive more sunlight than the north facing slopes (Figure A.6).

The increase in vegetation along drainages and the differences in vegetation growth along the slope faces are helpful when viewing the lineament bound blocks in the southeast corner of the study area. These blocks are clearly defined by the drainage patterns between and around them. The well-defined bedding and the character of the exposures in this image indicates that the blocks are composed of competent bedding. The lineament bound blocks are observed to have denser vegetation along the southern slopes. These characteristics are consistent with the Nanushuk Formation of the study area.

The northern fault is identifiable by a lineament of increased vegetation along the southern slope of the northern Big Bend anticline. This increase of vegetation is most likely due to an increase in soil or moisture associated with the fault as discussed in the previous section and for Figure A.5. The presence of this lineament in multiple types of data is further evidence that a structural feature is visible with satellite data.

A principal component analysis can be helpful for large areas that contain a high level of complexity. A principal component analysis can compress large amounts of information into a smaller number of bands (Amer et al., 2009). The first two or three components manage to explain the original variability thus reducing noise without losing valuable information (Eastman, 2001). For this research, seven components were created by principal component analysis from the Landsat seven band composite image. The first three proved to be of interest to this research. The first component (PC1) shows the common signatures of all seven bands (Figure A.7). This image shows primarily the topography of the region with some distinctions for water saturated areas. Water is dark with river gravels and some zones of exposed rock

rubble being brighter. Shadows are due to the sun illumination and the satellite-Sun-Earth geometry. There is no distinction of clay rich areas.

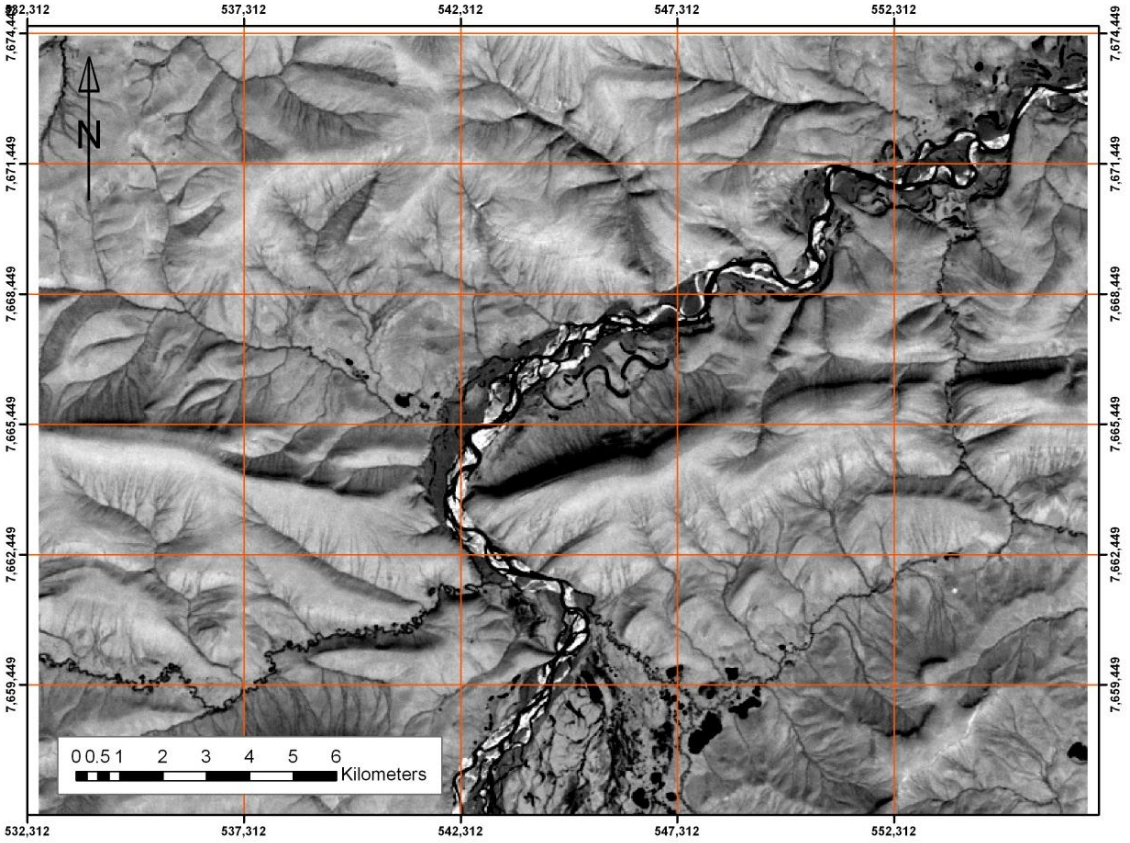

Figure A.7 PC1 image generated from a Landsat seven-band composite image, Landsat PC7-band 1. PC1 shows the common signatures of all seven bands. Water is dark. River gravels and some rubble zones are lightest. Basic topography is identifiable. Shadows are due to illumination form the sun and the Sun-Earth-satellite geometry. There is no differentiation of clays.

The second principal component (PC2) shows variances in vegetation (Figure A.8). Taller and denser vegetation is brighter and is evident in drainages and swampy areas along the river. The higher absorption values include areas of water and all exposed rocks including gravel and clays. A large swampy area near the river in the southern portion of the image is darker. This area is darker than other swampy areas because a large amount of river sediment underlies the

vegetation. This sediment was deposited as the river moved westward to its current position. There are also differences in density of vegetation between north or south facing slopes, as discussed with the vegetation indices, with the south facing slopes being brighter because they have denser vegetation. Areas with fine-grained sediment or clays are darker but are hard to differentiate from areas of increased soil moisture.

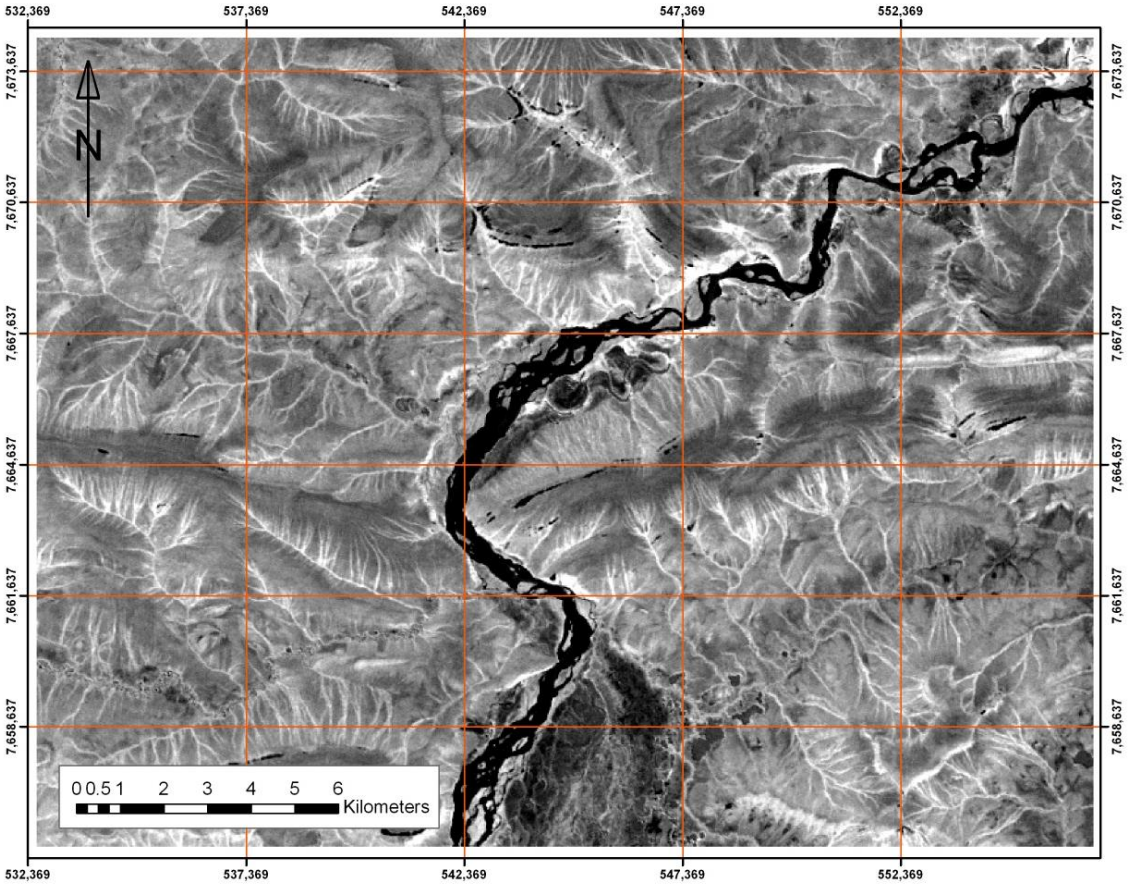

Figure A.8 PC2 image generated from a Landsat seven-band composite image, Landsat PC7-band 2. PC2 highlights differences in vegetation. Water, outcrops, rubble zones and unconsolidated clay sediments are dark. Taller and denser vegetation is light and shows mostly in the drainages.

The third principal component (PC3) highlights the lithology and is the most interesting (Figure A.9). All water is bright in this image but drainage areas are dark. Clays and fine-

grained sediment are light as are exposed beds and rubble zones. River gravel is dark, which is a contrast to most other images in which river gravel and exposed rocks are typically similar in reflectance value. The most interesting aspect of this image is that the sediment-rich area in the valley bottom east of the river in the southern part of the study area is much lighter than the river gravel from which it was derived. This suggests the possibility that there is another unknown explanation for the broad swampy area not covered in this study.

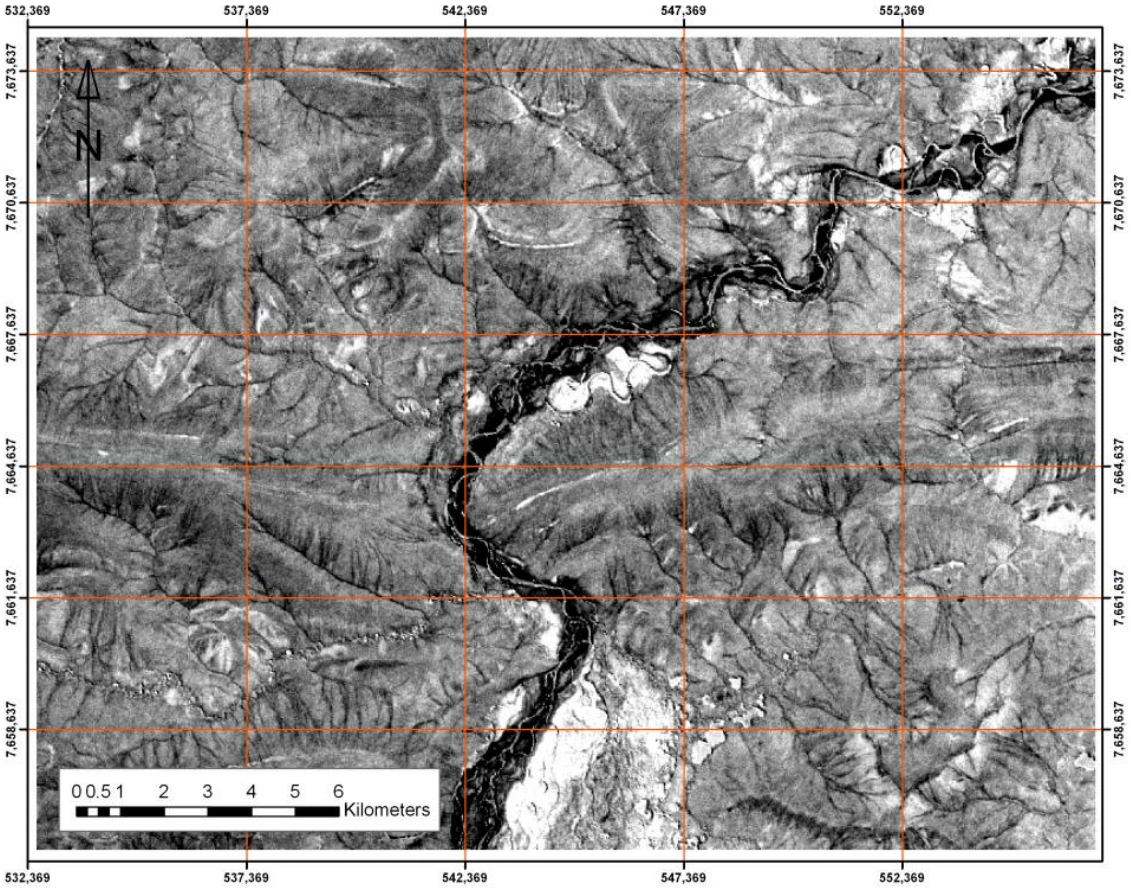

Figure A.9 PC3 image generated from a Landsat seven-band composite image, Landsat PC7-band 3. PC3 highlights the lithology. Moving water is medium to light. Still water is light. Exposed rock, river gravel and unconsolidated sediments are light. Clay-rich areas are lighter, whereas areas with coarser grain size are slightly darker in general. Drainages are dark.

I compiled the three principal components discussed above into an image where PC1, PC2 and PC3 are displayed in R, G, and B, respectively (Figure A.10). The common signatures for

all seven bands are highlighted in PC1 (red), vegetation is prominent in PC2 (green) and lithology is projected in PC3 (blue). By comparing the three single-component images with the color composite I was able to determine the characteristics indicated by the colors in this RGB image:

- Dark blue signifies clear moving water
- Lighter blue indicates still water and some rock and rubble exposures
- Red shows river gravel
- Yellow-green means an increased density of vegetation such as in drainages
- Purple denotes low lying swamps full of clay rich sediment
- Magenta and hot pink indicate coarser-grained rock such as sandstone

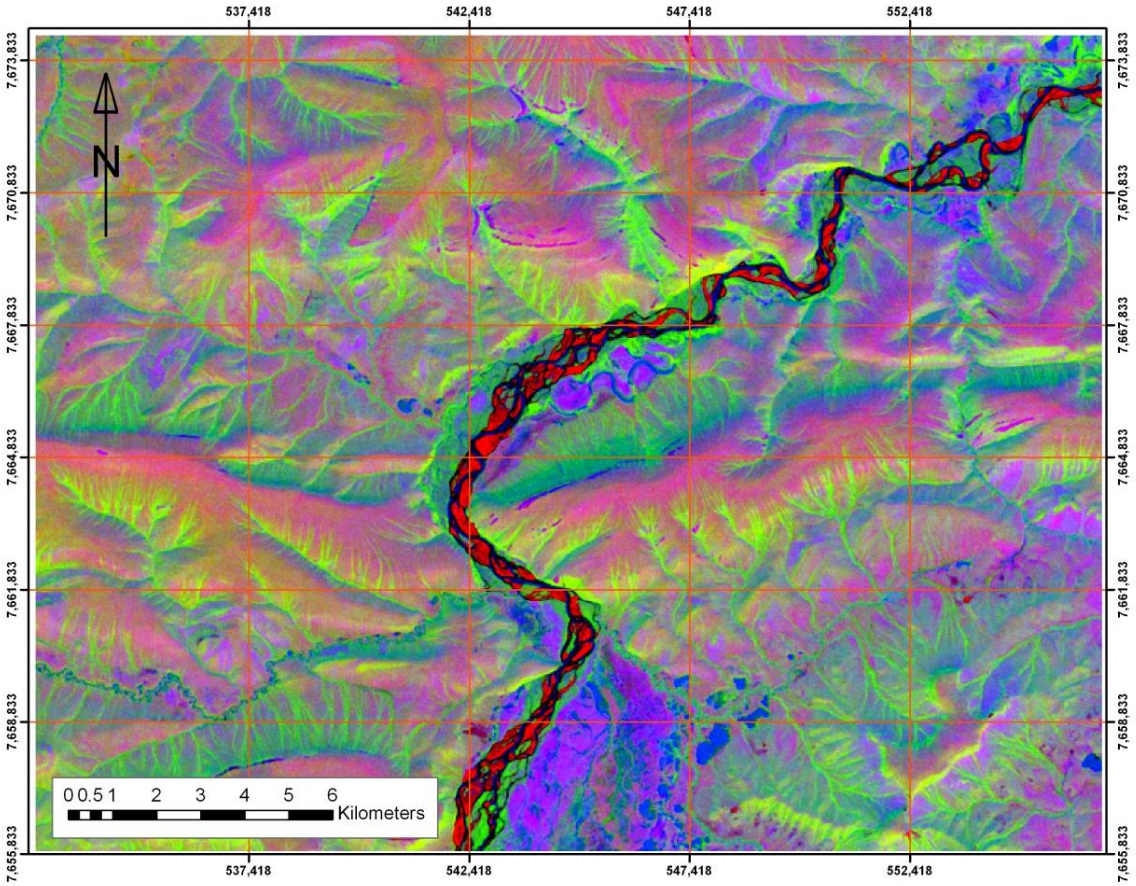

Figure A.10 PC bands 1, 2 and 3 derived from a 7-band Landsat image. Common signatures of all seven bands are shown in red. Vegetation is shown in green and lithology is shown in blue. Exact color associations are discussed fully in the text.

By looking at the range of values in each single-component image, features could be identified by band combination and color. For example, in the RGB composite, river gravel is red. The only single-component image in which river gravels are bright is for the first component, which is band 1 in the composite image, projected in red. This same reasoning was used to identify other features in the image such as clays and other fine-grained sediment created by river erosion. Density and abundance of vegetation is also discernible. Grain size of exposed rocks allows distinction between sandstone bedding and rubble and river gravel. Bedding traces and characteristics help to indicate the direction of bedding dip.

The composite image was helpful in identifying contacts between fine-grained sediment such as the clay of Seabee and Torok Formations and coarser-grained sediment such as is found in Nanushuk Formation (Figure A.11). However, no distinction is visible between Seabee Formation clay and Torok Formation shale. No distinction exists between fine-grained sediment deposited by the river and fine-grained sediment in exposed stratigraphy. The pattern shown in the image of coarser-grained units merging to the east is consistent with a branching anticline.

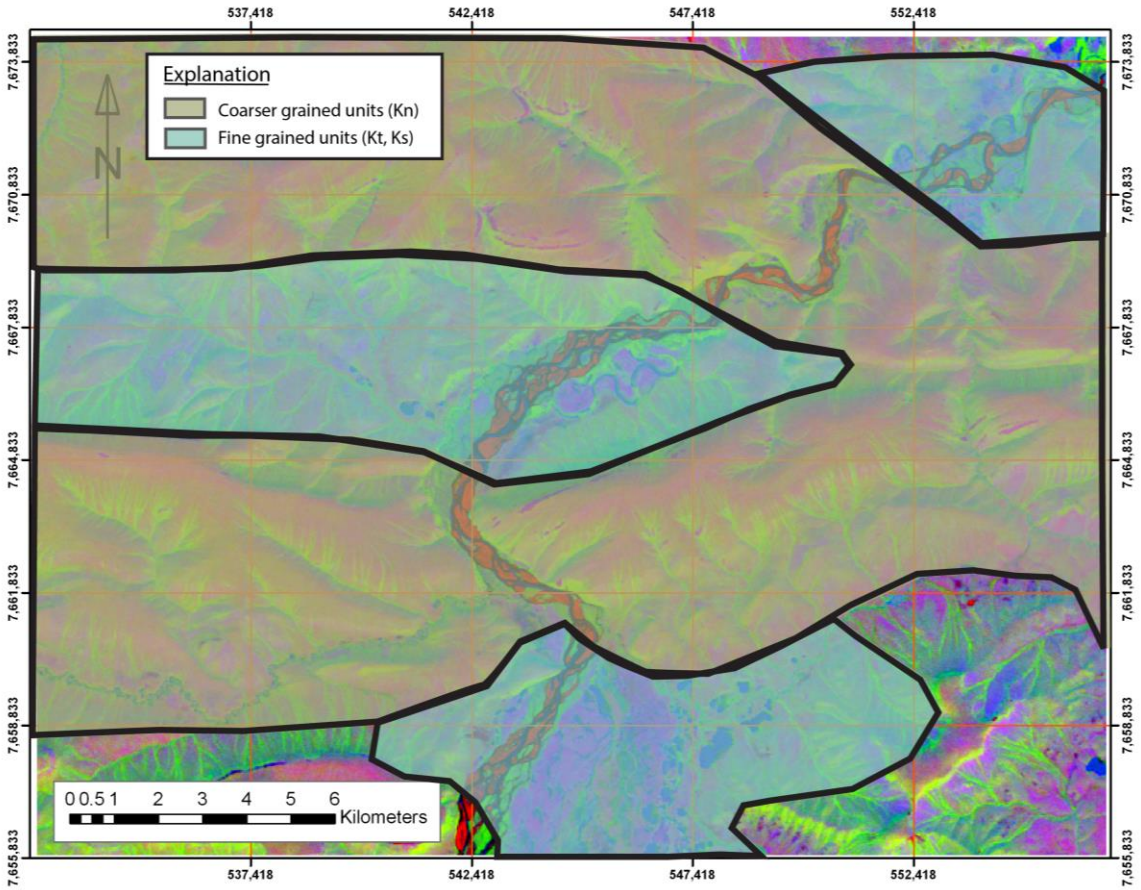

Figure A.11 PC3, derived from the Landsat 7 band composite image, interpreted to show lithologic units. Note there is no discernable distinction between Torok Formation shale and Seabee Formation clay.

A.5. SAR images: analysis and how it relates to the study area

Satellite images in the microwave range, such as ALOS-PALSAR, can be very helpful for geological interpretation because these wavelengths are less influenced by clouds and other atmospheric disturbances. The SAR interaction with vegetation and underlying lithology is considerably different from interaction in the visible and infrared regions. Therefore SAR provides a complementary dataset to study the Earth's surface, including topography, lithology, soil and sediment characteristics, presence of water, and geologic structures such as faults. The use of SAR images for this research has been effective in determining the location of and truncation of beds by faults for which there is little optical or field evidence.

The SAR images used for this research are the ALOS PALSAR and ERS-2 (European Remote Satellite) images. I was interested in the L-band from PALSAR and the C-band from ERS. Analysis of the SAR data included visual analysis of the polarized bands. I also combined SAR data with optical data in simple color composites to carry out integrated analysis of these data.

PALSAR data are polarimetric. The data used for this research included 5 scenes taken at different times each containing HH (horizontal) and HV (vertical) polarization (Table A.2). The initial processing of the PALSAR data included terrain correction and the creation of stacked images with three bands. The three bands include HH in red, HV in green and the ratio of HH/HV in blue. This initial processing was done by Rudi Gens at ASF (Alaska Satellite Facility at the Geophysical Institute, University of Alaska Fairbanks).

Table A.2 PALSAR Data Identification Information. Table includes the ID numbers and dates of acquisition. Band numbers relate to the stacked image that contains HV layers from each data set (Figure A.12).

Table A.2 PALSAR Data Identification Information		
Identification Number	Date Collected	Band/Layer Number
ALPSRP084351380	August 25,2007	1
ALPSRP091061380	October 10 2007	2
ALPSRP191711380	August 30,2009	3
ALPSRP245391380	September 2, 2010	4
ALPSRP252101380	October 18, 2010	5

In further visual analysis of different bands for individual images, I determined that the HV band of each image was the most helpful. This may be due to the east-west trend of most of the geologic structures of the area. An image was created using only the HV band from each of the five data sets. FCCs of the different combinations of HV bands were analyzed for geologic structures and stratigraphic features. Of all of the combinations analyzed, two images were most helpful. FCC 123 provides the best evidence for the location of the faults between the two anticline hinges (Figure A.12). This image shows a pattern of darker lineaments extending from

areas of known fault location. These dark lineaments are interpreted to be the location of major thrust faults. The dashed fault in the southern portion of the study area is a known detachment zone but it is unknown if there is displacement along the detachment. FCC 123 does help to identify the exact location of the detachment at the surface relative to the lineament bound blocks. The other image, FCC 125, also shows these same patterns but is in Appendix H.1 so as not to be redundant.

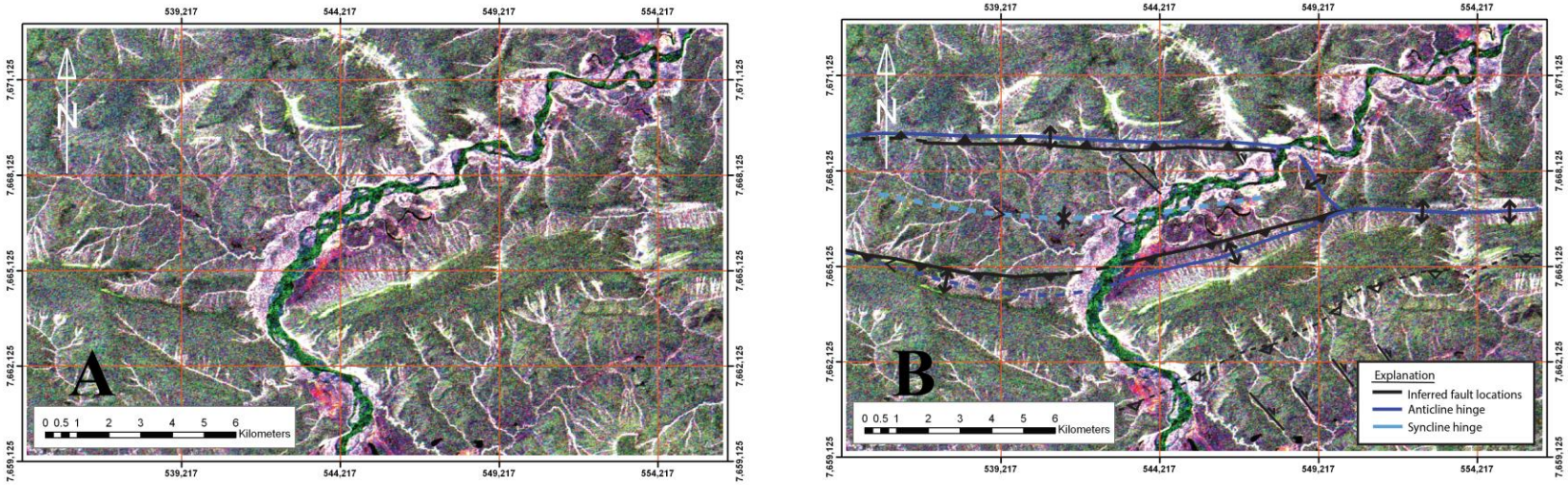

Figure A.12 Image combining band 2 (HV) of five PALSAR images. Uninterpreted (A, left), interpreted (B, right). Bands/layers 1,2 and 3. Clear, moving water is green. Gravel and eroded areas are light with some magenta. Coarse-grained rock such as sandstone has high reflectance. Purple is in areas with known clays and fine-grained sediment. The thrust faults here are defined by darker tones. Some bedding layers are also dark but are not as laterally continuous or dark as the interpreted fault locations.

I combined some of the PALSAR band 2 data with the Landsat 5 TM in order to make use of the complimentary information in these data sets. The image includes HV from ALPSRP084351380 as red, HV from ALPSRP091061380 as green and band 4 from the Landsat 5 TM image as blue (Figure A.13). This image was helpful for determining erosion patterns and sediment grain size. Areas that are very bright or yellow denote fine grained sediment. Blue colors show coarser-grained rock and increased vegetation. Some geologic features that are apparent are areas of high erosion along the northern slope of the rotated blocks and the southern Big Bend anticline, bedding traces that are normally covered by vegetation along the southern slope of the southern Big Bend anticline and near the hinge of the northern Big Bend anticline and increased soil moisture in areas such as the syncline between the two anticlines.

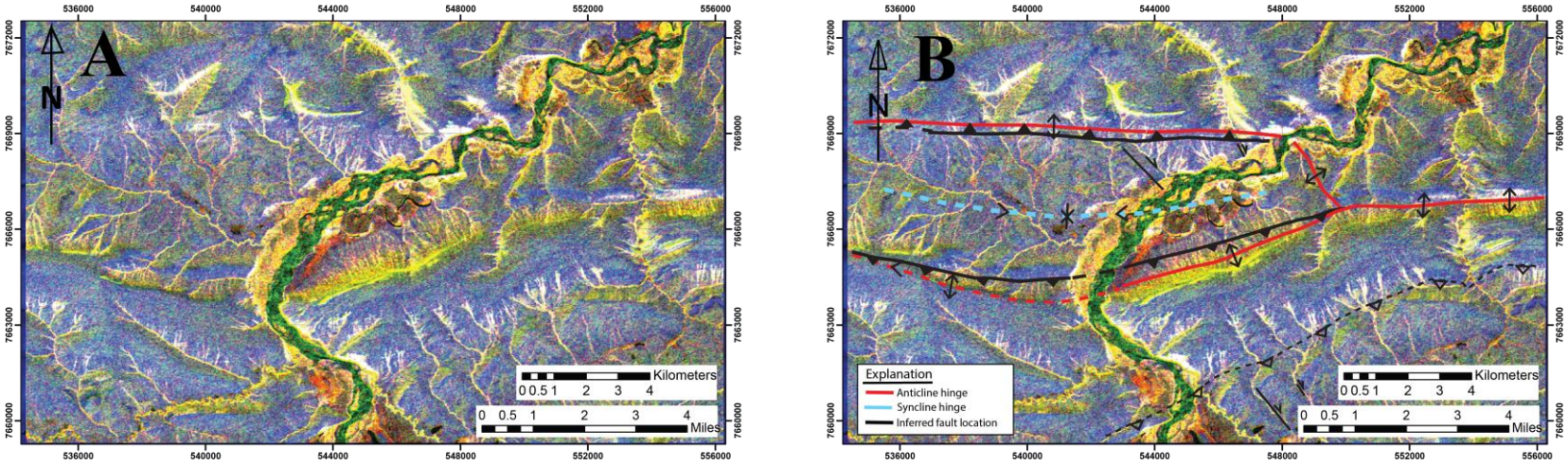

Figure A.13 Combined PALSAR and Landsat image; uninterpreted (A, left) and interpreted (B, right). These data are used in conjunction with known fault locations from field work. Major thrust faults show as dark blue east-west trending lineaments. The northern backthrust also has some very light areas associated with it that may be due to the reflection pattern associated with the slope of the hill or the local drainage pattern. Clear water is shown in green. Red and yellow show highly eroded areas such as the Seabee clay and gravel near the river. These areas commonly contain more water in sediment than better indurated sandstone beds would. The blue shows the areas of resistant rocks and bedding traces.

The most interesting and useful image stack including PALSAR data also includes ERS-2 data (Figure A.14). The image is composed of HV from ALPSRP084351380 in red, HV from ALPSRP091061380 in green and band 2 from the ERS-2 image in blue. All ERS identification information is presented in Appendix B. This image shows information on fault locations, bedding traces, exposed rock and vegetation similar to other images in this study. However, it also shows the eastward continuation of the northern thrust fault through the branch zone better than other images. Using all of the other information available, I could trace the fault only as far east as the west side of the Chandler River. In this image, the lineament associated with this fault continues across the river to the east, bends gently south and runs parallel to the single anticline at Trouble Creek. The dark lineament associated with the fault continues past Trouble Creek to the east out of the study area. The actual amount of displacement along this lineament is unknown as I found no evidence for the fault at Trouble Creek during field work. For this specific study the combination of PALSAR and ERS data provided information that other processing methods could not. Similar combinations of data could prove to be helpful in future geologic interpretations.

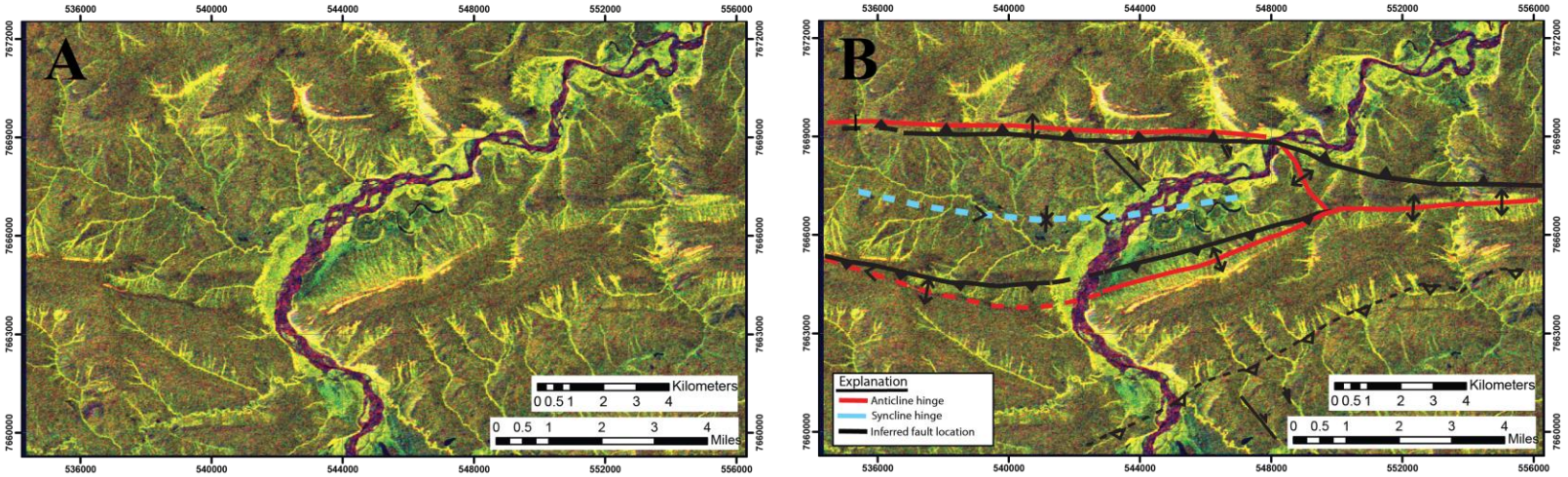

Figure A.14 Combined PALSAR and ERS-2 data in an FCC composed of HV polarized bands from two different date PALSAR and one ERS-2 image. Uninterpreted (A) and interpreted (B). Clear, moving water is green. Gravel and eroded areas are light with some magenta. Green is resistant rock. The thrust faults are seen here as darker lineaments. Some bedding traces are also dark but are not as laterally continuous or dark as the interpreted faults.

ERS-1 and Radarsat-1 data were also acquired and processed for this research. However, none of the processing provided any new information that could not be gained from either optical or PALSAR data. I concluded that for this study the L-band data were more useful than the C-band data. All of the data processed and analyzed is presented in Appendix H.

A.6. Remote predictive mapping (RPM): use of RPM in mapping remote areas and how it relates to this research

Remote predictive mapping (RPM) can be a very valuable tool for remote sensing analysts and geologists alike. RPM is mapping of an area using remote sensing data with limited or no field data. This is often done because of the remoteness of the area being mapped, such as the North Slope of Alaska, the Sahara or other planets. Mapping can be done for vegetation, watershed, geologic or other reasons. In an ideal situation, RPM would be done in conjunction with field work, but this is not always possible or practical. The next most useful approach includes some remote sensing analysis being done prior to field work in order to guide and direct the field work to maximize efficiency. Then the data from the field could be used to update, rework or continue the remote sensing analysis. This allows for the most effective use of all the data available.

For this research, RPM was used by processing most of the Landsat 5 TM data before field work was conducted. This allowed for a deeper understanding of the topography, stratigraphy and structure of the area. Camp sites location and initial areas to visit could be determined before travel to the field. This maximized helicopter time as well as on-foot traverses. After field work was completed, observations made in the field guided analysis done with PALSAR and ERS 1 and 2 data.

Information gained in the remote sensing portion of this research has allowed for more complete and informed mapping decisions to be made. Remote sensing analysis has also provided different data to be used to validate interpretations made from field data. This has proved very helpful for determining the exact location and extent of the thrust faults and the unit contacts.

B.1 Satellite identification information

Table B.1 All satellite images used in the analysis for this research

Image	Identification Number	Stacked units
ASTER DEM	ASTGTM_N69W152	
ASTER DEM	ASTGTM_N69W153	
Landsat 4/5 TM	LT50750112009200GLC00	
PALSAR	ALPSRP084351380	
PALSAR	ALPSRP091061380	
PALSAR	ALPSRP191711380	
PALSAR	ALPSRP245391380	
PALSAR	ALPSRP252101380	
Radarsat-1	R1_34102_ST2_F277	
Radarsat-1	R1_28957_ST2_F277	
Radarsat-1	R1_13522_ST2_F277	
Radarsat-1	R1_10435_ST2_F277	
Radarsat-1	R1_09063_ST2_F277	
ERS-1	E1_12341_STD_F276	Right 3
ERS-1	E1_11840_STD_F276	Right 3
ERS-1	E1_11339_STD_F276	Right 3
ERS-1	E1_10838_STD_F276	Right 3
ERS-1	E1_10337_STD_F276	Right 2
ERS-1	E1_09335_STD_F276	Right 2
ERS-1	E1_08834_STD_F276	Right 2
ERS-1	E1_08333_STD_F276	Right 2
ERS-1	E1_07832_STD_F276	Right 2
ERS-1	E1_07331_STD_F276	Right 1
ERS-1	E1_06329_STD_F276	Right 1
ERS-1	E1_05828_STD_F276	Right 1
ERS-1	E1_04826_STD_F276	Right 1
ERS-1	E1_04325_STD_F276	Right 1
ERS-1	E1_06378_STD_F174	Left 1
ERS-1	E1_05376_STD_F174	Left 1
ERS-2	E2_79963_STD_F174	Left 2
ERS-2	E2_79462_STD_F174	Left 2
ERS-2	E2_78961_STD_F174	Left 2
ERS-2	E2_80186_STD_F276	Right 2
ERS-2	E2_79184_STD_F276	Right 2
ERS-2	E2_78683_STD_F276	Right 2

C.1 Extra satellite analysis-Images and interpretation for remote sensing analysis not presented in the text: PALSAR, Radarsat-1 and ERS 1/2 data

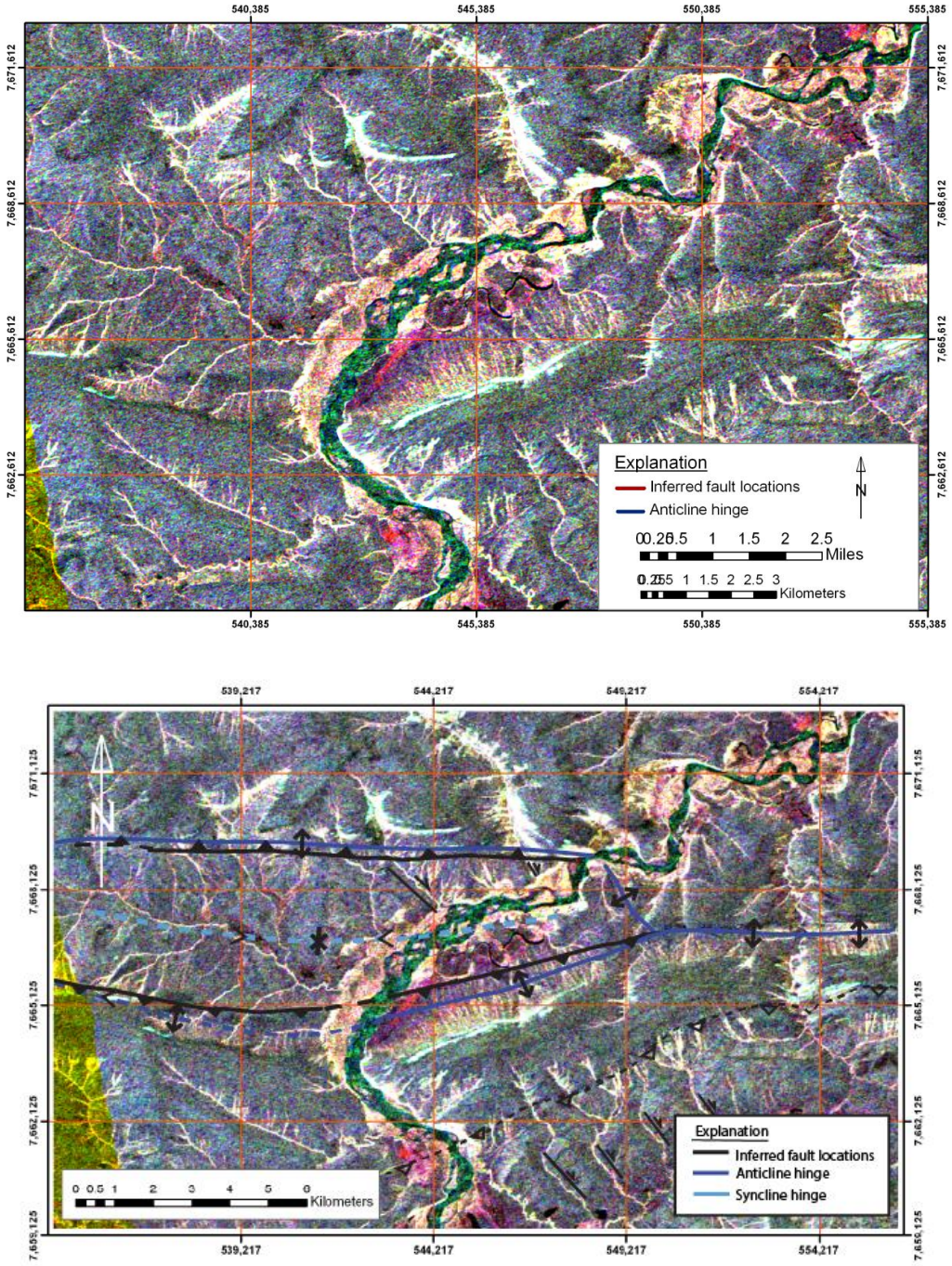

Figure C.1 PALSAR stack of all HV bands. FCC 125 similar to FCC 123 presented and discussed within Appendix A.

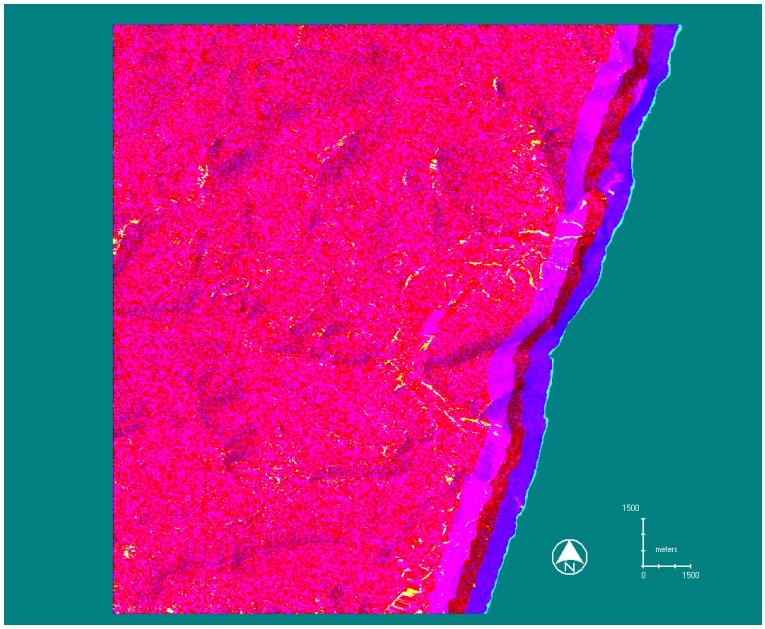

Figure C.2 ERS-1 right stack 2 principal component with 3x3 low pass filtering. Bands 1,2,5.

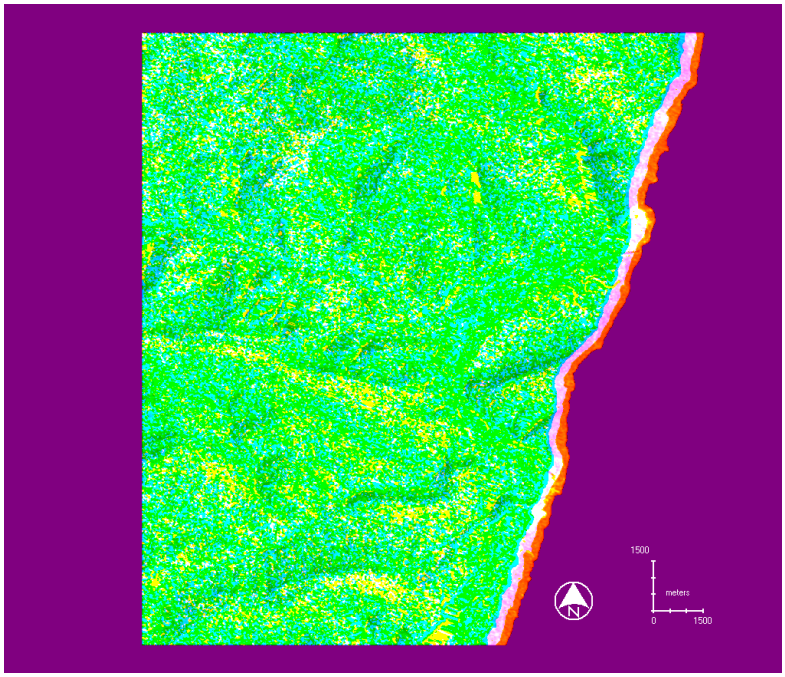

Figure C.3 ERS-1 right stack 3 principal component with 5x5 low pass. Bands 4,1,2.

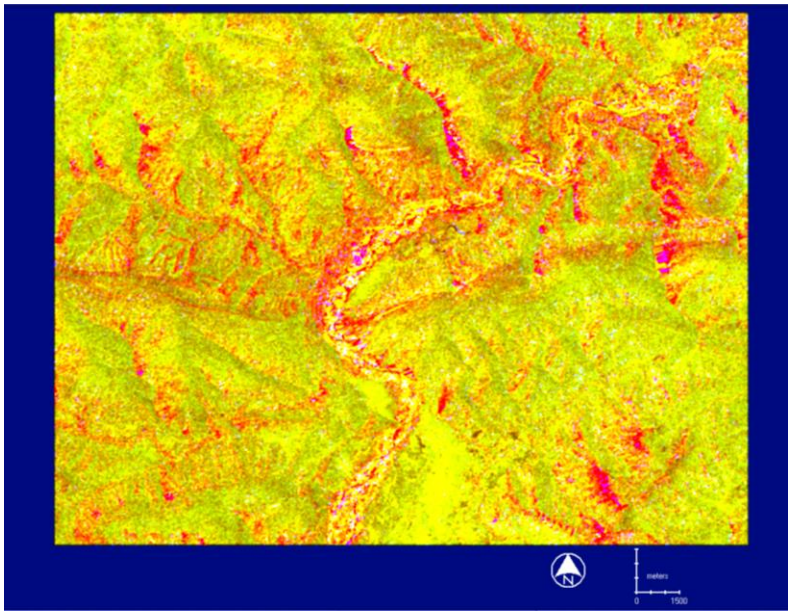

Figure C.4 ERS-2 right stack, principal component with low pass filter. Bands 1,2,3.

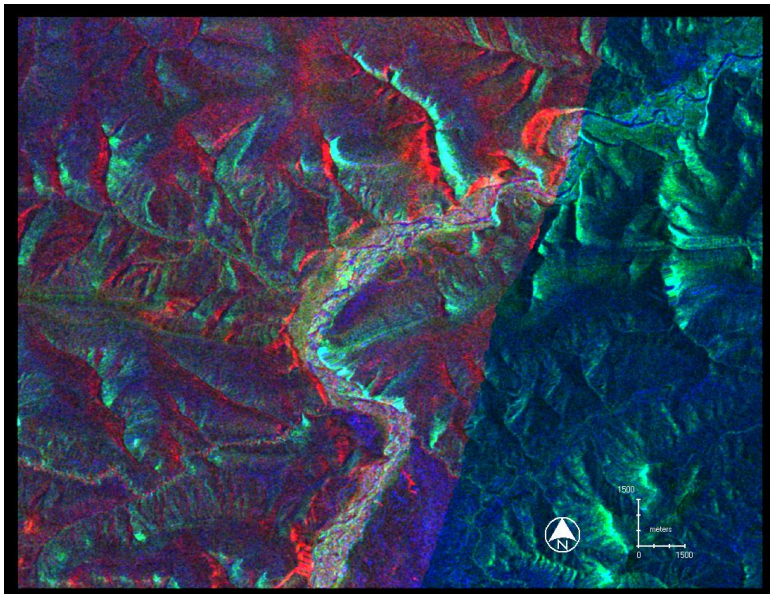

Figure C.5 ERS-2 all data and Landsat 4/5 TM image, principal component with 5x5 low pass filter. Bands 1,2,4.

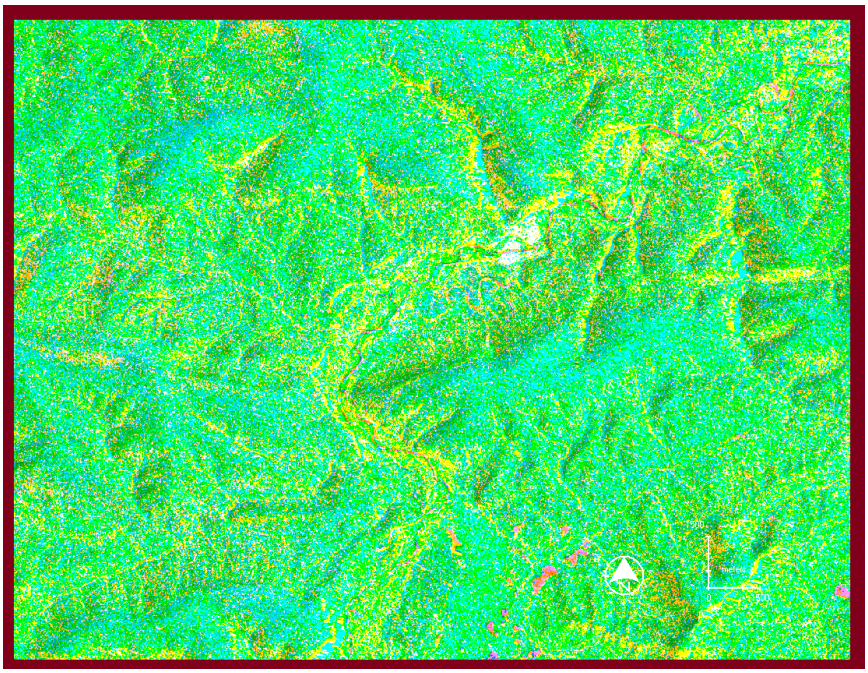

Figure C.6 Radarsat-1 all data, principal component. Bands 4,1,3.

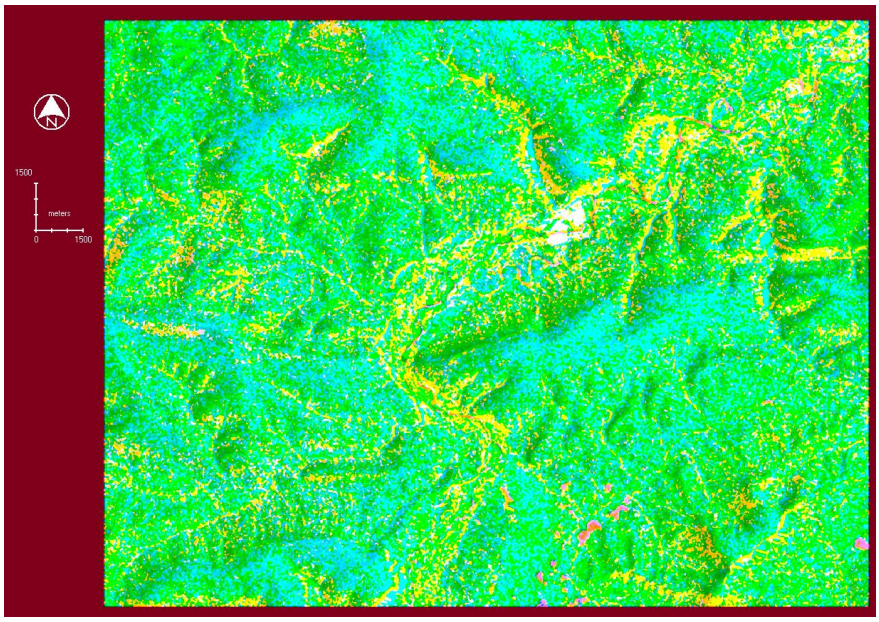

Figure C.7 Radarsat-1 all data, principal component with 5x5 low pass filter. Bands 4,1,3.

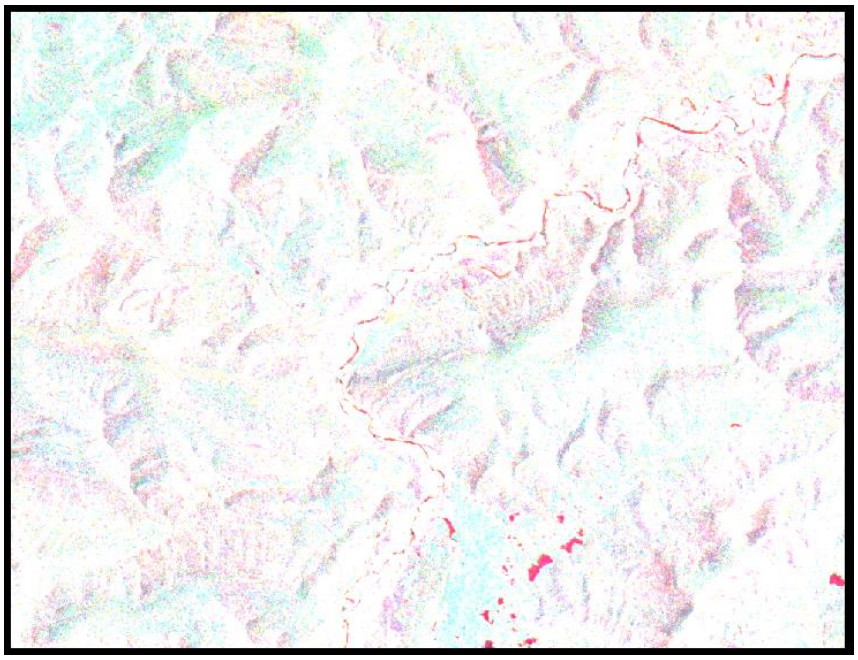

Figure C.8 Radarsat-1 multi-temporal filter 7x7 in RGB view with bands 4,2,1.

D.1-Samples of topographic maps used in the field

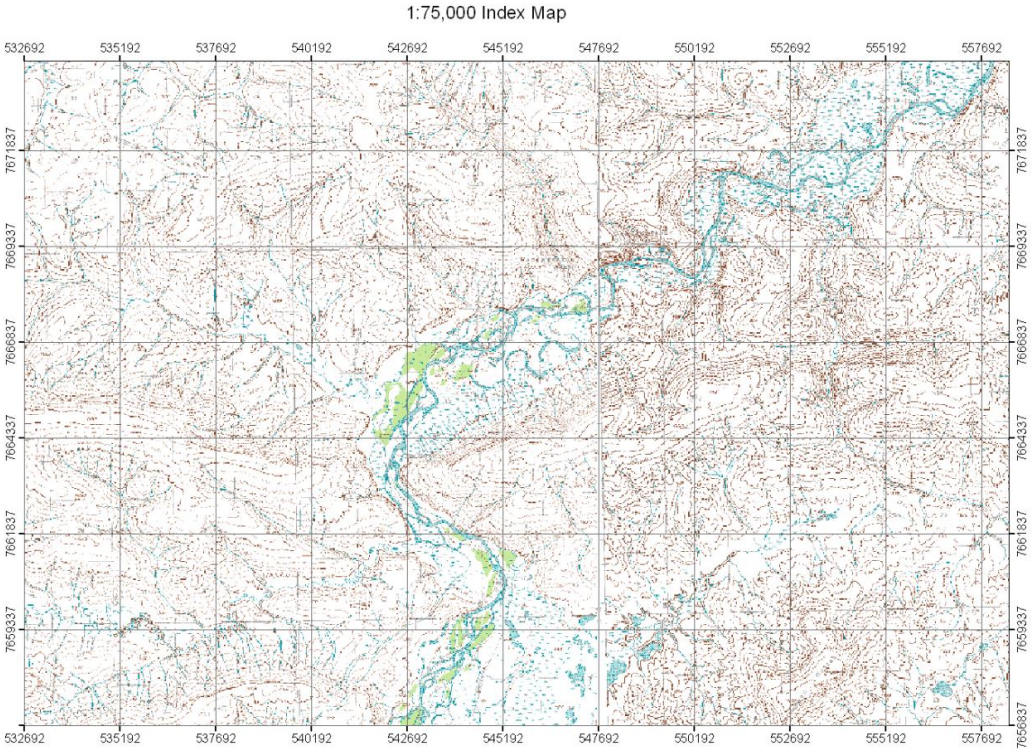

Figure D.1 Index map of the study area

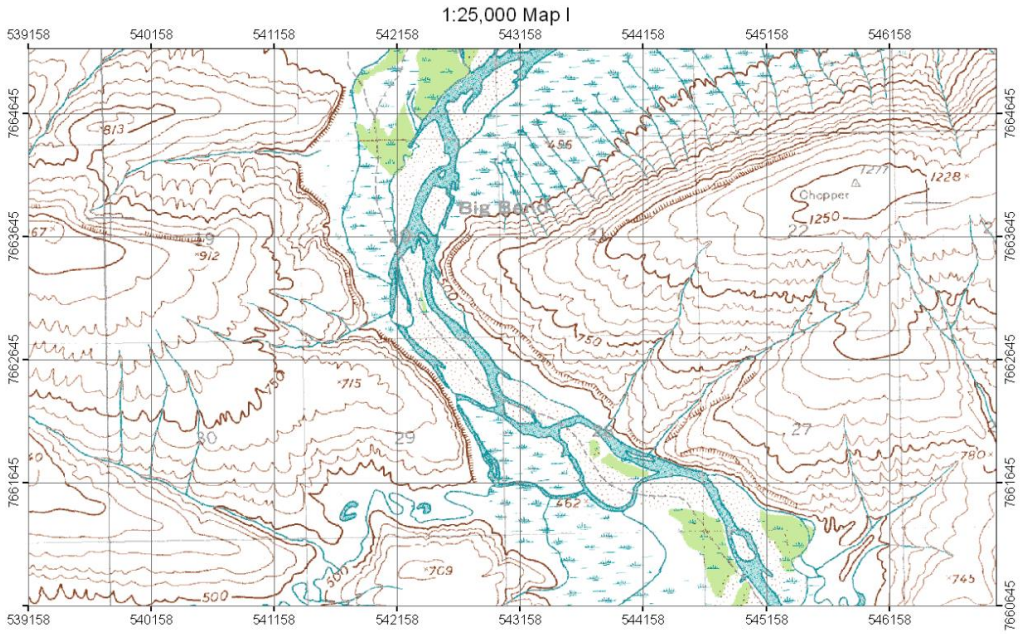

Figure D.2 Sample field map of the southern Big Bend anticline

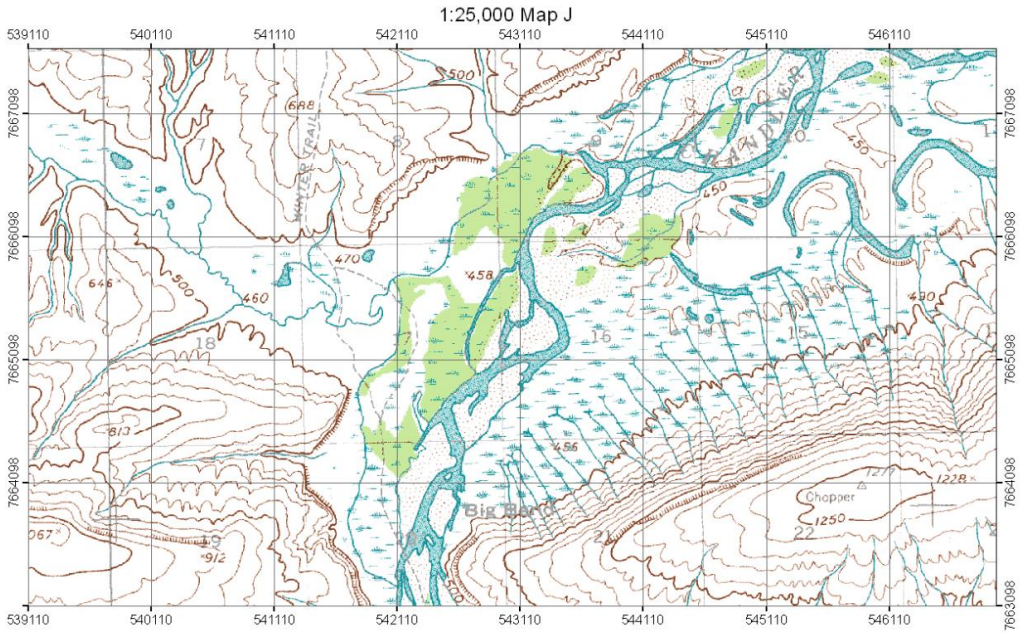

Figure D.3 Sample field map of the southern Big Bend anticline and Seabee syncline

E.1 Detterman et al., 1963 1:25,000 geologic map

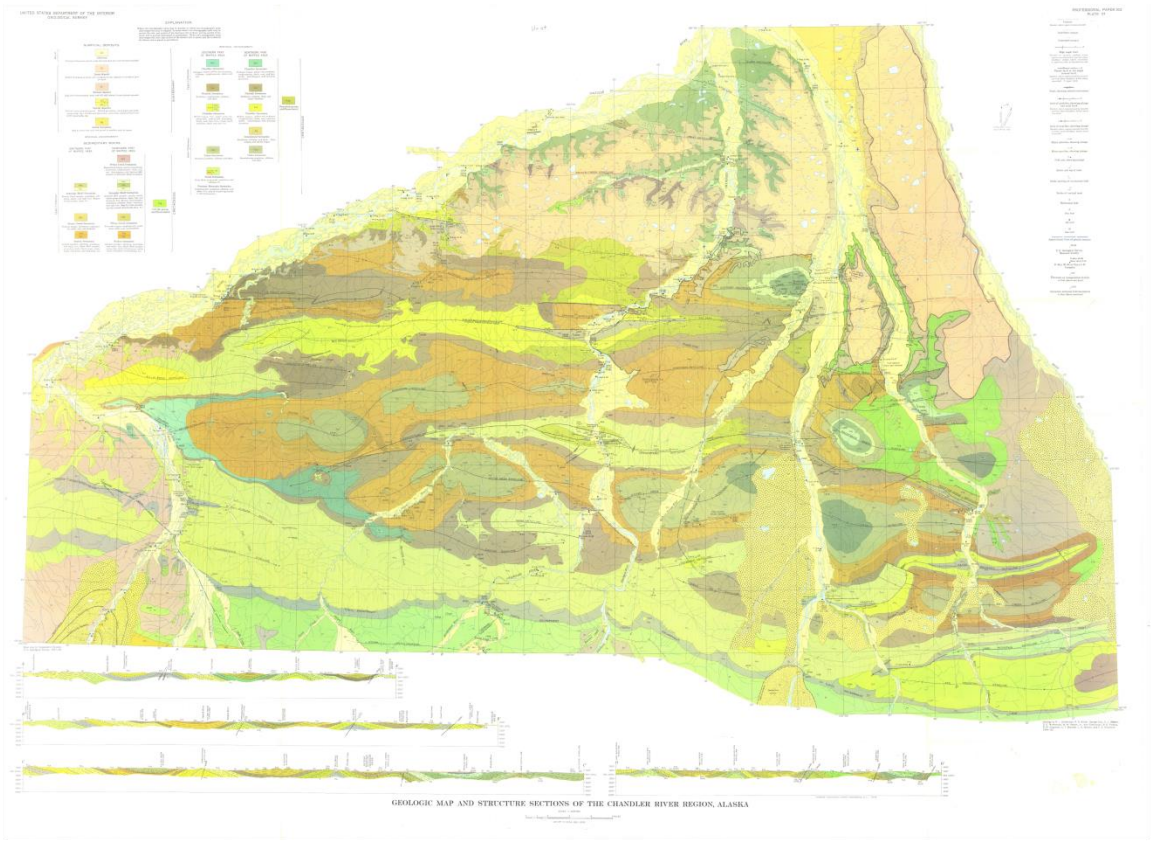

Figure B.1 Full Detterman et al, (1963) geologic map

F.1-Station locations and samples collected during field work summer 2010.

Table F.1 Field notes with waypoint information, sample numbers and coordinate data.

Date	Way Point	Sample	Latitude	Longitude
6/19/2010				
6/20/2010	2001		N69°04'28	W151°56'12
	2002		542377	7662877
	2003			
	2004		541852	7663112
	2005			
	2006		541830	7663134
	2007		541791	7663163
	2008		541739	7663204
	2009	2009-1	541547	7663731
	2010		541591	7663795
	2011	2011-2	541744	7663185
6/21/2010	2101	2101-1	541515	7664321
		2101-2		
	2102	2102-3	541526	7664531
		2102-4		
	2103		541553	7664501
	2104		541583	7664573
	2105		541601	7664610
	2106	2106-8 U-Th/He sa	541694	7664618
	2107	2107-9 U-Th/He	541661	7664609
	2108	2108-5	541612	7664638
		2108-6		
	2109		539552	7663891
	2110	2110-7	539504	7663816
	2111		539539	7663707
	2112		539697	7663672
	2113		539688	7663676
	2114		540314	7663640
6/22/2010	2201	2201-1	542754	7666739
	2202	2202-2	542759	7666737
	2203	2203-3	548192	7667779
	2204		548215	7667809
	2205		548172	7667831
	2206		548154	7667909
	2207		541881	7661496
	2208		541839	7661457
	2209		541857	7661477
	2210		541943	7661453
	2211		541946	7661455
6/23/2010	2301		546942	7668023
	2302		546992	7668122
	2303		546988	7668130
	2304		546983	7668130
	2305		546813	7668662

Seabee
Nanushuk
Torok
U-Th/He
Vitrinite

Date	Way Point	Sample	Latitude	Longitude
6/23/2010	2306		546789	7668751
	2307		546888	7668843
	2308		546855	7669314
	2310		547305	7668991
	2309		547354	7669236
	2311		547525	7668979
	2312		547572	7669019
	2313		547601	7669040
	2314		547747	7669077
	2315		547692	7669075
	2316		547454	7668896
	2317		547482	7668802
	2318		547436	7668814
	2319	2319-2 Vitrinite	547225	7668409
		2319-3 U-Th/He		
6/24/2010	2401		546734	7668101
	2402		546762	7668191
	2403		546666	7668086
	2404		546544	7667844
	2405		546458	7667898
	2406		545550	7667728
	2407		545536	7667701
	2408		545562	7667738
	2409		544366	7668007
	2410		544198	7667911
	2411	2411-1	543460	7667442
		2411-2		
6/25/2010	2501		548030	7667955
	2502		548077	76668856
	2503		548137	7668864
	2504		548168	7668865
	2505		548782	7669145
	Wes #1		549422	7669488
	Wes#2	Wes2-1	549685	7669243
	2506		549717	7668994
	2507		549758	7668864
	2508		549767	7668833

Date	Way Point	Sample	Latitude	Longitude
6/25/2010	2509		549815	7668745
	2510	2510-2	549841	7668720
6/26/2010	2601		545967	7664116
	2602		546803	7664538
	2603		547199	7664738
	2604		545902	7664083
	2605		545900	7664085
	2606	2606-1 U-Th/He	545760	7664309
	2607		545536	7664280
	2608		545192	7664234
	2609		545088	7664254
6/27/2010	2701		542619	7663129
	2702		542886	7662956
	2703		542897	7663005
	2704		542924	7662974
	2705		543030	7663053
	2706		543667	7663151
	2707		54385	7663000
	2708		544106	7662917
	2709		544419	7662810
	2710		544913	7662491
	2711		544815	7662409
	2712		544611	7662017
	2713	2713-1	544472	7661901
	2714	2714-2	544356	7661897
	2715		544219	7661884
	2716		544163	7661899
	2717		544120	7661932
6/28/2010	2801	2801-1	542747	7663111
	2802		542772	7663105
	2803		542862	7663071
	2804		542597	7663256
	2805	2805-2 U-Th/He	542546	7663321
	2806		542475	7663472
6/29/2010	2901		553931	7664175
	2902		553860	7664238
	2903		553763	7664282
	2904		553855	7664375
	2905		553637	7665151
	2906		553621	7665168
	2907		553486	7665465
	2908		553570	7665545
	2909		553647	7665422
	2910		553762	7665739
	2911		553754	7665824

Date	Way Point	Sample	Latitude	Longitude
6/29/2010	2912		553650	7665878
	2913		553814	7666153
	2914		554101	7666747
6/30/2010	3001	3001-1 U-Th/H	554086	7666875
	3002	3002-1	554102	7666924
	3003		554635	7667095
	3004		554507	7667164
	3005		554422	7667188
	3006		554365	7667229
	3007		554429	7667196
	3008		554681	7667426
	3009		554717	7667755
	3010		554304	7668042
	3011		554314	7668080
	3012		554437	7667999
	3013		554026	7668249
	3014		553843	7667083
7/1/2010	101	0101-2 U-Th/H	554338	7667152
	102		554096	7666292
	103		554150	7666123
	104		554245	7665787
	105	0105-3	554321	7665607
	106		554563	7665697
	107		554498	7666152

G.1 Attitude measurements collected in the field

Table G.1 All attitude measurements used for stereographic projections

BB south limb		Sanders' #		Wallace's #	
6/20/2010	2007	54	22.5		
6/21/2010	2010	110	26	195	15
	2111	85	26	192	26
	2112	78	4		
	2113	130	25		
6/22/2010	2210	26	9	142	19
		51	17	170	15
6/27/2010	2713	86	11		
		110	18		
	2714	95	15		
		70	20		
6/28/2010	2801	74	34		
	2804	68	13		
		45	13		
		60	17		

BB north limb		Sanders' #		Wallace's #	
6/21/2010	2106	245	7	15	45
	2108	270	20	1	26
		258	9		
6/24/2010	2404	231	13	352	8
	2405	224	4	283	12
	2411	135	38	154	8

NA north limb		Sanders' #		Wallace's #	
6/22/2010	2204	229	39.5	279	32
	2205	258	30	295	32
	2206	185	28		
6/23/2010	2319	85	46	352	40
		258	11		
6/24/2010	2404	231	13	352	8
	2405	224	4	283	12
6/25/2010	2503	275	24	4	17
		295	24		

NA south limb		Sanders' #		Wallace's #	
6/22/2010	2201	92	20	171	24
6/23/2010	2303	72	27	150	4
	2304	137	19	222	11
6/24/2010	2411	135	38	154	8

Mini Anticline		Sanders' #	
6/22/2010	2209	37	16
		42	16
		257	25
		198	4
		345	20
		270	6

Trouble Creek		Sanders' #	
6/29/2010	2903	100	18
		87	7
6/31/2010	3002	276	19
		290	15
	3014	276	21

H.1 -Bedding correlations between domains

Table H.1 Correlations made between bedding. Includes fault locations, strong correlations and potential correlations.

Domain B2 and C1	Domain B1 Near Chandler Rv.	Domain B1 near Trouble Creek	Domain A	Domain E	Domain D2	Domain D1	Domain C2
B2-1	B1-1	B1-1				D1-1	
	B1-2	B1-2					
	B1-3	B1-3					
	B1-4	B1-4				D1-2	
	B1-5	B1-5				D1-3	
B2-2	B1-6	B1-6				D1-4	
B2-3	B1-7	B1-7	A-1		D2-1	D1-5	
B2-4	B1-8	B1-8	A-2		D2-2		
	B1-9	B1-9	A-3		D2-3		
					D2-4		
					D2-5		
					D2-6		
					D2-7		
				E-1	D2-8		
	B1-10	B1-10	A-4	E-2	D2-9	D1-6	C2-1
B2-5	B1-11	B1-11	A-5	E-3		D1-7	
B2-6	B1-12	B1-12	A-6	E-4	D2-10	D1-8	C2-2
				E-5	D2-11	D1-9	C2-3
				E-6	D2-12		C2-4
	B1-13	B1-13	A-7	E-7	D2-13		C2-5
	B1-14	B1-14		E-8	D2-14		C2-6
				E-9			
				E-10			
				E-11			
B2-7	B1-15	B1-15	A-8				
	B1-16	B1-16	A-9				
B2-8	B1-17	B1-17	A-10	E-12			
				E-13			
				E-14			
B2-9	B1-18	B1-18	A-11	E-15			
B2-10	B1-19	B1-19		E-16			
B2-11	B1-20	B1-20		E-17			
	B1-21	B1-21		E-18			
B-12	B1-22	B1-22		E-19			
B2-13	B1-23	B1-23		E-20			
B2-14	B1-24	B1-24		E-21			
B2-15	B1-25	B1-25					
B2-16							
B2-17							
C1-1							
C1-2							
C1-3							
C1-4							
C1-5							

KEY
Bedding traces that correlate
Possible correlation
Possible fault location
Fault location

I.1-Test well depth information

Table I.1 Approximate stratigraphic thickness at each well site in meters

	Big Bend Well	Grandstand test #1	Seabee Well
Colville Group	300	30	140
Nanushuk Fm.	195	300	300
Torok Fm.	2500+	600+	3580